Master's thesis
Theoretical Physics

Nucleation Rate in a Radiatively Induced First-Order Phase Transition

Joonas Hirvonen

August 14, 2020

Supervisor(s): Aleksi Vuorinen and Oliver Gould

Examiner(s): Aleksi Vuorinen
Oliver Gould

University of Helsinki
Faculty of Science

PL 64 (Gustaf Hällströmin katu 2a)
00014 Helsingin yliopisto

HELSINGIN YLIOPISTO — HELSINGFORS UNIVERSITET — UNIVERSITY OF HELSINKI

Tiedekunta — Fakultet — Faculty	Koulutusohjelma — Utbildningsprogram — Degree programme
Faculty of Science	Theoretical Physics

Tekijä — Författare — Author

Joonas Hirvonen

Työn nimi — Arbetets titel — Title

Nucleation Rate in a Radiatively Induced First-Order Phase Transition

Työn laji — Arbetets art — Level	Aika — Datum — Month and year	Sivumäärä — Sidantal — Number of pages
Master's thesis	August 14, 2020	116

Tiivistelmä — Referat — Abstract

We apply the modern effective field theory framework to study the nucleation rate in high-temperature first-order phase transitions. With this framework, an effective description for the critical bubble can be constructed, and the exponentially large contributions to the nucleation rate can then be computed from the effective description. The results can be used to make more accurate predictions relating to cosmological first-order phase transitions, for example, the gravitational wave spectrum from a transition, which is important for the planned experiment LISA.

We start by reviewing a nucleation rate calculation for a classical scalar field to understand, how the critical bubble arises, via a saddle-point approximation, as the central object of the nucleation rate calculation. We then focus on the statistical part of the nucleation rate coming from the Boltzmann suppression of nucleating bubbles. This is done by the creation of an effective field theory from a thermal field theory that can describe the critical bubble. We give an example calculation with the renormalizable model of two $\mathbb{Z}_2$-symmetric scalar fields. The critical bubbles of the model and their Boltzmann suppression are studied numerically, for which we further develop a recently proposed method.

Avainsanat — Nyckelord — Keywords

nucleation rate, critical bubble, thermal field theory, effective field theory

Säilytyspaikka — Förvaringsställe — Where deposited

Muita tietoja — Övriga uppgifter — Additional information

Contents

1. Introduction

The first gravitational waves (GW) were detected directly by LIGO in 2015 [1]. This marked the beginning of gravitational wave cosmology. All of the knowledge on cosmology thus far had been gathered via observing electromagnetic waves. As a consequence, it is impossible to obtain a direct detection of events that happened before the universe became transparent at recombination. Observing GWs can probe the early universe directly, because the waves have essentially been decoupled, at least since the temperature dropped below the Planck mass [2]. Due to the decoupling, GWs from cosmological events have not changed due to interactions, albeit the evolution of the universe has had an effect on them [2].

First-order phase transitions in the early universe are potential candidates for producing a gravitational wave background, although none exist according to the Standard Model of particle physics (SM). Therefore, a detection of a signal from a transition would be a mark of physics beyond the SM. The first space-based gravitational wave observatory, LISA, is due to be launched in 2030s. This will make it possible to hear the waves from transitions that have happened below the scale of approximately 1TeV, because their peak amplitude is in the frequency window of the observatory [2].

One candidate transition would be the electroweak phase transition (EWPT). In the Standard Model, it is known to be a smooth cross-over [3, 4], but there is still a possibility that there is new physics that can render the transition into a first-order transition (e.g. [5]). The first-order EWPT is motivated with the possibility of explaining the baryon asymmetry of the universe via electroweak baryogenesis [6]. This would one example of finding physics that is beyond the Standard Model via observing gravitational waves from a first-order phase transition.

The possibility of observing new physics from cosmological phase transitions via their gravitational wave spectrum motivates a more careful study of the transitions. One important aspect of the transitions is their nucleation rate, which we will examine in this thesis. The other piece for a gravitational wave spectrum is the speed at which the walls of the nucleated bubbles convert an old phase into a new phase. From the nucleation rate, it is possible to extract the temperature of the transition and its duration [7]. Furthermore, it is possible to deduce the strength of the transition and the Hubble rate at the transition,

which are key elements in the computation of the gravitational wave spectrum from the transition [8].

A nucleation rate per unit volume is conventionally expressed in the following way:

$$\frac{\Gamma}{V} = Ae^{-S}, \tag{1.1}$$

where the two different contributions A and S come from different places. The exponential suppression, S, comes from the Boltzmann suppression of a critical bubble, which is, in a sense, a minimal bubble: In the absence of any perturbations, it would stay stationary, but if it is perturbed, it either grows filling the space with the new phase, or shrinks out of existence. The prefactor, A, contains the contributions from fluctuations around the critical bubble and also the time-evolution of a bubble configuration as it nucleates. Therefore, a critical bubble configuration plays a central role in a nucleation rate calculation. In a sufficiently stark first-order transition, it can already give by itself quite a bit of information on the transition and consequently, on the gravitational wave spectrum. The goal of the thesis is to be able to find the critical bubble and its exponential suppression in various situations.

As LISA will be launched in the near future, it is timely to revise our methods of calculating nucleation rates. Finding a critical bubble in a cosmological phase transition requires the creation of an effective description for the bubble. This is because the transition is driven by changes in thermal fluctuations due to the cooling of the universe. Hence, the fluctuations behind the transition must be taken into account as a background for the bubble to exist on. Previously, an effective description has been obtained via explicit resummations [9] or via a coarse-grained potential [10]. Here, we would like to present a framework that relies on modern effective field theory (EFT). The particular EFT, called dimensional reduction, has been developed in Refs. [11, 12].

The idea in the EFT, that can describe the critical bubbles, is to integrate out the short-scale fluctuations to the background while leaving the long-scale fluctuations to compose the critical bubble and to be the fluctuations around it. This is not always a straightforward task to complete, because it is possible that a field becomes much heavier on top of a bubble than it was in the old phase. In this case, the hierarchy needed to build a consistent EFT might break down in the old phase, while the fluctuations are needed to be integrated out on the critical bubble (cf. 3.3.4). With non-abelian gauge fields, the magnetic components are non-perturbative in the symmetric phase, where the gauge symmetry is not broken. This is called the Linde problem [13]. In these cases, the description of a critical bubble fails in the old phase, but the hope is that this kind of a mistake would not affect too much the exponential suppression, S, from the bubble or its shape. The mistake has also an effect on the prefactor, A, through the critical bubble configuration and the old phase, as it contains information of fluctuations around them.

The reason for using the EFT framework is that it is easier to know and to calculate the corrections that have to be taken into account. The possibility to systematically power count corrections allows the minimization of the running of the nucleation rate result with renormalization scale. Current methods give gauge dependent nucleation rates [14]. The power counting might also enable one to obtain gauge invariant results for the nucleation rate, as is the case for vacuum decay calculations [15]. Here, one obstacle compared to the vacuum decay might be the Linde problem mentioned above. However, the thesis will not specifically handle gauge fields.

In Ch. 2, we will study a calculation of the thermal nucleation rate for a classical scalar field and see how the calculation is founded on the critical bubble. We will also study the critical bubble itself and the fluctuations around it. The effective description is outlined in Ch. 3. We start by reviewing thermal field theory (TFT), which describes the quantum fields at a finite temperature i.e. it describes the field content in the early universe. Then, we go through the construction of an effective field theory, that describes the degree of freedom (DoF) undergoing the phase transition, from a TFT. We will also give an example calculation in a renormalizable model of two real scalars. Finally in Ch. 4, we will obtain numerical results from the example calculation. It is done with a method for finding the critical bubble from an effective action [16], which we will call the tunnelling potential method. The method and its numerical implementation will also be studied.

2. Nucleation Rate

A first-order phase transition usually[†] happens through nucleation. A familiar example is water boiling. There are bubbles nucleating into the water rather than the whole amount of water vaporizing immediately. The same is true for first-order phase transitions is quantum field theory. A field nucleates a bubble of new phase which then starts to grow and ultimately, these bubbles fill in the whole space.

At normal pressure, water boils always at 100°C. In cosmological phase transitions, there is an arm wrestling match between the Hubble rate and the nucleation rate. There is a critical temperature at which the new phase becomes favourable and bubbles begin to form. However, the nucleation rate can be so small that the expansion of the Universe wins. The bubbles will be left lonely in too quickly expanding space. As the temperature cools even more, the nucleation rate increases and at some temperature, bubbles nucleate at a quick enough rate so that they fill the whole Universe with the new phase. Therefore, the nucleation rate determines the temperature at which the phase transition truly occurs which is important in determining the amount of latent heat released in the phase transition and the pressure difference between the two phases. Another important quantity for the gravitational wave background from the phase transition is the duration of the transition which can also be determined from the nucleation rate.

A remarkably similar problem was first tackled by Coleman and Callan in Refs. [17] and [18]. The problem was the decay rate of a metastable state of a quantum field. We won't go into full details but look into how it paved the way for thermal nucleation rate calculations.

The decay rate per unit volume is given by the imaginary part of the energy density: $\Gamma/V = -2\,\mathrm{Im}\,\mathcal{E}$. Callan and Coleman used a clever trick to find the imaginary part of the lowest energy state in a metastable potential well. In the expectation value below,

[†]A first-order phase transition can happen through a spinodal decomposition, in which the old phase becomes absolutely unstable. Regular fluctuations are enough for the transition to take place and hence there is no bubble nucleation. This requires rapid changes in the system undergoing the transition so that there is no significant nucleation while the old phase is metastable. In cosmological phase transitions, which are our ultimate interest, the change in temperature is due to the Hubble expansion. At the scales of the electroweak phase transition, the internal timescales of the Higgs field are much quicker. Therefore the electroweak phase transition likely occurred through nucleation if it was a first-order transition.

the limit $\tau \to \infty$ skims out contributions from other states than the lowest energy state with an energy of E_0. This can be seen via inserting the unit operator in the basis of the Hamiltonian into the expectation value:

$$\langle\phi_+|\, e^{-\hat{H}\tau}\, |\phi_+\rangle = \sum_n |\langle\phi_+|n\rangle|^2 e^{-E_n\tau} \overset{\tau\to\infty}{\propto} e^{-E_0\tau}, \tag{2.1}$$

where $|\phi_+\rangle$ is a state in which a field ϕ is in the metastable field value everywhere (cf. Fig. 2.3) and $\hat{H}$ is the Hamiltonian of the field. The imaginary part of the energy density is found by solving for E_0. The expectation value can also be represented as a Euclidean path integral whose boundary conditions are $\phi = \phi_+$ at infinity:

$$\langle\phi_+|\, e^{-\hat{H}\tau}\, |\phi_+\rangle \to \int \mathcal{D}\phi e^{-S_\mathrm{E}}. \tag{2.2}$$

Here comes the reason why this problem is similar to thermal nucleation: Callan and Coleman used the saddle-point approximation for the path integral. The approximation was done around a stationary configuration of the Euclidean action called the bounce solution, which is analogous to the critical bubble in the thermal nucleation rate calculation, which will be studied in detail in Sec. 2.2. The use of a saddle-point approximation around a critical bubble is a key insight into performing the calculation of the thermal nucleation rate in Sec. 2.3.

The approximation has its limitations: It assumes that the bubbles that nucleate are similar to the critical bubble and takes the fluctuations around the critical bubble into account linearly. If a first-order transition is very weak, nucleating bubbles can differ drastically from the critical bubble and the saddle-point approximation breaks down.

In the vacuum decay calculation of Callan and Coleman, the saddle-point approximation is the trick for obtaining the imaginary part for the energy in Eq. (2.1). The bounce solution is not a minimum of the Euclidean action but rather a saddle-point and the imaginary part follows from an analytic continuation.

The first attempt of solving for a quantum field escaping a metastable state at finite temperature came from Linde [19]. It was based on an assumption that the decay rate would be given by the imaginary part of the free energy, F. However, Affleck showed [20] that in the case of a particle escaping a metastable state, the assumption of $\Gamma = -2\,\mathrm{Im}\,F$ holds only at low temperatures and breaks at high temperatures. This happens because the imaginary part of the free energy describes only quantum tunnelling. At high enough temperatures, thermal fluctuations cause the escape quicker than quantum tunnelling and therefore, the nucleation rate is not given by $\Gamma = -2\,\mathrm{Im}\,F$. The transition, that we are interested in, should happen above the temperature threshold of thermal fluctuations dominating. This matter will be discussed in more detail at the end of the section 2.3.

In this chapter, we will first go through the conceptually easier problem of a classical particle escaping a potential well in one dimension. Despite its simplicity, it is very

analogous to the nucleation rate of a field at high temperatures. In Sec. 2.2, we look into the much more complex nature of a field escaping a metastable state and establish the field configuration called the critical bubble being a central part of the nucleation rate. In the last section, we will generalize the escape rate of a classical particle to the nucleation rate of a classical field with the help of the critical bubble. We will also discuss subtleties relating to the exact solution of the nucleation rate for our purposes, which is probably still out of reach. Nevertheless, we will still be able to obtain the exponential contributions to the rate from the Boltzmann suppression of the nucleating bubbles. Ultimately, this is enough information to make predictions from phase transition as can be seen from Sec. 4.3.1.

2.1 Escape Rate of a Classical Particle

As a kind of a warm-up exercise for the thermal nucleation rate of a classical field, we will go through the thermal escape rate of a classical particle in one dimension. The escape rate essentially tells how quickly a particle trapped in a potential well will escape (Fig. 2.1). The question of escape rate is meaningful when the thermal agitations are small compared to the potential difference between the bottom of the well x_m and the top of the barrier x_b. Here, we will go through a quick estimate of the escape rate [20], discuss its shortcomings and then go through a more careful calculation [21].

The escape rate is the same as the probability flux over the top of the potential barrier x_b,

$$\Gamma = \int \mathrm{d}x\,\mathrm{d}p\,\frac{p}{m}\delta(x - x_b)\;\rho(x,p), \tag{2.3}$$

where ρ is the probability density of the state of the particle, p is its momentum and m is the mass. Since the potential barrier is high compared to the thermal energy of the particle, we can assume that the particle is in a thermal equilibrium in the potential well.

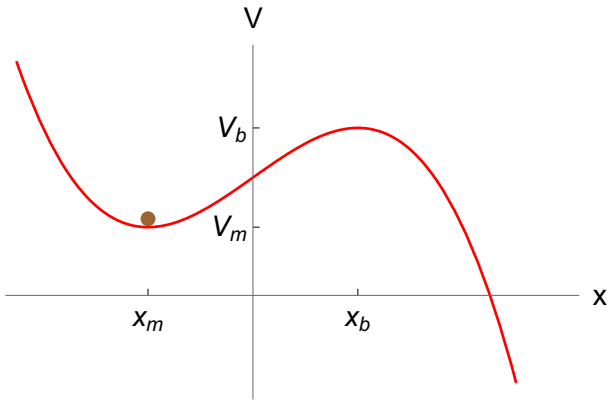

Figure 2.1: A one dimensional potential with potential well at x_m and a potential barrier at x_b.

For a first estimation, we will assume that the distribution is thermal on top of the barrier but there is no probability for the particle coming back from the other side of the barrier:

$$\Gamma = \frac{1}{Z}\int \mathrm{d}x\,\mathrm{d}p\,\frac{p}{m}\delta(x-x_b)\theta(p)\;e^{-H/T}, \tag{2.4}$$
$$H = \frac{p^2}{2m} + V(x),$$

where Z normalizes the probability density and $\theta(p)$ tells that all the probability flux coming into the well from the right hand side is zero. Z can be approximated with the saddle-point approximation around the bottom of the potential well because the bulk of the probability is in the well. With a quadratic approximation of the potential $V(x) \approx V_m + \frac{1}{2}m\omega_m^2(x-x_m)^2$:

$$Z \approx \int \mathrm{d}x\,\mathrm{d}p\,e^{-(\frac{p^2}{2m}+V_m+\frac{1}{2}m\omega_m^2(x-x_m)^2)/T} = \frac{2\pi T}{\omega_m}e^{-V_m/T} \tag{2.5}$$

The integrals in Eq. (2.4) can be carried out nicely giving

$$\Gamma = \frac{\omega_m}{2\pi}e^{-(V_b-V_m)/T}. \tag{2.6}$$

Interestingly, this is just the oscillation frequency of a harmonic oscillator in the approximated potential times the Boltzmann suppression from the potential barrier.

Here we would like to make a remark. The exponential suppression comes from the height of the potential barrier separating the potential well from the rest of space. The same is true for the nucleation rate but the potential barrier is a bit more subtle. For fields, the potential barrier does not exist in ordinary space but in the configuration space of the field. The barrier is a certain set of configurations and the lowest point on the barrier is the critical bubble. The critical bubble gives the exponential suppression of the nucleation rate. This will be studied in more detail in Sec. 2.2.

The calculation which was presented above is a bit naive. It was assumed that there are no particles coming back from the other side of the potential barrier. However, there is a possibility that the particle comes back due to a thermal nudge. Another point is that the probability is flowing over the barrier and it has to be replaced from the well. Therefore the likelihood of a particle being on the potential barrier is smaller than thermal distribution assumes.

A more refined calculation can be done by considering the time-evolution of the particle around the potential barrier [21] (Fig. 2.2). The classical time-evolution of a particle in a stochastic thermal medium is given by the Langevin equation and thus, the probability distribution satisfies the Fokker-Planck equation:

$$\frac{\partial}{\partial t}\rho(x,v,t) = -\left(v\frac{\partial}{\partial x} - \frac{1}{m}\frac{\partial}{\partial v}(\gamma m v + V'(x)) - \frac{\gamma T}{m}\frac{\partial^2}{\partial v^2}\right)\rho(x,v,t), \tag{2.7}$$

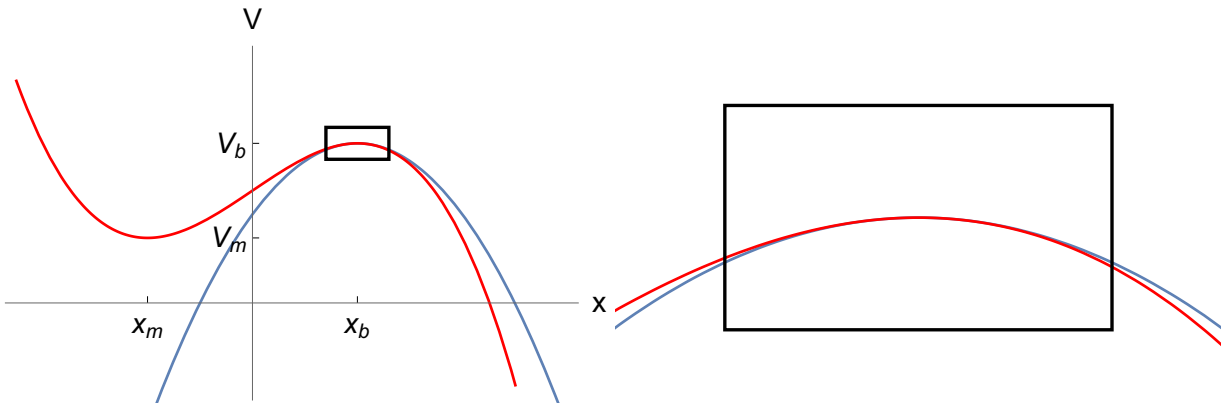

Figure 2.2: A quadratic approximation to the potential at the top of the potential barrier.

in which γ is a friction coefficient due to the the thermal medium.

We are looking for a solution for the Fokker-Planck equation which satisfies three conditions: the distribution is time-independent due to the thermal supply of the potential well, the distribution becomes thermal inside the well and is zero on the outside of the barrier. We want the solution around the top of the potential barrier and therefore, we can approximate the potential barrier to be parabolic: $V(x) \approx V(x_b) - \frac{1}{2}m\omega_b^2(x-x_b)^2$. The solution to the Fokker-Planck equation is

$$\rho(x,v) = \rho_{\text{thermal}}(x,v) \cdot \sqrt{\frac{m\omega_b^4}{2\pi\gamma\lambda T}} \int_u^\infty \mathrm{d}z \exp\left(-\frac{m\omega_b^4}{2\gamma\lambda T}z^2\right), \tag{2.8}$$

$$u = (x - x_b) + \frac{\lambda}{\omega_b^2}v, \tag{2.9}$$

$$\lambda = \sqrt{\omega_b^2 + \left(\frac{\gamma}{2}\right)^2} - \frac{\gamma}{2}. \tag{2.10}$$

Now that we have a better estimate of the probability density on the top of the potential barrier, we can use again Eq. (2.3) to obtain the escape rate:

$$\Gamma = \frac{\sqrt{\omega_b^2 + \frac{\gamma^2}{4}} - \frac{\gamma}{2}}{\omega_b} \cdot \frac{\omega_m}{2\pi} e^{-(V_b - V_m)/T}. \tag{2.11}$$

There is an addition to the prefactor from the friction coefficient γ which tells how the thermal medium affects the travel on top of the barrier. As one would expect, this result reduces to the more naive one if $\gamma = 0$, i.e. when the effects of the thermal medium to the motion of the particle can be neglected.

Even though we have now taken into account damping from the medium, the exponential suppression is exactly the same as before and comes form the height of the potential barrier. This will carry over to the nucleation rate of the field; the exponential suppression of the nucleation rate comes from the Boltzmann factor of the critical bubble configuration.

2.2 Nucleation and Critical Bubble

The escape rate of a classical field is somewhat more complicated than the escape rate of a classical particle. It cannot be described by a one-dimensional potential like the case of a particle. The field does not have just one degree of freedom but infinitely many. The escape rate of a field is called a nucleation rate because the field does not escape the potential well uniformly everywhere. This would require an amount of energy which is proportional to the volume of the field: $V\,\Delta U_{\text{barrier}}$. The escape rate for a uniform escape is then suppressed exponentially by this energy. For this reason, the field escapes first only locally. The escaped part of the field drags the rest of the field with it to the other side of the potential barrier. These small volumes of the field which have escaped are called bubbles. Therefore the task with a field is to compute the nucleation rate of bubbles that start to grow and fill the space.

If a stationary particle was in the potential of Fig. 2.1 over the location x_b, the particle would escape in the absence of thermal medium. Let us have a field that is described with a Hamiltonian function

$$H = \int \mathrm{d}^3x \left(\frac{1}{2}\pi^2 + \frac{1}{2}(\boldsymbol{\nabla}\phi)^2 + U(\phi) \right) \tag{2.12}$$

and the potential from Fig. 2.3. How could one tell if a configuration with boundary condition $\lim_{r\to\infty} \phi = \phi_+$ would eventually escape to the value ϕ_-? It is simply not enough to have a field value which is over the top of the potential bump in Fig. 2.3. There is also energy stored in the gradient term of the Hamiltonian function which means that neighbouring regions of the field could still pull the field value back to the metastable well.

We will start to unravel the question of a field nucleating and escaping to the stable state through a configuration called a critical bubble. It is kind of a similar gatekeeper as

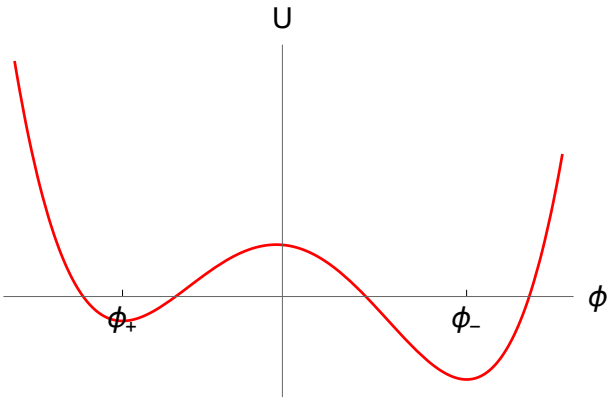

Figure 2.3: A potential for a field. The field undergoes nucleation if it is trapped to the metastable state at ϕ_+.

is the location of the top of the potential barrier in the previous section. Simplistically, if a bubble is large enough, it starts to pull field elsewhere with it, but if it is too small, the rest of the field wins and the bubble shrinks out of existence. The critical bubble is in the middle. It is a stationary configuration but perturbing it will make it either grow or shrink. The field has escaped locally from the metastable state if there is a bubble that is larger than the critical bubble – a nucleation has happened.

The rest of this section is devoted to studying the critical bubble. We will first look into finding the configuration. Then we show in which cases the critical bubble exists. The method, used to prove the existence, also allows us to study the shape of the critical bubble. We then move onto decomposing fluctuations around the critical bubble with a natural choice of basis functions. This helps us to see if a bubble is "bigger" or "smaller" than the critical bubble. It also helps us to understand the analogy between the location of the potential barrier and the critical bubble configuration. The decomposition of fluctuations developed here is also crucial for the nucleation rate calculation of the next section.

As the critical bubble is a stationary configuration, it is also a stationary point of the Hamiltonian function:

$$\frac{\delta}{\delta\pi}H = 0 \quad \Rightarrow \quad \pi = 0, \tag{2.13}$$

$$\frac{\delta}{\delta\phi}H = 0 \quad \Rightarrow \quad \boldsymbol{\nabla}^2\phi = U'(\phi). \tag{2.14}$$

The latter equation can be simplified considerably due to the rotational invariance of the critical bubble around its centre [22]:

$$\ddot{\phi}(r) + \frac{d-1}{r}\dot{\phi}(r) = U'(\phi(r)), \tag{2.15}$$

where a dot represents a derivative with respect to the radial coordinate. The remaining task is to find a solution to this equation, which we shall refer to as the equation of motion (EoM)) of the critical bubble, with the following boundary conditions:

$$\lim_{r\to\infty}\phi(r) = \phi_+, \tag{2.16}$$

$$\dot{\phi}(0) = 0. \tag{2.17}$$

The former condition tells that the critical bubble configuration lies in the metastable field value at infinity and the latter just says that the critical bubble is well-behaved at its centre.

We will now move onto showing that there exists a solution which can be identified as the critical bubble (besides the trivial solution $\phi(r) = \phi_+$). The EoM (2.15) is similar to Newton's second law in which time is replaced by the radial coordinate and the position

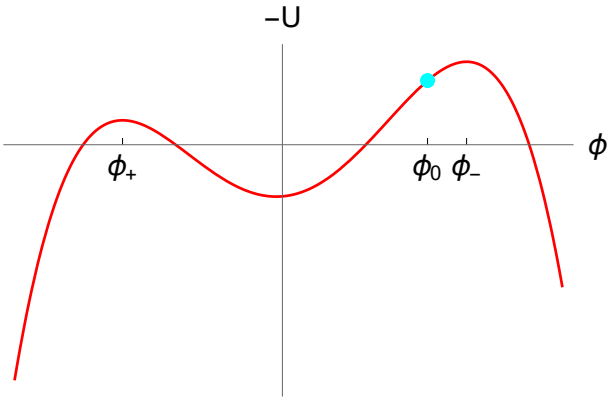

Figure 2.4: A negative potential appears in the EoM of the critical bubble (2.15). ϕ_0 is the field value at the centre of the critical bubble.

is replaced by the field value. Also, there is an interesting friction term and the potential is inverted as in Fig. 2.4. The critical bubble is found if we can find a field value ϕ_0 for which

$$\begin{cases} \phi(0) = \phi_0 \\ \dot{\phi}(0) = 0 \end{cases} \quad \Rightarrow \quad \lim_{r\to\infty} \phi(r) = \phi_+. \tag{2.18}$$

The method for showing the existence of ϕ_0 (and therefore the critical bubble) is the undershoot–overshoot method [18]. We show that there exist values for $\phi(0)$ for which it is possible to go over ϕ_+ and fall short from it in the limit of $r \to \infty$. Therefore by continuity there exists a ϕ_0 with which the boundary conditions of the critical bubble are satisfied.

We start the undershoot–overshoot method by defining a quantity which resembles the energy of a particle in the inverted potential:

$$\tilde{E} = \frac{1}{2}\dot{\phi}^2 - U. \tag{2.19}$$

This quantity always decreases as r increases:

$$\frac{\partial \tilde{E}}{\partial r} = \left(\ddot{\phi} - U'\right)\dot{\phi} = -\frac{d-1}{r}\dot{\phi}^2 < 0. \tag{2.20}$$

On the second line, the EoM (2.15) was used. From the latter boundary condition (2.17), it follows that

$$\tilde{E} = -U(\phi(0)), \quad \text{at } r = 0, \tag{2.21}$$

$$\tilde{E} < -U(\phi(0)), \quad \text{when } r > 0. \tag{2.22}$$

Now, we have enough information to complete our undershoot–overshoot. The undershoot is rather trivial. We can pick $\phi(0)$ so that it is on the other side of the potential

barrier and $U(\phi(0)) = U(\phi_+)$. Then $\tilde{E} < -U(\phi_+)$ for $r > 0$ and the solution for the EoM (2.15) can never climb up to the metastable field value ϕ_+. The overshoot is a bit trickier. One can choose $\phi(0)$ to be very, very close to the value ϕ_-. What happens is that the solution to the EoM stays near the top as long as one wants, depending on how close they choose $\phi(0)$ to be to ϕ_-. That way the friction term nearly vanishes and $\tilde{E}$ becomes almost conserved (cf. (2.20)). Now, we have $\tilde{E} \approx -U(\phi_-) > -U(\phi_+)$ and the solution overshoots. Therefore there exists a value ϕ_0 with which the boundary conditions for the critical bubble are satisfied and therefore the critical bubble solution exists for potentials like that shown in Fig. 2.3 with a metastable field value.

This undershoot–overshoot logic can be used to find that the critical bubble becomes really wide and flat with certain potentials. If the potential minima had almost the same potential value, $U(\phi_-) \approx U(\phi_+)$, then there is not much room to lose $\tilde{E}$. As we saw above, the way to make $\tilde{E}$ almost conserved is to start very near the field value ϕ_-. That way the field value $\phi(r)$ stays near the value ϕ_- to a large radial coordinate value (Fig. 2.5). The bubbles of this type are called thin-wall bubbles because the region in which the field value changes from ϕ_- to ϕ_+, the wall, is very narrow compared to the radius of the bubble. A critical bubble is a thin-wall bubble if the transition happens near its critical temperature (at which $U(\phi_-) = U(\phi_+)$). With supercooling, the separation in the energies of the different minima grows and the critical bubble becomes thick walled.

If a critical bubble is a far larger fluctuation than the regular thermal fluctuations, all the bubbles that nucleate resemble it. However, it is impossible for a bubble to be exactly like a critical bubble during its evolution. Therefore, it is important to understand fluctuations around the critical bubble. Another very important reason for studying fluctuations is to understand what kinds of bubbles are larger than the critical bubble in

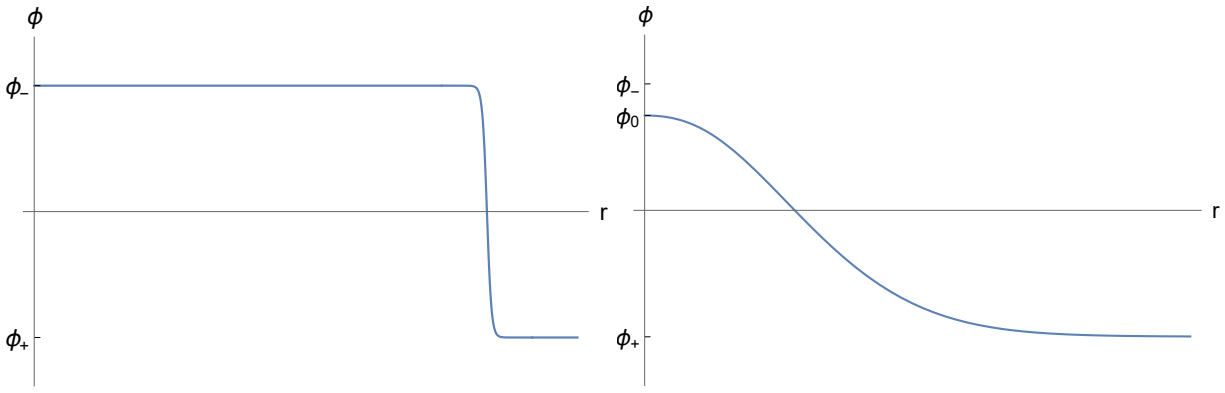

Figure 2.5: A depiction of a thin-wall bubble (left) and a thick wall bubble (right). r is the radial coordinate, ϕ is the field value. For a thin-wall bubble, the field value at the centre is very close to the stable field value ϕ_-. The bubble profile has a plateau in the middle with a wall which is thin in comparison to the size of the plateau. Whereas, in the case of a thick wall bubble, the field value at the centre, ϕ_0, is not that close to ϕ_- and starts to slide towards the metastable value, ϕ_+, right away.

the sense that they keep growing.

There is a natural and useful way of decomposing fluctuations around the critical bubble with an orthonormal basis of functions. A Hermitian operator can be constructed from the Hamiltonian and the critical bubble solution:

$$\frac{\delta^2 H}{\delta\phi^2}\bigg|_{\phi=\phi_\mathrm{B}} = \delta(\mathbf{y}-\mathbf{x})\Big(-\boldsymbol{\nabla}^2_{\mathbf{x}} + U''(\phi_\mathrm{B}(\mathbf{x}))\Big), \tag{2.23}$$

where ϕ_B is the critical bubble configuration. The neat properties of Hermitian operators guarantee that this operator has an orthonormal basis of eigenfunctions f_n with real eigenvalues ξ_n:

$$\int_{\mathbf{x}} \frac{\delta^2 H}{\delta\phi^2}\bigg|_{\phi=\phi_\mathrm{B}} f_n(\mathbf{x}) = \xi_n f_n(\mathbf{y}), \tag{2.24}$$

$$\int_{\mathbf{x}} f_n(\mathbf{x}) f_m(\mathbf{x}) = \delta_{nm}. \tag{2.25}$$

Actually, if the eigenvalue is above $U''(\phi_+)$, the index n becomes continuous and, for example, the orthonormality condition has Dirac delta instead of the Kronecker delta. This can be seen from the fact that the operator in Eq. (2.23) is identical to the Hamiltonian operator in single-particle quantum mechanics with $U''(\phi_\mathrm{B}(\mathbf{x}))$ as the potential. However, this does not affect our discussion in any significant way, so we will keep using simplified notation with sums and Kronecker deltas.

The physical meaning of the eigenfunctions can be seen through the Taylor expansion of the Hamiltonian around the critical bubble.

$$\begin{aligned}
H[\phi_\mathrm{B}+\Delta\phi] &\approx H[\phi_\mathrm{B}] + \frac{1}{2}\int \mathrm{d}^3x\mathrm{d}^3y\, \Delta\phi(\mathbf{y})\frac{\delta^2 H}{\delta\phi^2}\Delta\phi(\mathbf{x}) \\
&= H[\phi_\mathrm{B}] + \frac{1}{2}\int \mathrm{d}^3x\mathrm{d}^3y \sum_m c_m f_m(\mathbf{y})\frac{\delta^2 H}{\delta\phi^2}\sum_n c_n f_n(\mathbf{x}) \\
&= H[\phi_\mathrm{B}] + \frac{1}{2}\int \mathrm{d}^3y \sum_{m,n} c_m f_m(\mathbf{y})\xi_n c_n f_n(\mathbf{y}) \\
&= H[\phi_\mathrm{B}] + \frac{1}{2}\sum_n \xi_n c_n^2.
\end{aligned} \tag{2.26}$$

On the first line we expanded the functional to second order around the critical bubble solution. The linear term vanishes since the critical bubble is a stationary point of the Hamiltonian. On the second line we decomposed the fluctuation into the eigenfunctions of the operator which we then used on the third line. Finally on the last line, we used the orthonormality of the eigenfunctions.

The decomposition into the eigenfunctions and their eigenvalues tells how a fluctuation changes the energy of the bubble to the quadratic order. This gives us a natural way of classifying the eigenfunctions: If the eigenvalue is negative, a fluctuation of the form of the corresponding eigenfunction lowers the energy. If the eigenvalue is zero, the

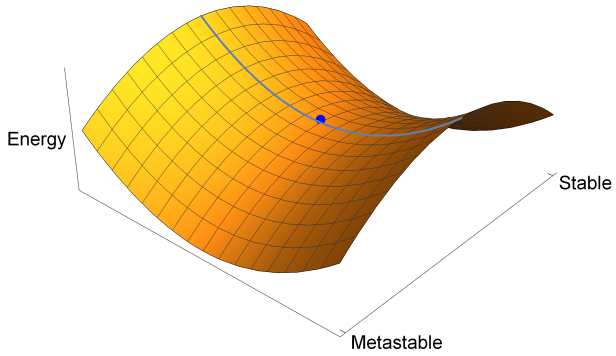

Figure 2.6: A two dimensional slice of a field configuration space around a critical bubble (blue dot). The direction from metastable to stable corresponds to the negative eigenmode. The other direction is a positive eigenmode. The blue line marks the top of the potential barrier in the configuration space.

eigenfunction does not change the energy. The rest of the eigenfunctions increase the energy and are not that important.

An important characteristic of the critical bubble is that it has only one negative eigenfunction [23]. The negative eigenmode is the unstable direction of the critical bubble and therefore the direction over the potential barrier. What we meant by saying that the bubble grows or shrinks is that it changes shape according to this negative eigenmode. Growing means obviously that the bubble goes closer to the stable state. (Fig. 2.6)

Besides the negative eigenmode, there are zero modes – one for each symmetry broken by the critical bubble. In this case, there are three zero modes due to translational symmetry being broken by the critical bubble. Therefore the critical bubble is not completely unique as can be seen from Fig. 2.7. There are no rotational zero modes because the rotational symmetry is not broken by the critical bubble. Since these zero modes are related to the translation of the critical bubble, all three are just derivatives of the bubble:

$$f_{0,\,i} = \frac{1}{N}\frac{\partial}{\partial x_i}\phi_{\mathrm{B}}, \tag{2.27}$$

which can be shown straightforwardly by using the EoM (2.15):

$$\left(-\boldsymbol{\nabla}^2 + U''(\phi_{\mathrm{B}}(\boldsymbol{x}))\right)\frac{\partial}{\partial x_i}\phi_{\mathrm{B}}(\boldsymbol{x}) = \frac{\partial}{\partial x_i}\underbrace{\left(-\boldsymbol{\nabla}^2\phi^B(\boldsymbol{x}) + U'(\phi_{\mathrm{B}}(\boldsymbol{x}))\right)}_{=0}. \tag{2.28}$$

The normalization factor N will be important for the nucleation rate because it basically is the conversion factor between the physical volume of the system and the configuration space area on the flat part of the potential barrier shown in Fig. 2.7.

The factor N can be found by using a scaling argument. It will be covered in a bit more general situation in Sec. 4.1, because it plays a crucial role there, but I explain

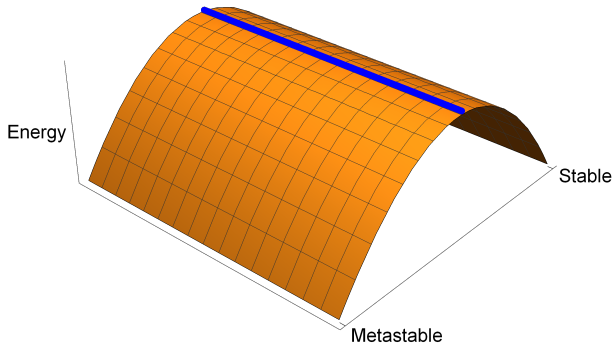

Figure 2.7: A two dimensional slice of a field configuration space. Due to the translational invariance, a critical bubble configuration is not unique. All the configurations along the blue line are critical bubbles and the direction of the line corresponds to a zero mode. There is one zero mode for each symmetry broken by the critical bubble. The direction from metastable to stable corresponds to the negative eigenmode.

the argument also here. The critical bubble configuration is a stationary point of the Hamiltonian. We can create a new configuration which is the critical bubble only when a parameter Λ is equal to one: $\tilde{\phi}_{\mathrm{B},\Lambda}(r) \equiv \phi_{\mathrm{B}}(\Lambda r)$. Due to the extremality of the critical bubble

$$\left(\frac{\mathrm{d}}{\mathrm{d}\Lambda} H\left[\tilde{\phi}_{\mathrm{B},\Lambda}, \pi = 0\right]\right)\Big|_{\Lambda=1} = 0. \tag{2.29}$$

This gives a condition between the gradient term and the potential with which one can solve that

$$\int \mathrm{d}^3x \, (\boldsymbol{\nabla}\phi_{\mathrm{B}})^2 = 3H[\phi_{\mathrm{B}}, \pi = 0]. \tag{2.30}$$

From the spherical invariance and the normalization condition, we get that $N = H[\phi_{\mathrm{B}}, 0]^{1/2}$:

$$f_{0,\,i} = H[\phi_{\mathrm{B}}, 0]^{-1/2} \frac{\partial}{\partial x_i}\phi_{\mathrm{B}}. \tag{2.31}$$

The rest of the eigenfunctions are rather ordinary. In these directions of the field configuration space, the energy of the bubble rises. It creates a valley on top of the potential barrier. The field must go through the valley to get to the stable state as shown in Fig. 2.6. The rising energy cost forces the nucleating fields to be rather similar to the critical bubble.

The exception to all bubbles being similar to the critical bubble is a weak first-order phase transition in which thermal fluctuations are already close to the size of the critical bubble. There are two possibilities: a transition that is near a second order phase transition or near a spinodal decomposition mentioned in the footnote in the beginning of this chapter. In the former, the potential barrier separating the two different phases is

already low near the critical temperature and in the latter, the barrier is lowered due to extreme supercooling.

It is important to stress that in these kinds of transitions, the exponential suppression from the critical bubble is not the only significant part of the nucleation rate. If the transition is not very weak, the nucleation rate also receives an exponential contribution from the fluctuations around the critical bubble. In a very weak transition, the saddle-point approximation around the critical bubble breaks, and it cannot be studied via its critical bubble configuration.

In the previous section, we computed the escape rate of a classical particle in one dimension. There, we found that there is an exponential suppression to the rate which comes from the height of the potential barrier (Fig. 2.1). In the field case, the barrier exists in the configuration space of the field and the lowest point on the barrier is the critical bubble as shown in Figs. 2.6 and 2.7. The critical bubble is the gatekeeper of the new phase which the field has to pass and therefore one could guess that the critical bubble gives an exponential suppression of the nucleation rate. This is exactly what we will see in the next section.

2.3 Nucleation Rate of a Classical Field

Now, we are ready to set up a calculation for the nucleation rate. We have actually done most of the work in the previous two sections. In Sec. 2.1, we studied two calculations for the escape rate of a classical particle. The calculations were heavily circulating around the top of the potential barrier which had trapped the particle to a potential well (Fig. 2.1). In Sec. 2.2, we found the potential barrier for a field from the configuration space of the field and studied its properties around the lowest point, the critical bubble configuration.

The bubble nucleation is a messy event for the system. Let us assume that an infinite field is in a metastable field value at some time. Afterwards, there will be infinitely many bubbles nucleating. To make sense out of the whole complexity, one could just calculate how quickly a single bubble nucleate in a system with volume V which is much larger than the volume of the critical bubble. Due to the translational invariance the rate at which one bubble nucleates in the volume is proportional to V. If the nucleation rate is small enough, the nucleating bubbles are independent of each other. Then, the answer for the rate of a single bubble nucleating per volume is the nucleation rate per volume for the entire field.

The independence of bubbles needs two things: the bubbles are quite sparse and the bubble configuration dies off exponentially to the metastable field value outside the bubble. If the bubbles nucleated on top of each other regularly, this would mean that the bubble formation is very rapid. That is the case where the thermal fluctuations are of the

same order as the critical bubble and, as we discussed at the end of the previous section, these transitions cannot be studied through the critical bubble. The exponential tail of the bubble can be found with the EoM of the critical bubble (2.15). Far enough from the centre, the friction term can be neglected and, due to the first boundary condition (2.16), the gradient of the potential can also be approximated with a linear term in the field value:

$$\ddot{\phi} = U''(\phi_+)\phi. \tag{2.32}$$

The solution that satisfies the boundary condition at infinity is the exponential function:

$$\phi \propto e^{-\sqrt{U''(\phi_+)}\, r}. \tag{2.33}$$

Therefore, the bubble configuration dies off exponentially at some large distance away from its centre. This does not, however, mean that the critical bubble could not be arbitrarily large in the thin-wall limit (discussed in the previous section). For thin-wall bubbles, it means that the wall dies off exponentially on the outside.

We can now generalize the escape rate from Sec. 2.1 to the nucleation rate of a single bubble. Eq. (2.4) in this case is

$$\Gamma = \frac{\int \mathcal{D}\phi\mathcal{D}\pi\ \pi_-^{\mathrm{B}}\theta(\pi_-^{\mathrm{B}})\delta(\phi_-^{\mathrm{B}})\ e^{-\beta H}}{\int \mathcal{D}\phi\mathcal{D}\pi\ e^{-\beta H}}, \tag{2.34}$$

where H is the Hamiltonian function from Eq. (2.12) and β is the inverse of temperature. The delta function restricts the integrals to be on top of the potential barrier in the field configuration space shown in Fig. 2.8. ϕ_-^{B} is the negative eigenmode of the critical bubble, which is the direction over the potential barrier along the arrows in the figure, and π_-^{B} is the conjugate momentum to the direction of the negative eigenmode. The step function takes only the flux going away from the metastable state into account i.e. only growing bubbles.

In the previous section, we found an orthonormal set of basis functions f_n with the Hermitian operator in Eq. (2.23). We can make a change of basis in the integral in the numerator according to this basis and then integrate over the conjugate momentum. For the denominator, we can do the same trick but with the second variation of the Hamiltonian function evaluated on the trivial solution to the EoM, $\phi = \phi_+$. All the momentum conjugate integrals are pure Gaussian integrals, except for the momentum conjugate relating to the negative eigenmode in the numerator. Hence, they can be carried out straightforwardly:

$$\Gamma = \frac{1}{\sqrt{2\pi\beta}} \frac{\int[\mathrm{d}\phi^B] e^{-\beta\tilde{H}}\delta(\phi_-^{\mathrm{B}})}{\int[\mathrm{d}\phi^0] e^{-\beta\tilde{H}}}, \tag{2.35}$$

$$\tilde{H} = \int \mathrm{d}^3x \Big(\frac{1}{2}(\boldsymbol{\nabla}\phi)^2 + U(\phi)\Big). \tag{2.36}$$

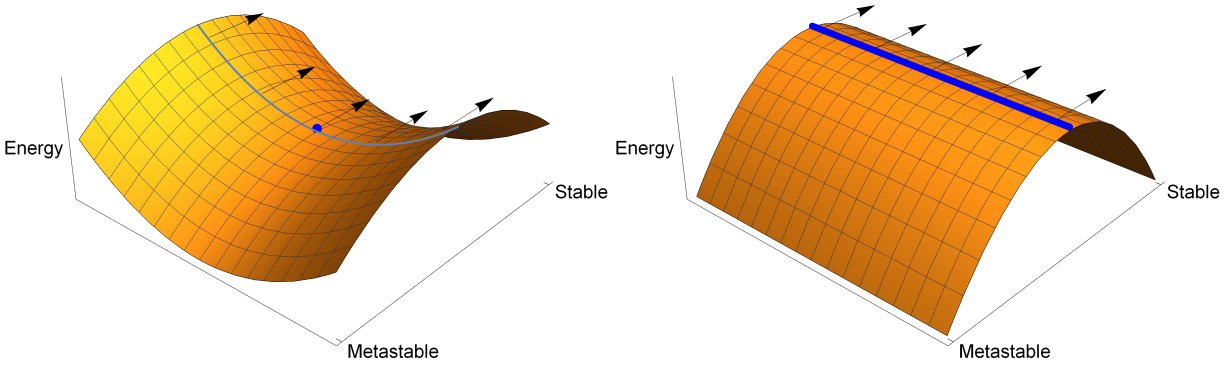

Figure 2.8: Both of the figures are two dimensional slices of a field configuration space showing the potential barrier for nucleating a bubble. The nucleation rate is the flux over the potential barrier to the direction of the negative eigenmode marked with arrows.

In the nucleation rate, the integral that is left in the numerator gives us the Boltzmann weighted hypersurface area, through which the nucleation can happen.

Here, we will make the saddle-point approximation in the integral in the numerator by expanding the Hamiltonian to the second order around the critical bubble configuration, ϕ_{B}. We use a little bit of renaming compared to Eq. (2.26):

$$\tilde{H} \approx \tilde{H}[\phi_{\mathrm{B}}] - \frac{1}{2}(\lambda_{-}^{\mathrm{B}}\phi_{-}^{\mathrm{B}})^2 + \frac{1}{2}\sum_{n>0}(\lambda_{n}^{\mathrm{B}}\phi_{n}^{\mathrm{B}})^2, \tag{2.37}$$

where λ^{B}s relate to eigenvalues and ϕ^{B}s are the coefficients of the eigenmode expansion of a fluctuation. Note, that there is only one negative eigenvalue and the zero modes do not contribute to the energy of the bubble.

The integral over the negative eigenmode is trivial due to the delta function and the integrals over the positive eigenfunctions are just Gaussian integrals. The three zero modes cannot be done that straightforwardly. Doing the "Gaussian" integrals blindly to the constant directions results in an infinity. There actually is an infinity due to the zero modes but it is linked to the infinite volume of the system. The three zero modes are related to the translational invariance and we can perform the integrals explicitly by switching the integral from integrating over the zero modes in the configuration space to integrating over the location of the centre of the bubble:

$$\int \prod_{i=1}^{3} \mathrm{d}\phi_{0,i}^{B} = \left(\tilde{H}[\phi_{\mathrm{B}}]\right)^{3/2} \int \mathrm{d}^3x = \left(\tilde{H}[\phi_{\mathrm{B}}]\right)^{3/2} V, \tag{2.38}$$

where the Jacobian comes from the normalization of the zero modes (2.31). The emergence of the energy of the critical bubble here might seem like a surprise. The square root of the energy of the critical bubble tells how far has the critical bubble configuration moved

in the configuration space when it is been displaced in ordinary space. Therefore the cube of the square root tells how much more hypersurface area is formed for the zero modes (Fig. 2.7). So, it appears in the conversion factor between the volume of the system and the hypersurface area, through which the bubble can nucleate.

The integral of the numerator in Eq. (2.35) is now completed:

$$\int [\mathrm{d}\phi^B] e^{-\beta\tilde{H}} \delta(\phi_-) = V\tilde{H}[\phi_\mathrm{B}]^{3/2} \left[\prod_{n>0} \left(\sqrt{\beta}\lambda_n^\mathrm{B} \right)^{-1} \right] e^{-\beta\tilde{H}[\phi_\mathrm{B}]}. \tag{2.39}$$

The integral in the denominator of Eq. (2.35) can be approximated similarly with a saddle-point approximation around the metastable phase, which is equivalent to one-loop order. The resulting eigenvalue products can be expressed with determinants of the second variations of the Hamiltonians around the critical bubble and the metastable configuration respectively. The determinants are called fluctuation determinants.

This gives us an expression for the nucleation rate:

$$\frac{\Gamma}{V} = \frac{1}{2\pi} \left(\frac{\tilde{H}[\phi_\mathrm{B}]}{2\pi T} \right)^{3/2} \sqrt{\frac{\det\left[-\boldsymbol{\nabla}^2 + U''(\phi_+) \right]}{\det^+\left[-\boldsymbol{\nabla}^2 + U''(\phi_\mathrm{B}) \right]}} e^{-\beta(\tilde{H}[\phi_\mathrm{B}] - \tilde{H}[\phi_+])}, \tag{2.40}$$

where the plus symbol as a subscript on the determinant means omission of the negative and zero eigenvalues. The determinants are UV-divergent and would need regularization and counterterms to be handled properly. In a transition that is suppressed strongly by the critical bubble, they contribute to the nucleation rate compared to the exponential suppression from the critical bubble. However, in a weak first-order transition they can give a contribution that is the same order as the exponent. If the transition is too weakly first order, the whole saddle-point approximation fails, and the equation above does not give a good approximation for the rate.

A more careful analysis was done in Ref. [21]. Similarly to the escape rate of a particle in Sec. 2.1, it was assumed that the field obeys the Langevin equation:

$$\left(\frac{\partial^2}{\partial t^2} - \boldsymbol{\nabla}^2 + \gamma \frac{\partial}{\partial t} \right) \phi + U'(\phi) = \xi, \tag{2.41}$$

where γ is the damping coefficient and ξ is the noise term which is Gaussian and satisfies:

$$\langle \xi(\mathbf{x}, t) \rangle = 0, \qquad \langle \xi(\mathbf{x}, t) \xi(\mathbf{x}', t') \rangle = 2\gamma T \delta(\mathbf{x}' - \mathbf{x}) \delta(t' - t). \tag{2.42}$$

Therefore, the probability distribution obeys a Fokker-Planck equation. Once again, a static solution to the Fokker-Planck equation was obtained for the part of the field configuration space in which the energy of the configuration can be approximated through quadratic function as in Eq. (2.37). This region is depicted in Fig. 2.8. From the solution to the Fokker-Planck equation, the flux over the potential barrier can be solved. This

gives us the nucleation rate. Similarly to the escape rate, there is a change only in the prefactor and not in the exponential suppression:

$$\frac{\Gamma}{V} = \frac{1}{2\pi}\left(\frac{\tilde{H}[\phi_{\rm B}]}{2\pi T}\right)^{3/2} \frac{\sqrt{\lambda_-^2 + \frac{\gamma^2}{4}} - \frac{\gamma}{2}}{\lambda_-} \sqrt{\frac{\det\left[-\boldsymbol{\nabla}^2 + U''(\phi_+)\right]}{\det^+\left[-\boldsymbol{\nabla}^2 + U''(\phi_{\rm B})\right]}} e^{-\beta(\tilde{H}[\phi_{\rm B}] - \tilde{H}[\phi_+])}. \tag{2.43}$$

These results cannot (probably) be applied straightforwardly to the models we are going to go through in Sec. 3.3. A problem is that the minimum of the potential for the new phase is induced by another field by its fluctuations. As a consequence, the inducing field has to be able to relax on top of a bubble so that the bubble can grow. This complicates the time-evolution and might make the prefactor of the nucleation rate much smaller. The exponential contributions to the nucleation rate should still come from the statistical part, which is the Boltzmann weighted hypersurface area over the barrier in the configuration space. The next chapter is devoted to finding this part of the rate.

At the end of this section, I would like to discuss why the thermal nucleation rate is enough and the quantum tunnelling is not needed. However, this is not a strict proof. In Ref. [20], Affleck found that the thermal escape rate was dominant if $T > \frac{\omega_b}{2\pi}$ in the escape rate of a particle. Due to the similarities between the cases of particles and fields, one could expect that the thermal rate is enough for $T > \frac{\lambda_-}{2\pi}$. Solving the negative eigenvalue is beyond the scope of this thesis, but we can give a lower bound for the eigenvalue. It can be found by noting again that the operator in Eq. (2.23) is identical to the Hamiltonian operator of the single-particle quantum mechanics with the potential being $U''(\phi_{\rm B}(\mathbf{x}))$. With this view, the eigenfunctions are eigenstates of the Hamiltonian operator and the eigenvalues correspond to the energies of the states. All the states must have energy that is larger than the minimum of the potential. For the negative eigenvalue, this means that $\lambda_- > \sqrt{|\min\{U''(\phi_{\rm B}(\mathbf{x}))\}|}$. The lower bound is usually the same order as the mass of the nucleating degree of freedom. Thus, it is enough that the DoF is light compared to the temperature.

The question of sufficiency of the thermal nucleation rate can also be tackled from another perspective. The type of a phase transition we are studying happens for low momentum modes of the nucleating field. Due to large occupation numbers at high temperatures, they can be treated classically [24]. This type of treatment is possible only if the effective masses of the low energy modes are much lower than the temperature. Therefore, the region of validity discussed here is the same as in the paragraph above.

3. Effective Description for the Critical Bubble

The ultimate goal of a nucleation rate calculation is to obtain observable quantities, for example relating to the gravitational wave spectrum from a transition. For predicting these quantities, a nucleation rate can tell us the temperature and duration of a transition (in Eqs. (4.81) and (4.85) respectively). To this end, it is quite enough to have the exponential contributions to the rate and only a rough order of magnitude estimate of the prefactor in front of the exponential. As discussed in the previous chapter, the contributions that are exponentially large, come from the statistical part of the nucleation rate, shown as the ratio of the integrals in Eq. (2.35). It is the Boltzmann weighted hypersurface area in the configuration space of the nucleating field, through which the nucleation can happen. If a transition is strong enough, the only exponential contribution comes from the critical bubble, as the fluctuations around it do not contribute much. The objective of this chapter is to find $\tilde{H}$ in Eq. (2.35) for a cosmological phase transition, which gives us control over the critical bubble and the statistical part of the nucleation rate.

In the transition of the previous chapter, the only role of thermal fluctuations was to produce bubbles that would nucleate into the new phase. Here, it is important to understand that the fluctuations have another important role. The state of a system is dictated by the minimum of its free energy which incorporates the effects of the thermal fluctuations of the system. Phase transitions happen because changes in thermodynamical variables change the thermal fluctuations and consequently the free energy. Hence, the thermal fluctuations dictate whether there is a transition in the first place, in addition to being responsible for the nucleation if there is one. Due to these two jobs for fluctuations, there is a danger of double counting their effects in the critical bubble. On the one hand, the fluctuations are responsible for the stability of the new phase and the metastability of the old phase. Therefore, the stability of the critical bubble, that is between the two phases, depends on the fluctuations that make the new phase stable. On the other hand, the critical bubble itself consists of thermal fluctuations. Therefore, we need an effective description for the critical bubble, that can describe the fluctuations building up the

bubble on top of the background from the fluctuations responsible for the stability of the bubble.

The physics of the early Universe is described through thermal field theory. Its imaginary time formulation, which is enough for finding the statistical part of the nucleation rate, is reviewed briefly in Sec. 3.1. In Sec. 3.2, we will employ the modern effective field theory framework for taking correctly into account the effects of different fluctuations, i.e. for solving the problem of double counting. This is a framework that is suitable, when there exists a hierarchy of scales. In transitions that happen at high temperatures, there is usually a hierarchy between the temperature and the mass of the nucleating degree of freedom. The useful EFT for these situations was originally developed in Refs. [11, 12], and it is reviewed in Subsec. 3.2.1. Near a symmetry breaking phase transition, the mass of the nucleating field can become very small. As a consequence, it is quite natural that there is a mass scale between the nucleating field and the temperature. We will focus on this scale in Subsec. 3.2.2. An example calculation of finding an effective description for critical bubble is given in Sec. 3.3. The model of the example was studied in the case of vacuum decay in Ref. [25], where a heavy field is integrated out for finding the critical bubble for a lighter field. We will also discuss the thin-wall limit, whose treatment differs from the thick wall case, in Subsec. 3.2.3.

3.1 Thermal Field Theory

In the phase transitions of the early Universe, the nucleating degrees of freedom were quantum fields at very high temperatures. Therefore, to describe those phase transitions, we need thermal field theory (TFT) which is quantum statistics with fields as quantum objects i.e. quantum fields at finite temperature. In this section, we will review all the tools needed in TFT for the last sections of this chapter. A more in-depth text, such as Ref. [26], might be needed if you are not already familiar with TFT. We start this section by going through the very basics of TFT relating to the density operator. We then proceed to introduce a formalism of TFT for static quantities called the imaginary time formalism and explain why it is enough for our purposes even though bubble nucleation is inherently a real-time phenomenon. The rest of this section is for the proper handling of the perturbative expansion in the coupling constant.

In quantum mechanics, the state of a system is represented with an element $|\Psi\rangle$ of a Hilbert space $\mathcal{H}$. The observables are Hermitian operators $\hat{A} : \mathcal{H} \to \mathcal{H}$ and their expectation value in a certain quantum state is given by the inner product of the Hilbert space:

$$\langle \hat{A} \rangle_\Psi = \langle \Psi | \, \hat{A} \, | \Psi \rangle \, . \tag{3.1}$$

In thermal field theory, we have statistical uncertainty of the quantum state of the system. This is encoded into an operator called the density operator or density matrix $\hat{\rho}$. Expectation values of observables on a system described by a density operator $\hat{\rho}$ take the form

$$\langle \hat{A} \rangle_{\hat{\rho}} = \text{Tr } \hat{\rho}\hat{A}. \tag{3.2}$$

The density matrix must satisfy three conditions:

- $\text{Tr } \hat{\rho} = 1$
- $\hat{\rho}^\dagger = \hat{\rho}$
- $\langle \Psi | \hat{\rho} | \Psi \rangle \geq 0, \quad \forall \, |\Psi\rangle \in \mathcal{H}$

The first one states that the expectation value of the unit operator is one, the second tells that there is an orthogonal eigenbasis with real eigenvalues and the last one says that none of the eigenvalues are negative.

One special case for the density operator is the one with no statistical uncertainty. The density matrix is then given by the quantum state of the system:

$$\hat{\rho} = |\Psi\rangle \langle \Psi| . \tag{3.3}$$

We can see that the definitions of the expectation values do match in this case.

3.1.1 Imaginary Time Formalism

We are going to review a formulation of thermal field theory which is suitable for obtaining equal-time correlation functions and thermodynamical quantities. The nucleation is inherently a real-time phenomenon and cannot be studied in full detail using the imaginary time formulation. However, we argue that the statistical part of the nucleation rate can be obtained from the formalism. Thus, we have access to the exponential suppression of the rate.

The phase transitions under study occur when the location of the global minimum of the free energy shifts and the transitions can be first order if the shift is discontinuous. The phase transitions happen because thermal fluctuations change when the temperature changes. The thermal fluctuations, that are responsible for the new phase becoming the stable phase, must also be in equilibrium on top of the critical bubble. This is due to the fact that the critical bubble is a configuration that interpolates between the two phases. Therefore, the imaginary time formalism is suited for handling the important fluctuations on top of a nucleating bubble.

Another crucial point is that the Boltzmann weight is embedded into the thermal distribution. The statistical part is just the Boltzmann weighted hypersurface area in

the configuration space of the nucleating field, through which the nucleation can happen. (This is discussed more in-detail in the previous chapter and it is illustrated in Fig. 2.8.) Therefore we can find the statistical part of the nucleation rate with the imaginary time formalism presented below.

We can now begin the review of the imaginary time formulation of thermal field theory. First, we will find the density operator in thermal equilibrium. Due to the form of the density operator, we can express n-point functions as path integrals which are then ripe for perturbative calculations. The perturbation series of the n-point functions in weak coupling are discussed but the exact computational tools are postponed to the next subsection where regularization and renormalization methods are discussed. Lastly, we will look at the propagator which has a peculiar form and get a glimpse of the degree of freedom undergoing a phase transition.

In thermal equilibrium the entropy of the system is maximized. Therefore, the density operator of a system in equilibrium is obtained by maximizing the von Neumann entropy

$$S = -\operatorname{Tr}\, \hat{\rho} \ln \hat{\rho}. \tag{3.4}$$

There are physical conditions for the maximization that must hold. For us, the only one is that the expectation value of the Hamiltonian is fixed:

$$\langle \hat{H} \rangle_{\hat{\rho}} = E. \tag{3.5}$$

We assume that any possible chemical potentials are irrelevant. It could be that there would be an asymmetry in a current which is effectively conserved at the scale of the phase transition. However, this can be neglected at least at the electroweak phase transition because the temperature is much larger than any possible chemical potentials. Also, there are no conserved currents in the example model of Sec. 3.3.

The result for the equilibrium density operator is

$$\hat{\rho} = \frac{1}{Z} e^{-\beta \hat{H}}, \quad Z = \operatorname{Tr}\, e^{-\beta \hat{H}} \text{ and } \beta = \frac{1}{T}, \tag{3.6}$$

where T is the temperature of the system and Z is called the partition function.

The partition function Z contains all the thermodynamical information of the system. For example, the free energy and the energy are

$$F = -T \ln Z, \tag{3.7}$$

$$E = -\frac{\partial}{\partial \beta} \ln Z. \tag{3.8}$$

We will now focus only on one real scalar field. Other types of fields are not necessary for understanding the thesis and the reader may consult e.g. Ref. [26] for details of other types of fields.

The partition function can be expressed as a Euclidean path integral:

$$Z = \mathrm{Tr}\ e^{-\beta\hat{H}} = \int_{\mathrm{per.}} \mathcal{D}\phi\, e^{-S_{\mathrm{E}}}, \tag{3.9}$$

where per. means periodicity: $\phi(\tau = 0) = \phi(\tau = \beta)$, and the Euclidean action for a single real scalar is

$$S_{\mathrm{E}} = \int_0^\beta \mathrm{d}\tau \int_{\mathbf{x}} \left(\frac{1}{2}\partial_\mu\phi\partial_\mu\phi + U(\phi)\right). \tag{3.10}$$

The Euclidean nature of the path integral comes from the operator $e^{-\beta\hat{H}}$ having the form of an imaginary time evolution operator. Hence, the extent of this Euclidean time dimension is β. The periodicity comes from the trace.

There is actually a piece of information regarding fermions which will be important in Subsec. 3.2.1. It is that the fermionic path integral is actually anti-periodic.

Similarly to the partition function, the equal-time correlation functions can be expressed as a path integral:

$$\begin{aligned}\langle\hat{\phi}(\mathbf{x})\hat{\phi}(\mathbf{y})...\rangle &= \frac{1}{Z}\,\mathrm{Tr}\left[e^{-\beta\hat{H}}\hat{\phi}(\mathbf{x})\hat{\phi}(\mathbf{y})...\right] \\ &= \frac{1}{Z}\int_{\mathrm{per.}} \mathcal{D}\phi\ \phi(\tau=0,\mathbf{x})\phi(\tau=0,\mathbf{y})...\, e^{-S_{\mathrm{E}}}.\end{aligned} \tag{3.11}$$

This is just classical statistical field theory in $\mathbb{R}^3 \times S^1$ whose compact dimension has the extent of $1/T$ and whose correlation functions for fields at $\tau = 0$ correspond to the physical equal-time correlation functions (cf. Fig. 3.1).

The correlation functions play a very important role in the next section. The perturbative approximation of the correlation functions in small coupling constants is explained

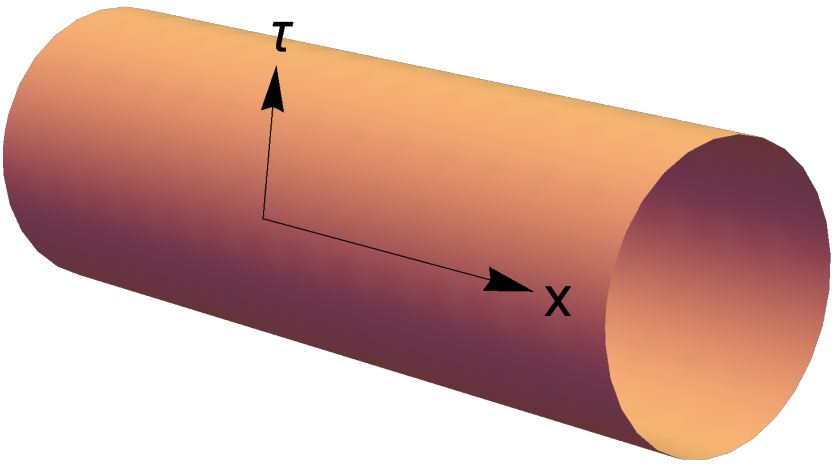

Figure 3.1: Structure of the space in the imaginary time formalism: τ represents the Euclidean time direction with periodicity of the inverse temperature and x represents the three spatial dimensions.

below. It will be the tool to create the effective field theory we need to describe the critical bubble. We split the action into the free part and the interaction part,

$$S_{\mathrm{E}} = S_0 + S_{\mathrm{I}}, \quad S_0 = \int_0^\beta \mathrm{d}\tau \int_{\mathbf{x}} \Big(\frac{1}{2}\partial_\mu\phi\partial_\mu\phi + \frac{1}{2}m^2\phi^2\Big), \tag{3.12}$$

and then expand the exponential inside the path integral into its Taylor series in the interaction action:

$$\begin{aligned}\langle\hat{\phi}(\mathbf{x})\hat{\phi}(\mathbf{y})...\rangle &= \frac{1}{Z}\int_{\text{per.}} \mathcal{D}\phi\ \phi(0,\mathbf{x})\phi(0,\mathbf{y})... \sum_{n=0}^{\infty}\frac{(-S_{\mathrm{I}})^n}{n!}\,e^{-S_0} \\ &= \sum_{n=0}^{\infty}\frac{(-1)^n}{n!}\langle\phi(0,\mathbf{x})\phi(0,\mathbf{y})...S_{\mathrm{I}}^n\rangle_{0,\mathrm{c}},\end{aligned} \tag{3.13}$$

where subscript 0 stands for the free theory (action is just S_0 and the denominator is the free partition function Z_0 instead of Z). The subscript c states that there are no disconnected parts called vacuum bubble diagrams. The disconnected parts were cancelled by the full partition function from the first line. In a real computation, one has to find a precision, which is enough, and truncate the series to the precision.

These correlation functions in the free theory can be decomposed into propagators using Wick's theorem:

$$\langle\phi(X_1)...\phi(X_k)\rangle_0 = \sum_\sigma \langle\phi(X_{\sigma(1)})...\phi(X_{\sigma(2)})\rangle_0...\langle\phi(X_{\sigma(k-1)})...\phi(X_{\sigma(k)})\rangle_0, \tag{3.14}$$

where σ does not stand for all permutations but for all different possibilities of pairing. As an example, the $n = 1$ term from (3.13) in ϕ^4-theory ($S_{\mathrm{I}} = \int_{\mathbf{x}} \frac{\lambda}{4!}\phi^4$) with two field operators in the correlation function:

$$\begin{aligned}\langle\phi(0,\mathbf{x})\phi(0,\mathbf{y})S_{\mathrm{I}}\rangle_{0,\mathrm{c}} &= \Big\langle\phi(0,\mathbf{x})\phi(0,\mathbf{y})\int_W \frac{\lambda}{4!}\phi(W)^4\Big\rangle_{0,\mathrm{c}}, \qquad W=(\tau_w,\mathbf{w}) \\ &= \int_W \frac{\lambda}{4!}4\langle\phi(0,\mathbf{x})\phi(W)\rangle_0\langle\phi(0,\mathbf{y})\phi(W)^3\rangle_{0,\mathrm{c}} \\ &= \int_W \frac{\lambda}{4!}4\cdot 3\langle\phi(0,\mathbf{x})\phi(W)\rangle_0\langle\phi(0,\mathbf{y})\phi(W)\rangle_0\langle\phi(W)^2\rangle_0.\end{aligned}$$

There are four ways to connect $\phi(0,\mathbf{x})$ to a $\phi(W)$ and then three ways to connect $\phi(0,\mathbf{y})$ to a $\phi(W)$. The contraction $\langle\phi(0,\mathbf{x})\phi(0,\mathbf{y})\rangle_0$ is dropped because it would leave a disconnected peace behind. ($\langle\phi(W)^4\rangle_0$-piece would be left disconnected.) In a diagrammatic representation, this would be

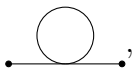 , (3.15)

in which the centre point represents the point W and the endpoints are $(0,\mathbf{x})$ and $(0,\mathbf{y})$.

The only missing piece is now the propagator, which is given by

$$\begin{aligned}\langle\phi(X)\phi(Y)\rangle_0 &= \sum\!\!\!\!\!\!\int_P \frac{e^{-iP(X-Y)}}{P^2+m^2}, \qquad P=(2\pi nT,\,\mathbf{p}),\ n\in\mathbb{Z} \\ &\equiv T\sum_{n=-\infty}^{\infty}\int_{\mathbf{p}}\frac{e^{-iP(X-Y)}}{\mathbf{p}^2+(2\pi nT)^2+m^2}.\end{aligned} \tag{3.16}$$

The integral over $\mathbf{p}$ is the normal integral over the three-momentum. However, the zeroth component is a bit peculiar. There are only discrete Fourier modes due to the periodicity of the imaginary time dimension. Possible values are the integer multiples of $2\pi T$ because the length of the dimension is T^{-1}. These modes are called the Matsubara modes,

$$\Phi = \sum_{n=-\infty}^{\infty} \Phi_n e^{i\omega_n \tau}, \quad \omega_n = 2\pi n T. \tag{3.17}$$

Note also the signs in the propagator are not the same as in regular zero-temperature QFT due to the Euclidean signature.

If $\tau_X = \tau_Y$, the bare propagator in Eq. (3.16) can be viewed as an infinite sum of three-dimensional propagators. The mass of non-zero Matsubara modes in the propagator is much larger than the mass of a Matsubara zero mode, when the temperature is high, $T \gg m$. In the following section, we will find that, at high temperatures, it is possible to construct an effective field theory for Matsubara zero modes and that a nucleating degree of freedom is a Matsubara zero mode.

3.1.2 Renormalization and Dimensional Regularization

In this subsection, we will see how to regulate the UV-divergences present in thermal field theory. First, I show that the first order in the weak-coupling expansion of the free energy in Eq. (3.7) would be UV-divergent if the parameters of the Euclidean action were not divergent. I introduce a regularization scheme called dimensional regularization to compute the first order in the expansion of the free energy. At the end of this section, I show how to do the renormalization using correlation functions.

In perturbation theory, the free energy (3.7) contains all the connected diagrams with no external legs. For the ϕ^4-theory, the first order in this expansion is the following diagram:

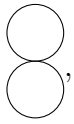 , (3.18)

which consists of two propagators and one interaction vertex. We are not interested in the number of possible Wick contractions now. Without the symmetry factor, the diagram is:

$$T \int_X \lambda \left(\not{\sum\!\!\!\!\!\!\int}_P \frac{1}{P^2 + m^2} \right)^2, \tag{3.19}$$

where the integral over X gives just a factor of V/T.

We would like to be able to compute the sum-integral that appears in the diagram (3.19) but we need to regulate the integral. The regularization scheme we will use is dimensional regularization. Due to the regularization scheme, the number of spatial

dimensions is

$$d = 3 - 2\epsilon, \tag{3.20}$$

where ϵ is taken to zero from above at the end of the computation. Because the dimensionality of space is not actually three, we need to make some changes. The quantity in (3.19) should have the same mass dimension as the free energy. At the same time, the temperature, the mass parameter and the coupling constants should retain their dimensionality. To achieve this, we must introduce a dimensionful parameter, the renormalization scale μ, which has the dimensions of mass, and replace the coupling in the Lagrangian according to:

$$\lambda \to \mu^{2\epsilon}\lambda. \tag{3.21}$$

This is enough to keep the action dimensionless. One more thing to note is the dimensions of the field are now

$$[\phi] = 1 - \epsilon \tag{3.22}$$

but this does not play a big role for us.

Dimensional regularization is nice in the sense that it hides divergences that are present in other regularization schemes. Only the physically relevant logarithmic divergences are present which eases the renormalization procedure. This happens via redefinitions through analytic continuation:

$$\int_{\mathbf{p}} \frac{1}{(\mathbf{p}^2 + \Delta^2)^l} = \frac{\Gamma(l - d/2)}{(4\pi)^{d/2}\Gamma(l)} \frac{1}{(\Delta^2)^{l-d/2}}, \tag{3.23}$$

$$\sum_{n=1}^{\infty} n^{-z} = \zeta(z). \tag{3.24}$$

In the first equation, the beta function is used to analytically continue the solution of the integral to be in the form of gamma functions and, in the second one, the analytical continuation happens via the zeta function. Also, so called scale-free integrals vanish in dimensional regularization which will streamline the matching process in the section.

In thermal nucleation, we are interested in the high temperature limit $T^2 \gg m^2$. In this limit, it is convenient to split the calculation into two pieces: the zero Matsubara mode and the non-zero Matsubara modes. The zero mode does not have the temperature to regulate its IR-behaviour and therefore acts differently from other Matsubara modes at high temperatures. This is an important feature in dimensional reduction discussed in the next section. The zero mode is exactly the form of the integral in Eq. (3.23) and it is not divergent:

$$\mu^{2\epsilon} T \int_{\mathbf{p}} \frac{1}{\mathbf{p}^2 + m^2} = -\frac{mT}{4\pi} + \mathcal{O}(\epsilon), \tag{3.25}$$

where we introduced the renormalization scale to keep the units nice. For the non-zero

modes, we can expand in $m^2/T^2 \ll 1$ and obtain:

$$\mu^{2\epsilon}\sum\!\!\!\!\!\!\int_P{}' \frac{1}{P^2+m^2} = \frac{T^2}{12} - \frac{2m^2}{(4\pi)^2}\left(\frac{1}{2\epsilon} + \ln\left(\frac{e^{\gamma/2}\mu}{(4\pi)^{1/2}T}\right)\right) + \mathcal{O}\left(\frac{m^4}{T^4}\right) + \mathcal{O}(\epsilon), \tag{3.26}$$

where the dash means that the zero mode is excluded from the sum.

The result is divergent due to $1/\epsilon$ and, in the free energy, the divergence is mixed with the temperature. (There is the square of this sum-integral in the free energy.) This is obviously not physically acceptable. The solution is to realize that the mass parameter in the Lagrangian can be divergent to cancel the divergences from physical quantities. So, we split the parameter into two pieces

$$m^2 \to m^2 + \delta_{m^2}. \tag{3.27}$$

The second part contains all the divergences and is called the mass counterterm. The first part is the renormalized mass parameter.

The Euclidean Lagrangian which is obtained from the Hamiltonian does not contain temperature, therefore, neither does the mass counterterm. Hence the renormalization can be done in zero temperature in which sum-integrals become regular four-dimensional integrals.

$$T = 0: \quad \sum\!\!\!\!\!\!\int_P \to \int_P. \tag{3.28}$$

The method for finding the counterterms is to renormalize correlation functions. The mass counterterm on one-loop level is obtained from:

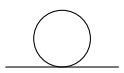

$$= -\frac{\mu^{2\epsilon}\lambda}{2}\int_P \frac{1}{P^2+m^2} - \delta_{m^2}$$
$$= \frac{\lambda m^2}{(4\pi)^2}\frac{1}{2\epsilon} - \delta_{m^2} + \mathcal{O}\big(\lambda m^2\big),$$

which should be finite as a whole.

There is an (unphysical) ambiguity in which parts to include into the mass counterterm and which parts should be in the renormalized mass parameter. One possibility is that the renormalized mass parameter would be the pole mass. This is called the pole mass scheme. We will use the computationally easier scheme called the $\overline{\text{MS}}$-scheme, in which only the divergent part is included into the counterterms. In this scheme, the renormalized mass parameter might not equal the physical (pole) mass and the relation has to be further worked out if one is interested in the physical mass. In the $\overline{\text{MS}}$-scheme, we have

$$\delta_{m^2} = \frac{\lambda m^2}{(4\pi)^2}\frac{1}{2\epsilon}. \tag{3.29}$$

We leave the full renormalization for later when we have a specific theory to apply it. Later on we will see another feature of the $\overline{\text{MS}}$-scheme

which is absorbing certain numerical factors into the renormalization scale μ.

To summarize the renormalization procedure:

The number of spatial dimensions is $d = 3 - 2\epsilon$ and, at the end of the computation, ϵ is taken to zero from above. The Euclidean Lagrangian contains bare parameters m_0^2, λ_0 and ϕ_0. (The field might also need renormalization.) They can be split into two parts: a divergent part which is the counterterm and a finite part which is the renormalized parameter:

$$m_0^2 = m^2 + \delta_{m^2}, \tag{3.30}$$

$$\lambda_0 = \mu^{2\epsilon}(\lambda + \delta_\lambda), \tag{3.31}$$

$$\phi_0^2 = \mu^{-2\epsilon}(1 + \delta_Z)\phi^2. \tag{3.32}$$

The renormalization scale keeps the dimensions of the renormalized coupling physically correct. The counterterms are computed through zero temperature correlation functions so that the correlation functions are finite. In $\overline{\text{MS}}$-scheme, only the divergences are included into the counterterms.

3.1.3 IR-Problems of the Naive Perturbation Expansion

The model that we are going to study in this thesis has a field with negative renormalized mass parameter. Looking at the result in Eq. (3.25), it seems that the contribution of the zero Matsubara mode to the free energy is imaginary. Thus, it seems like the theory is not perturbative around the field value $\phi = 0$. However, this can be illusory when the mass parameter is small compared to the temperature $|m^2| \ll T^2$.

The full propagator can be expressed in terms of two-point one-particle irreducible diagrams

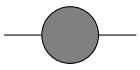

$$= -\Pi(P) \tag{3.33}$$

as

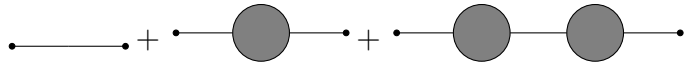

$$= \frac{1}{P^2 + m^2} - \frac{1}{P^2 + m^2}\Pi(P^2)\frac{1}{P^2 + m^2} + \frac{1}{P^2 + m^2}\Pi(P^2)\frac{1}{P^2 + m^2}\Pi(P^2)\frac{1}{P^2 + m^2} + ...$$

$$= \frac{1}{P^2 + m^2 + \Pi(P^2)} \tag{3.34}$$

The theory can be perturbative around $\phi = 0$ if $m^2 + \Pi(P^2) > 0$.

On the one-loop level, the leading contribution to $\Pi(P^2)$ at high temperature is from

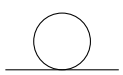

$$= -\lambda\frac{T^2}{24} + ... \tag{3.35}$$

Therefore, we get that the theory is perturbative around $\phi = 0$ when the temperature satisfies

$$T^2 \gtrsim -\frac{24m^2}{\lambda}. \tag{3.36}$$

A nice thing about constructing an effective theory, which we will do in the next section, is that the resummation is done implicitly and we do not need to worry about it too much.

One important note is that there is clearly a some kind of a transition in the ϕ^4-theory with negative mass parameter. At very high temperatures, the minimum of the effective potential is at $\phi = 0$ and at zero temperature the minimum is at $\phi \neq 0$. The transition happens at

$$T \approx \sqrt{-\frac{24m^2}{\lambda}}. \tag{3.37}$$

3.2 Effective Field Theory

A phase transition, in some sense, is never visible from the bare Euclidean action that describes a thermal field theory. Phase transitions happen because thermal fluctuations change with temperature, which may cause a new phase being stable and the current phase just metastable. Therefore, these fluctuations must be taken into account on top of the Euclidean action. If there is a scale hierarchy between the mass of the nucleating degree of freedom and the temperature, as there usually is in cosmological phase transitions, the effective field theory (EFT) framework is well suited to describe the phase transition.

We will first go through a bit more in general about effective field theories. Then, we revisit the reasons why the EFT framework is suited for our quest of the exponential suppression of the nucleation rate and how it guides the handling of fluctuations at different length scales. There, we will also make a remark on where our methods fail. Finally, we study the two steps of EFT that are needed for the description of the critical bubble and note that in the special case of the thin-wall limit, even these are not enough. This problem is discussed more in-depth in the last section of this chapter. An example of a calculation in which the two steps are needed is given in the following section.

An effective theory is just a theory with a limited range of applicability. A familiar example is Newtonian mechanics which breaks down, for example, when the objects have speeds comparable to the speed of light. Therefore, the range of applicability is restricted to $v \ll c$. Similarly an EFT is just a field theory with a limited range of applicability. For example, the 4-Fermi theory describes the weak interaction at low energies compared to the mass of the bosons of the weak interaction and the chiral perturbation theory describes QCD at low energies. Also, the standard model of particle physics is an EFT of a more general theory, at the very least because it fails to describe gravity at energies

near and above the Planck mass.

Usually, the limitation for the applicability of an EFT is that it can describe phenomena below a certain momentum threshold called the cut-off scale of the EFT, Λ. This also means that the describable phenomena have to happen at length scales longer than the inverse cut-off length scale, Λ^{-1}. The usefulness of an EFT comes partly from these limitations: The full theory of an EFT (FT) can be really clumsy because it contains all the information from the short length and high momentum scales. The EFT is free from the extra information and the long length scale phenomena are much easier to deal with it than with the FT.

We will now discuss the construction of an EFT, which contains four steps:

1. identification of the degrees of freedom in the EFT,
2. construction of the action describing the EFT,
3. fixing the coefficients to match the full theory at wanted length scales,
4. truncation of the action.

The construction of an EFT begins with the identification of the IR degrees of freedom which are described by the EFT. This is not always straightforward. For example, QCD is confining at energies where the chiral perturbation theory is valid and, therefore, the field content of the chiral perturbation theory does not consist of the elementary fields of QCD. However, this is not a problem in our case. The specific identifications are discussed in the Subsects. 3.2.1 and 3.2.2.

The EFT is described through an action for the IR DoFs. The construction of an effective action is only restricted by the symmetries of the full theory: if an operator breaks the symmetries, it should not be included into the action. Otherwise, all the operators consisting of the fields in the EFT must be included.

The coefficients of an action are determined via a process called matching. The matching is done by requiring that the observables within the EFT are the same as the corresponding observables in the full theory. This is one of the clever parts of EFTs because one can kind of cheat here [27]. The (complicated) IR physics is the same in the EFT and in the FT, so it can be bypassed. We regulate the infrared regions via dimensional regularization presented in Subsec. 3.1.2 instead of the masses and resummations of the IR degrees of freedom (cf. Subsec. 3.1.3). The mistake is the same on both sides and does not affect the result of the matching. As a bonus, all the loop integrals on the side of the EFT are now scale free. Due to dimensional regularization, scale free integrals are identically zero.

An EFT action contains an infinite number of terms. However, it is not possible in practice to fix all of their coefficients. Hence, the action must be truncated, which causes

the EFT to replicate the full theory only with finite precision. Also, the coefficients of the action cannot be matched exactly. Therefore, we need to know what precision satisfies our needs and whether the EFT fulfils the precision.

The EFT action is just a series expansion in different expansion parameters and the precision of the action is obtained by power counting in these parameters. One of the expansion parameters is the inverse of the cut-off scale of the EFT. The mass dimensions of an operator, induced by integrating out the higher momentum scale, determines the inverse power of the cut-off in the coefficient of the operator. Therefore, operators with higher mass dimension should be suppressed by more inverse powers. It is possible that the suppression is not enough, and the action as a series expansion diverges due to operators with higher dimensionality. This is a sign that one is trying to apply the EFT beyond its range of applicability, i.e. in the region beyond the cut-off scale. Often, there are also weak-coupling parameters for which the power counting must also be done.

Here, I would like to make a remark for the EFT describing bubble nucleation. It can happen that the field value inside a bubble becomes so large that it causes the expansion discussed above to fail. The situation can be remedied with resumming all the terms in the failing part of the expansion [28]. Then the action of an EFT holds also in the region in which the former series expansion failed. This will be needed in the Subsec. 3.2.2 and is also mentioned in Subsec. 3.2.1.

Let us now turn back to the nucleation after a more general review of effective field theories and revisit why the EFT framework is well-suited for our goal to find the statistical part of the nucleation rate.

If one integrates every fluctuation out in a constant background, the resulting action for the background is the effective free energy divided by the temperature. (The action is actually more like a potential because the background is constant.) Therefore, the expectation value of the field is given by the global minimum of the action. A first-order phase transition exists if the global minimum shifts discontinuously.

However, a bubble is not a constant background and so the fluctuations that make up the bubble cannot be integrated out. Neither is it allowed to integrate out fluctuations at the length scale of the bubble or longer. The EFT framework tells us a consistent way to integrate out fluctuations necessary for the description of the critical bubble. The remaining action for the relevant degrees of freedom is the analogue of $\beta\tilde{H}$ from Eq. (2.35): It contains the critical bubble as its stationary point and gives the Boltzmann suppression of different bubble configurations.

The creation of an EFT requires a hierarchy. However, there is a possibility that the stability of the new phase needs the free energy contributions of the light[†] fluctuations. There is no hierarchy that would allow us to integrate out the light fluctuations, leaving the nucleating field described by a new EFT. As is shown by the undershoot–overshoot

argument in Sec. 2.2, the action of an EFT contains the critical bubble at its tree-level only if the new phase has a lower potential value than the old phase. Thus, it is clear that an EFT containing the critical bubble at its tree-level cannot be created for the nucleating field in a situation where the contributions from light fluctuations are needed for the stability of the new phase.

The situation described above is discussed more in-depth in Subsec. 3.2.3. The essence is that, in a situation where the light fluctuations give only a small (but crucial) contribution to the free energy, the critical bubble is a thin-wall bubble, i.e. it has a large plateau inside (cf. Fig. 2.5). Within the plateau, the integration out of the light fluctuations is allowed. The bubble wall width is of the order of the inverse mass of the nucleating field [18] and therefore, light DoFs cannot be integrated out within the walls. This creates an effective theory for the walls of the bubble from which the critical bubble can be found. In Subsec. 3.2.3, an effective theory is not actually derived but the critical bubble is approximated via the thin-wall approximation explained in the subsection.

This still leaves out a situation in which the light fluctuations give a major contribution to the free energy near the phase transition. It is certainly not too easy to come up with this type of a situation in which there is a strong enough first-order transition that it could be studied via its critical bubble. A transition that is basically solely due to light fluctuations is the symmetry breaking transition in ϕ^4-theory, but it is a second order transition in nature. The same thing holds in the cubic anisotropy model studied in Subsec. 3.3.4: If the transition is first order, the other field becomes heavy on top of the bubble as it induces the transition. It could be that, if a transition is strong enough to be studied via its critical bubble, the transition is either induced by heavy fluctuations or that the critical bubble is a thin-wall bubble and consequently, the light fluctuations can be integrated out within the plateau.

We have now discussed exhaustively about the short scale fluctuations that end up into the effective action of the EFT describing the critical bubble. There are also fluctuations on longer length scales that are not integrated out, yet. These fluctuations contribute to the nucleation rate through fluctuation determinants of which there is an example in Eq. (2.40). The determinants exist always in pairs, one is evaluated on the critical bubble configuration and the other in the metastable phase. The ratio cancels outside the bubble, which is easier to see if the determinants are exponentiated. The example, given in the equation, is somewhat of an exception because the negative eigenmode, related to the nucleation, and the zero modes, relating to the translational symmetry, are singled out. There are no other negative eigenmodes in the fluctuations of other degrees of freedom. However, there can be zero modes from internal symmetries being broken by the critical

[†]For brevity, we shall refer to fields on the mass scale of the nucleating field or even lighter fields as light.

bubble configuration.

As one might expect, fields that are very weakly coupled to the nucleating field contribute very little to the rate. This manifests in the two determinants cancelling almost completely because the determinant on the bubble is not different from the determinant in the metastable phase. On the other hand in a symmetry breaking transition, if a field is very strongly coupled to the nucleating degree of freedom, it ends up picking a large mass on the critical bubble (cf. Fig. 3.4). This means that its correlation length becomes short, and the field will be integrated out. In this case, there would be no fluctuation determinant for the field. However, there are subtleties relating to the symmetric phase. When integrating out the field on the bubble, it is also integrated out in the symmetric phase. In the phase, there is no scale hierarchy, so the EFT does not describe it correctly. The hope is that this would have an effect only on the out-skirts of the critical bubble, so that error would not be too large.

The situations, in which the long length-scale fluctuations are more important than might be expected, are the ones in which an internal continuous symmetry is broken by the critical bubble configuration. Then, the zero mode must be dealt with separately as was done for the translational zero mode in the previous chapter. The zero mode can give a significant contribution on its own, but not exponential though. One example of this is a model of $O(2)$-symmetric pair of real scalars which nucleate. Here, the critical bubble breaks the $O(2)$-symmetry giving a corresponding zero mode.

Now, we are going to discuss the truncation of the effective action. This might be a bit abstract because no precise model is in question. The truncation in a specific model will be discussed in Sec. 3.3. The discussion of the thin-wall limit is left into Subsec. 3.2.3 so here we will discuss only thick wall bubbles.

The natural truncation for the action describing the critical bubble is to have only the terms which are larger than the order of unity in power counting. The reason is that we won't be able to evaluate the full pre-factor of the nucleation rate yet (including the part that comes from the time-evolution of nucleation). The pre-factor amounts to at least logarithmic contributions when exponentiated. Therefore the effects from the order of unity contribution to the action are washed out by the pre-factor.

This truncation also helps us to see whether the transition can be described through a critical bubble. If the action describing the critical bubble has no contributions that are larger than unity, the truncation says that there are not any large enough terms to be kept in the action. This corresponds physically to the bubble not giving any significant suppression and to the fluctuations in the pre-factor dominating. Hence, the transition is not describable via a critical bubble.

The order of a contribution to the Boltzmann suppression from a term in the action is obtained from two things: the size of the corresponding Lagrangian term and the

volume of the critical bubble. The size estimate for the first one can be attained via the power counting. The Lagrangian term has an effect to the Boltzmann suppression only within the bubble and, hence, the volume affects the size of the contribution. In the thick-wall case, the length scale of a critical bubble is the inverse mass of the nucleating field. Consequently, the volume is $\sim \tilde{m}^{-3}$.

Based on the size of a critical bubble in a thick wall case, we can argue that the determinants in the statistical part of the nucleation rate do not contribute exponentially (cf. Eq. (2.40)). The determinant in the numerator is the one-loop free energy of the nucleating field in the metastable phase when it is exponentiated (with an appropriate power of temperature). As the determinant in the denominator is exponentiated as well, the contributions of these two cancel outside the bubble. The free energy density of the nucleating field in the metastable phase is $\sim \tilde{m}^3$ and, therefore, the exponential contribution of the fluctuation determinants seems to be the order of unity, i.e. not exponential. This might be a bit misleading because the determinants are in the prefactor and not in the exponent. The determinants most likely amount to some order, for example, in small couplings in the prefactor and become logarithmic in the power counting when exponentiated. Therefore, they can be larger than plain order of unity.

In Refs. [29] and [30], it was found that the fluctuation determinants give an exponential contribution to the nucleation rate. However, the contributions came from the momentum scale $\sim T$. A consistent treatment at temperatures $T \gg \tilde{m}$ requires that this scale is included into the effective action of the critical bubble via integrating it out. Hence, it does not enter into the determinants when integrating over the fluctuations of the nucleating field. As the critical bubble can be much larger in the thin-wall limit, the argument given here for the non-exponential contribution of the fluctuations of the nucleating field breaks down. This matter will be discussed in Subsec. 3.2.3.

Ref. [31] discusses the cubic anisotropy model, which we will cover in Subsec. 3.3.4. In the reference it was found that there is an exponential contribution coming from the fluctuation determinants of the inducing field, which breaks the method they are using to study the nucleation rate. In our treatment, the field is integrated out due to being heavy on the critical bubble. However, we create another problem by doing so, which is that the symmetric phase is not properly described by the EFT.

In the following two subsections, we will discuss the two layers of EFT necessary for describing the critical bubble if it is thick walled. The terminology for the different scales is that the scale of the temperature (or higher) is called the super-heavy scale, the possible scale between the super-heavy scale and the nucleating degree of freedom is called the heavy scale and the scale of the nucleating degree of freedom (or lower) is called the light scale. The names are in accordance with Ref. [11]. There is an important point to keep in mind, which is that a field that becomes heavy on a critical bubble is in the heavy

scale even if it was light in the metastable phase. Further discussion of the thin-wall limit is left for its own section, Sec. 3.2.3.

3.2.1 Dimensional Reduction

In this subsection, we will go through the first layer of the EFT describing the critical bubble of a phase transition. Obviously, there can be higher scales that need to be integrated out before this step, but this is the first step specific to a thermal phase transition. Here, we will see how to handle the momentum scale of the temperature, which contains the dominant thermal effects. The EFT discussed here can be constructed only if the mass of the nucleating field is much lighter than the temperature at the time of nucleation. This is usually the case for phase transitions of weakly coupled fields. An example calculation is done in Subsec. 3.3.2.

The infrared degrees of freedom of the EFT are the Matsubara zero modes of bosonic fields with masses much smaller than the temperature. This is rather straight forward to spot by looking at the bare propagator in Eq. (3.16). In the case of physical equal-time correlation functions (Eq. (3.11)), the propagator can be viewed as an infinite sum of three-dimensional Euclidean propagators with different masses, $m_n^2 = m^2 + (2\pi n T)^2$. When $m \ll T$, there is a clear hierarchy between the zero and non-zero Matsubara modes and the non-zero ones can be integrated out.

The remaining DoFs are constant in the Euclidean time direction and so it is effectively removed from the EFT. The spatial structure of the EFT is $\mathbb{R}^3$ rather than $\mathbb{R}^3 \times S^1$ of the full theory and this is where the process of integrating out non-zero Matsubara modes gets its name.

I mentioned that the IR DoFs are zero modes of *bosonic* fields. This is due to the fact that fermionic fields do not have zero modes because of their anti-periodicity in the Euclidean time direction. Masses of the fermions are $m_n^2 = m^2 + ((2n+1)\pi T)^2$ and so all of the modes have a mass from the super-heavy scale, which is integrated out.

The range of applicability of an EFT is governed by the momentum scales integrated out. In this case, the cut-off is of order πT and, therefore, length scales that can be described by the EFT are much longer than $(\pi T)^{-1}$. This seemingly puts constraints on which length scales there can be changes in the critical bubble. However, the bubble varies over length scales of the inverse mass of the nucleating degree of freedom, which is already much longer than the constraint from the EFT. If the dimensional reduction can be done for the nucleating degree of freedom, the resulting EFT is able to describe the critical bubble.

In our example in Subsec. 3.3.2, the following straightforward identification is

enough:

$$\phi = T^{-1/2}\Phi_0, \tag{3.38}$$

where ϕ is the three dimensional field and Φ_0 is the zero Matsubara mode of the four-dimensional field from Eq. (3.17). The temperature appears in the identification to make the EFT fields canonically normalized. The kinetic term of the three-dimensional field arises from the kinetic term of the four-dimensional field:

$$\int_X \frac{1}{2}(\partial_\mu \Phi)^2 = \int_X \sum_{n=-\infty}^{\infty} \frac{1}{2}\Big(\partial_\mu\Big(\Phi_n e^{i\omega_n \tau}\Big)\Big)^2$$
$$\text{Only } n=0: \quad \to \int_{\mathbf{x}} \frac{\beta}{2}(\boldsymbol{\nabla}\Phi_0)^2 = \int_{\mathbf{x}} \frac{1}{2}(\boldsymbol{\nabla}\phi)^2.$$

Of course, there can be gradient terms which come from the matching. Making the EFT fields canonically normalized would then need a more complicated identification [11]. However, there will be no need to take into account higher order derivative terms in our example.

The fluctuations at the scale of the temperature are the predominant thermal fluctuations and consequently, this step of integrating out gives the dominant thermal contributions to the description of a critical bubble. They approximately determine the temperature of the transition even though some of the finer details of the transition are missing. These details are studied in the next subsection and an example calculation is given in Subsec. 3.3.3.

There are features of transitions described with an EFT obtained via dimensional reduction that cannot be seen from our example computation. For example, a first-order phase transition can be induced already in the dimensional reduction step. This can happen, if there are interaction terms that break the $\mathbb{Z}_2$-symmetry, e.g. Yukawa coupling to a fermion, $y\Phi\bar{\Psi}\Psi$.

A Yukawa term can give a significant contribution to the mass of a fermionic field in the centre of the critical bubble. If the contribution is of the same order as temperature, the perturbative expansion in the coupling breaks down. This happens because the mass contribution is at the same scale as the cut-off scale of the effective theory and a next term in expansion in $\Delta M_{\mathrm{Y}}(\Phi)/T$ is the same order as the previous one. To regain the validity of the EFT, the Yukawa interaction must be resummed.

The same thing can happen to a bosonic field, for example to a scalar field X through $\lambda_{\mathrm{X}}\Phi^2\mathrm{X}^2$. The difference with the fermionic case is that, now, the Matsubara zero mode of the X field will not be part of the dimensionally reduced theory. The mass of the zero mode is too large inside a critical bubble to be included into the EFT. In the example calculation, we do not consider situations in which a resummation must be done within dimensional reduction but this will be demonstrated in the second step in the example.

I would like to make one last note on dimensional reduction. In symmetry breaking transitions, the mass parameter of the nucleating degree of freedom is usually negative in the full theory. This poses an illusory IR problem for the FT discussed in Subsec. 3.1.3. The matching of dimensional reduction takes care of the seeming problem as can be seen in Sec. 3.3.

3.2.2 Integrating out Heavy Fields

Now, we have discussed integrating out the super-heavy scale T in the limit of $\tilde{m} \ll T$. However, there can still be degrees of freedom that are much more massive than the nucleating field but much lighter than the temperature. Therefore, they need to be integrated out. These, so-called, heavy fields can exist in any type of transition but we are going to focus mainly on symmetry breaking phase transitions (SBPT) in which the expectation value of the nucleating field transitions away from zero value. In SBPTs, the heavy scale can exist quite naturally and give a significant impact on the nature of a phase transition. In this subsection, we will first discuss, how the heavy scale arises and, then, how it can induce a first-order phase transition. At the end of the subsection, we will discuss subtleties of integrating out the heavy scale and the need to be careful when identifying the degrees of freedom belonging to the scale.

Regarding symmetry breaking transitions, the most important contribution from the super-heavy scale is the enhancement of the mass of a three dimensional field. As discussed in Subsec. 3.1.3, a negative renormalized mass parameter almost cancels the mass near a SBPT. Therefore, the nucleating field can be very light near its phase transition, which leaves room for the heavy scale to exist.

There are two mechanism that can make a field become part of the heavy scale if the renormalized mass parameter of the full theory is light: through thermal enhancement of its mass or through the vacuum expectation value of the nucleating field. We will see examples of both with a scalar field in Sec. 3.3.

Gauge fields are very natural candidates for being heavy scale since their renormalized mass parameter is identically zero in the full theory. The electro-static part of a gauge field receives a thermal mass which is of order gT, where g is the gauge coupling. The magnetic components do not have a thermal mass this large, which leads to them not being perturbative. This is known as the Linde problem [13]. However, both electric and magnetic components receive modification to their masses from the field value of the nucleating field, if the gauge field is coupled to it. The modification is of order $g^2T|\phi^2|$, where ϕ is the three-dimensional field and the temperature comes from the identification (3.38). Therefore, gauge fields can be at the heavy scale rather naturally.

As discussed in the previous subsection, fermionic fields are all super-heavy due to

their anti-periodicity in the Euclidean time direction of the full theory. Hence, they have already been integrated out from the effective field theory.

We will now discuss the power counting of this step of EFT. The current step can have lot more complexity to it than DR, and the power counting is at the root of it. For example, the induction of a new minimum has subtleties to be understood via the power counting. Also, the expansion parameter of quartic couplings is no longer just the coupling, because it is not dimensionless in three dimensions. This makes it possible, that a mass too small can break the perturbative series.

The cut-off scale comes from the masses of fields integrated out in this step. The cut-off scale is now much closer to the energy scale of nucleation. As a consequence, the suppression of operators with higher dimensionality is weaker. Therefore, it can be that the field value at the centre of a critical bubble can be so large that the cut-off cannot make the power series of an effective action converge. In a usual case, this type of a breakdown can be seen by noticing that the contribution to the mass of a heavy field from coupling to the nucleating field is as large or larger than its own mass. The correct treatment is then to resum the ill-converging part [28]. In the usual case, this can be viewed as a contribution to the mass of the heavy field, as discussed above. This plays a crucial role in inducing a first-order phase transition through the heavy scale. Another consequence of the low cut-off is that derivative operators might need to be included into the effective action.

The power counting in coupling constants is different from four-dimensional theories. This happens because the dimensions of couplings are different in three dimensions. An example, that is useful in our example calculation, is the quartic self-coupling of a scalar field. Its mass dimension is one and, therefore, the small expansion parameter (without numerical coefficient) is λ_3/m_3 [26], where m_3 is the mass of the scalar field which might depend on the nucleating field. This expansion parameter dictates how many loop-orders are needed for a certain precision. Another important piece of information that comes from the expansion parameter is whether a field is perturbative or not. If the mass of the nucleating field decreases too much, the ratio might become order one. Physically, this means that the field fluctuates so much that the quartic self-coupling cannot be treated perturbatively. Consequently, the EFT description of the transition fails to predict if the transition is first order. This is further discussed with the example in Subsec. 3.3.5.

Let us now look into how the heavy scale can induce a first-order phase transition. It boils down to two things: the nucleating field can increase the mass of a field and a larger mass means less free energy for a field in equilibrium. Therefore, a larger expectation value of the nucleating field can reduce the free energy of another field giving a new minimum with non-zero expectation value. Often, when the new minimum is induced, the mass contribution from the nucleating field is at least comparable to the mass of a

heavy field in the symmetric phase. Hence, the contribution has to be resummed.

Some caution is necessary, if a field, that is light in the symmetric phase but heavy on the bubble, is integrated out. In this case, the EFT breaks down near the symmetric phase, because the removed field has no hierarchy, or the hierarchy is inverted, with the nucleating field. The hope is that this matters only for the end of the tail of the bubble, which would not change the exponential suppression much. Usually, the behaviour of the field value far from the centre is given by Eq. (2.33) which follows from a simple equation of motion for the critical bubble in Eq. (2.15). Additional derivative terms to the effective action from the light field might give a large contribution, if the bubble tail behaves as in the equation. Therefore, the additional derivative terms could change the behaviour of the end of the tail significantly.

3.2.3 Thin-Wall Limit

Now, we have gone through both steps of constructing the effective field theory. Here, we will extend the formalism to a situation in which the transition is first order but the two steps might not be sufficient. We will first discuss on physical grounds, why the EFT fails as a description in the thin-wall limit. Then, we will explain the necessary extra step, how the step changes the fluctuation determinants. The proper extension would require an effective theory for bubble walls, which will not be derived here from first principles. We will show the leading order approximation to the exponential suppression from the critical bubble, which is from Ref. [18]. At the end, we will examine the cross-over from the EFT description to the extension and propose a diagnostic for switching from the EFT to the extension.

On the contrary to other discussions in the thesis, it is now fruitful to approach the thin-wall limit from the thick-wall case. This means that the temperature goes towards the critical temperature from below. The discussion is done this way because the thick-wall is known to be described by the EFT obtained from the two steps above. Hence, we can identify how it breaks down when the critical bubble becomes more and more thin-walled.

As a quick recap, a thick-wall critical bubble is described by an effective action which contains the effects of scales higher than the light scale. The action evaluated on the critical bubble gives an exponential suppression for the nucleation rate and the effects of the light scale fluctuations around the critical bubble go into fluctuation determinants (cf. Eq. (2.40)).

As the free energy difference between the phases shrinks, the undershoot–overshoot method from Sec. 2.2 tells that a plateau starts to form in the interior of the critical bubble. A plateau is illustrated in Fig. 2.5. At this point the EFT still describes the

critical bubble.

When the free energy difference is very small, the plateau becomes much larger than the width of the wall and the bubble is now a thin-wall bubble. The plateau is large enough for the light fluctuations to relax inside it, changing the pressure within the bubble. As a consequence, it is possible that the relaxed light fluctuations are important for the shape of the critical bubble. These fluctuations are not included into the effective action of the critical bubble and hence, the action does not properly describe the critical bubble. In the extreme case, it could even be that the new phase is not stable without the light fluctuations. In this case, the effective action would not even contain a critical bubble at its tree-level.

The extra step is now rather clear: For the description, the relevant light degrees of freedom need to be integrated out on the plateau of the thin-wall critical bubble. This is allowed due to the plateau being large enough for the light fluctuations.

It is still illegal to integrate out light degrees of freedom inside the walls, because the width is at the order of the inverse mass of the nucleating field [18]. Since the bump in the field potential between two phases describes the internal structure of the bubble wall, it is crucially important that it does not originate from the light scale, which cannot be integrated out.

To construct the geometric effective theory for infinitely thin walls in Ref. [29], the light internal fluctuations would need to be integrated out as well. However, the internal fluctuations of the walls do not contribute on the leading order, and the geometric effective theory can give a good approximations.

One thing to note is that after integrating over the light fluctuations on the inside of the critical bubble, they no longer enter the fluctuation determinants. The determinants come now solely from the internal and external deformations of the bubble wall. The latter part has been evaluated in Ref. [32].

Now, we can move onto the approximation from Ref. [18]. In the thin-wall limit, a bubble can be approximated to be consisting of only two components: a wall and a volume on the inside of the wall. The wall contributes to the exponential suppression through a surface tension σ and the volume through the pressure difference between the two phases p. The pressure is just the difference of the free energy density between the two phases:

$$p = f_{\text{old}} - f_{\text{new}}. \tag{3.39}$$

We will see below how to compute the surface tension. The exponential suppression, S, can be given by

$$TS = \sigma A - pV. \tag{3.40}$$

The critical bubble is spherical [22] and so $A = 4\pi R^2$, $V = \frac{4}{3}\pi R^3$ in three dimen-

sions. We can now solve for the radius of the critical bubble by extremizing the action:

$$R = \frac{2\sigma}{p}. \tag{3.41}$$

For a light field to be integrated out on the plateau, the radius has to be much longer than the inverse mass of the field.

Now that we have the radius, we can solve the exponential suppression from the thin-wall critical bubble:

$$S = \frac{16\pi\sigma^3}{3p^2T}. \tag{3.42}$$

The surface tension is the exponential suppression from the wall per unit area. Inside the wall, we cannot integrate out the light fields, so the wall is described via the effective action obtained from the previous two steps. The internal structure of the wall does not change appreciably within the thin-wall limit and therefore, it can be well approximated as being a solution that extremizes the action and interpolates between the two minima at the critical temperature of the effective action (cf. Fig. 3.2). As the radius of the bubble is very large compared to the width of the wall, the wall is almost flat. Hence, the surface tension is the exponential suppression of a plane wall per unit area.

One can solve for the form of the approximated flat wall with the full effective action. For the sake of a simpler numerical estimate, we will use a less accurate surface tension, that does not take into account any extra gradient terms besides the kinetic term. This helps us to get a very simple integral for the tension [18]:

$$\sigma = T \int_{\phi_+}^{\phi_-} \mathrm{d}\phi \, \sqrt{2U_{\text{eff}}(\phi)}, \tag{3.43}$$

where the integration bounds are the two minima of the potential. The temperature appears due to the factor of temperature in Eq. (3.40). The potential U_{eff} is from the effective action and does not contain contributions from the light scale. At least, with the

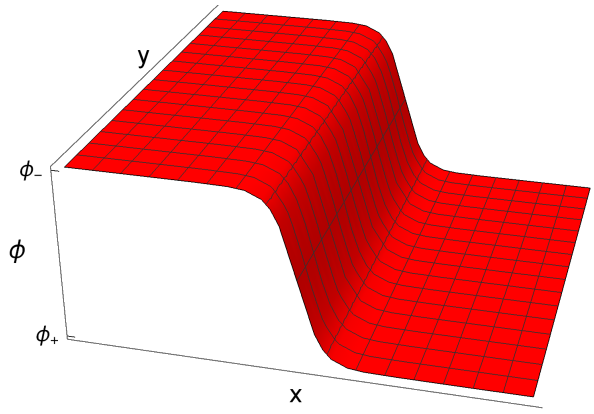

Figure 3.2: Figure illustrates the approximation relating to the wall of a thin-wall bubble. It is approximated as a field configuration, that extremizes the action with boundary conditions $\lim_{x\to\pm\infty} \phi = \phi_\pm$.

benchmark points, that are chosen in Sec. 4.3, the reduction in accuracy is not large. This is due to the wave function renormalization, in Eqs. (3.103) and (3.113), not contributing much in relation to the full exponential suppression.

We have now a simple recipe for the leading order exponential suppression from the critical bubble in the thin-wall limit. The only variable, that changes as the system starts supercooling, is the pressure.

Let us discuss the cross-over between the two descriptions, the EFT and the extension. There are three different situations for the critical bubble: thick-wall, thin-wall and a grey area in between. We know that the EFT holds in thick-wall cases, as the light fluctuations cannot be integrated out into the effective action, and the extension holds in thin-wall cases. However, there are situations in which light fluctuations are not crucial for the critical bubble but can be integrated out on the plateau. It is in this grey area that the two descriptions differ from each other in the handling of the light fluctuations: the EFT keeps their contribution in the determinants whereas the extension takes it straight to the exponent. In the grey area, the contribution of the light fluctuations on the plateau can be retrieved from the fluctuation determinants as long as their contribution to the pressure inside the critical bubble does not change the size of the bubble too much (cf. Fig. 4.13). As the critical bubble becomes more and more thin-walled, the light fluctuations give greater and greater contribution, and eventually, the contribution changes the critical bubble so much that the EFT no longer describes it correctly.

There is a rather straightforward two-step diagnostic for including certain light fluctuations into the critical bubble. The first step is to make sure that the plateau is large enough for the particular light fluctuations to relax on it. The second step estimates how much the light fluctuations change the size of the critical bubble. An estimate for the radius can be obtained from the thin-wall approximation in Eq. (3.41). These approximations for the radius are calculated with and without the contribution from the light fluctuations to the pressure of the new phase. If the estimates differ noticeably, the extension should be used. This estimation is done in Fig. 4.13.

3.3 Example: Two Real Scalars

We have established a framework for finding the statistical part of the nucleation rate which contains the exponential suppression. In this section, we will go through the simplest example in which there is a first-order phase transition, radiatively induced by the heavy scale..

The model we are going to study is the renormalizable theory with two weakly

coupled $\mathbb{Z}_2$-symmetric real scalar. It is described by the following Euclidean action:

$$S_{\mathrm{E}} = \int_{\mathbf{x}} \int_0^\beta \mathrm{d}\tau \left(\frac{1}{2}(\partial_\nu \Phi)^2 + \frac{m^2}{2}\Phi^2 + \frac{1}{2}(\partial_\nu \mathrm{X})^2 + \frac{M^2}{2}\mathrm{X}^2 + \mu^{2\epsilon}\frac{\lambda}{4!}\Phi^4 + \mu^{2\epsilon}\frac{f}{4!}\mathrm{X}^4 + \mu^{2\epsilon}\frac{g^2}{4}\Phi^2\mathrm{X}^2 + \frac{\delta_{m^2}}{2}\Phi^2 + \mu^{2\epsilon}\frac{\delta_\lambda}{4!}\Phi^4 + \mu^{2\epsilon}\frac{\delta_{g^2}}{4}\Phi^2\mathrm{X}^2 \right). \tag{3.44}$$

Needless counterterms have already been dropped for simplicity. The renormalization scale μ has been introduced in accordance with the regularization scheme, which is dimensional regularization from Subsec. 3.1.2. The renormalization of this model is done in App. B.1.

We will choose the situation to be such that the degree of freedom undergoing a symmetry breaking phase transition is the Matsubara zero mode of the Φ-field and that the zero mode of the X-field induces a first-order transition. From this, we already know that the renormalized mass parameter of the Φ-field has to be negative and that the cross-coupling needs to be much larger than the self-coupling of the Φ-field:

$$m^2 < 0, \tag{3.45}$$

$$g^2 \gg \lambda. \tag{3.46}$$

There can be an induced transition even with weaker cross coupling, but it is a second order transition, as is shown in Subsecs. 3.3.1 and 3.3.4.

The approximate transition temperature can also be deduced, as was done for a simpler model in Subsec. 3.1.3. Now, the leading contribution to the self-energy of the Φ-field comes from interacting with the X-field:

$$= -g^2\frac{T^2}{24}, \tag{3.47}$$

where the dashed line represents a X-propagator and the solid lines Φ-propagators. The approximate transition temperature is the one at which the self-energy is zero. Therefore, the temperature is

$$T^2 \approx -\frac{24m^2}{g^2}. \tag{3.48}$$

This is confirmed in Subsec. 3.2.1.

There are actually two rather distinct example possibilities within the full Euclidean action: an asymmetric model and the cubic anisotropy model. In the first model, the inducing field X is heavier than the nucleating field Φ and it is more strongly coupled to itself. This was a model in which Eric Weinberg studied vacuum decay in Ref. [25]. In the cubic anisotropy model, the scalars are identical, $M^2 = m^2$ and $f = \lambda$. Here, a bubble breaks the symmetry between the fields and chooses which one nucleates the bubble and which one becomes heavy on the bubble. (Due to the symmetry between the fields, we have the power to label the field nucleating the bubble as Φ.)

In this section, we will first go through the creation of the effective field theory for the asymmetric model, and then in Subsec. 3.3.4, we look at the cubic anisotropy model. Basically, all the work for the cubic anisotropy model is done examining the asymmetric model. In the first subsection, we go through the power counting in the asymmetric model for both steps of integrating out and give size estimations for certain parameters. The actual calculation is divided into two subsections. The first contains dimensional reduction. There, we will see that the physically most important contribution is the thermal contribution to the mass of a three-dimensional field. The hard field is integrated out in Subsec. 3.3.3. There, the physically most important contribution is the one-loop free energy of the hard field: it induces the first-order transition. In the last subsection, we discuss the limitations of the effective field theory framework of ours through the example models.

3.3.1 Power counting

In the current subsection, we will discuss the power counting of the asymmetric model. First, we will restrict the values of a few parameters to ease the power counting. Then, we will discuss the size of terms in the effective actions of both steps. After the proper power counting, we will see that there are restrictions for the sizes of certain parameters due to the constraint of a first-order phase transition. We will also estimate the size of the field value at the centre of a critical bubble in different transitions. At the end, we will touch on the subject of the truncation of the effective action.

The restrictions, we make, relate to the parameters of the inducing field X:

$$f \sim g^2, \tag{3.49}$$

$$\left|M^2\right| \lesssim g^2 T^2, \tag{3.50}$$

where T is the temperature at the transition. The self-coupling of the inducing field has to be large enough to keep it from breaking its $\mathbb{Z}_2$-symmetry. A larger size for f would just mean that more diagrams would become important in the matchings. The renormalized mass parameter of the inducing field cannot be too negative so that the symmetry is not broken before the other field undergoes a transition. Also, if the mass is too large compared to the temperature, it already suppresses the fluctuations that should induce the transition. Therefore, a too large mass hinders the ability to induce transitions. Note, that the restriction from above is not strictly the limit at which it is no longer possible to induce a first-order transition.

An important part of the power counting is estimating the leading order of a term in the effective action. With this knowledge, it is possible to know which terms to exclude in the truncation. An effective action has mass dimension zero. Therefore, the mass

dimension of a term is given by the dimensionality of the space(time) which is three in both of the effective field theories. The correct dimensions for a term are reached with the proper inverse power of the cut-off. In dimensional reduction, the cut-off is the temperature and, when integrating out the heavy field, it is the mass of the heavy particle.

The leading order of an operator, coming from DR, is from the one-loop of the X-field because both fields couple strongly to it. There are two exceptions to this rule, and they are the operators $\phi\boldsymbol{\nabla}^{2k}\phi$ and $\chi\boldsymbol{\nabla}^{2k}\chi$, where χ is the three-dimensional field relating to the zero Matsubara mode of the inducing field, X_0. These operators appear only at two-loop level, because the one-loop, two-point diagram is independent of external momentum. Also, there are operators which come from the tree-level of the full theory and hence, do not obey the counting below. For a regular term from the one-loop, we have

$$\frac{(g^2)^n f^m}{T^{2k+n+m-3}}\boldsymbol{\nabla}^{2k}\Big((\phi^2)^n(\chi^2)^m\Big). \tag{3.51}$$

One weakness, that this formula has, is that logarithms are not taken into account. In some cases, they might be important. Also, the numerical factor is not estimated.

When integrating out the heavy scale, the situation looks a bit different. Here, the field value grows so large, that we need to resum external ϕ^2-legs in the χ-propagator. This leads to the modification of the χ-mass, $M_3^2(\phi)$. For example, the one-loop contribution is now of order $M_3(\phi)^3 - M_3(0)^3$, where the subtraction takes away the one-loop free energy of χ (cf. the exponent in Eq. (2.40)). The non-gradient contributions from the pure χ-diagrams can be estimated with

$$(fT)^n\Big(M_3(\phi)^{3-n} - M_3(0)^{3-n}\Big), \tag{3.52}$$

where n tells the number of self-interaction vertices in the corresponding diagram. fT is the leading order of the self-coupling of χ, which is shown is Subsec. 3.3.2. As discussed in Subsec. 3.2.2, the expansion parameter without numerical coefficient is f_3/M_3 and the expansion breaks down, if the mass is too low.

The formula (3.52) does not encompass all the possible operators. For example, there can be an internal ϕ-contraction, in which the ϕ-propagator has a momentum from the heavy scale. Therefore, there can be sole external ϕ-legs not associated with the resummation. Also, gradient terms were not included. The formula is the following:

$$\frac{(fT)^n(g^2T)^{m+2l}}{M_3(\phi)^{n+2m+2k+3l-3}}\boldsymbol{\nabla}^{2k}(\phi^2)^{m+l}, \tag{3.53}$$

where l is the number of single legs and m is the number of double legs associated with a non-zero external momentum in the derivative expansion. There is no need for subtracting the symmetric phase because it is already zero. Once again, the $\phi\boldsymbol{\nabla}^{2k}\phi$-operator does not exist on one-loop level, $n = 0$.

We have already fixed parameters M^2 and f. In the next subsection, we find that the mass of χ-field is $M_3^2 \sim g^2T^2$. Also, we have the parametric order of m^2 on physical grounds from Eq. (3.48), $m^2 \sim -g^2T^2$. This leaves the cross-coupling g^2, the self-coupling of the Φ-field, λ and the mass of ϕ-field, m_3^2 to be free parameters of which the former is fixed in a model and the latter decreases as the transition supercools. However, we will find constraints on λ and m_3^2 from the condition of the transition being first order. We will also find the parametric order for the field value at the centre of a critical bubble ϕ_0 and for the volume of the bubble V_B in different ranges of transitions.

In order to study the field value at the centre and the conditions for m_3^2 and λ, we have to "cheat" a bit by looking at the leading form of the resulting potential from Subsec. 3.3.3.

$$U(\phi) = \frac{m_3^2}{2}\phi^2 - \frac{1}{12\pi}\left[\left(M_3^2 + \frac{g^2T}{2}\phi^2\right)^{3/2} - M_3^3\right] + \frac{\tilde{\lambda}T}{4!}\phi^4. \tag{3.54}$$

The middle term will be called the cubic term. It is the one responsible for the radiatively induced phase transition. The constant inside the cubic term is there to set the potential to equal zero when $\phi = 0$. The term can be compared with expected one-loop contribution from a heavy field in (3.52).

We can see that the broken phase field value, ϕ_-, has two identical possibilities due to the $\mathbb{Z}_2$-symmetry. A bubble breaks the symmetry, but we can always choose the direction to be positive, $\phi_- > 0$. The field value of the symmetric phase is obviously zero, $\phi_+ = 0$. The transition can happen only below or at the critical temperature, when $U(\phi_-) \leq U(\phi_+)$.

The parameters will be computed if Subsecs. 3.3.2 and 3.3.3. Here, we give their leading forms:

$$m_3^2 = m^2 + \frac{g^2T^2}{24} + \mathcal{O}\Big(g^3T^2\Big), \tag{3.55}$$

$$M_3^2 = M^2 + \frac{(g^2+f)T^2}{24} + \mathcal{O}\Big(g^4T^2\Big), \tag{3.56}$$

$$\tilde{\lambda} = \lambda + \mathcal{O}\Big(g^4 \ln T\Big). \tag{3.57}$$

From the first orderedness, we can see two conditions that must hold for the potential at the transition: $U''(0) \geq 0$ and $U''''(0) < 0$. There has to be a barrier in the potential between the two minima for the transition being a first-order transition. Hence, the first condition. The second condition is bit more subtle. If it does not hold, the cubic term is always overpowered by the quadratic and the quartic terms. Hence, there would be no

dip in the potential and no phase transition. These conditions lead to

$$m_3^2 > \frac{g^2 T M_3}{8\pi}, \tag{3.58}$$

$$\tilde{\lambda} < \frac{3g^4 T}{16\pi M_3}. \tag{3.59}$$

These two are not sufficient but they are necessary.

A crucial piece of information for the size of a term in the effective action describing the critical bubble is the field value at the centre, ϕ_0. We are going to estimate it parametrically in two distinct scenarios.

We will first look at the order of ϕ_0 near the critical temperature, T_c. (There has to be a bit of supercooling for the critical bubble to be thick walled.) The field value at the centre of the critical bubble is close to ϕ_- according to the undershoot–overshoot argument in Sec. 2.2. We assume that the field value of the local minimum is large enough for the cubic term to be of order $g^3 T^{3/2} \phi_0^3$. At the local minimum, near the critical temperature, all three terms in the potential must be of the same order: The minimum is found where the cubic term and the quartic term are of the same order. However, for the minimum to have potential value near zero, the quadratic term must be at the same order as the other two terms. We get an order of magnitude equation

$$m_3^2 \phi_0^2 \sim g^3 T^{3/2} \phi_0^3 \sim \tilde{\lambda} T \phi_0^4. \tag{3.60}$$

We can quickly obtain the order of magnitude for ϕ_0 and m_3^2 in terms of the couplings and the temperature:

$$\phi_0^2 \sim \frac{g^6}{\tilde{\lambda}^2} T \sim \frac{m_3^4}{g^6 T^3}, \tag{3.61}$$

$$m_3^2 \sim \frac{g^6}{\tilde{\lambda}} T^2. \tag{3.62}$$

If $\tilde{\lambda} \sim g^4$, then the mass parameter m_3^2 given in (3.55) might never reach the critical temperature value estimated in (3.62). This would mean that there is no critical temperature and that the $\langle\phi\rangle \neq 0$ phase is always favoured. However, ϕ_0 from (3.61) would be so large that the treatment in Subsec. 3.3.2 breaks down. Therefore, the potential in Eq. (3.54) does not have predictive power any more, so this might just be an artefact of our treatment.

Let's now look at a more sophisticated way of getting the order of magnitude of the field. By doing it, we obtain understanding on when this approximation fails and a loose upper bound on m_3^2 at the transition, that agrees with the order of magnitude of m_3^2 at the critical temperature.

We can find local minima (and other extrema) by finding the roots of the derivative

of the potential. The $\phi > 0$ minimum is at

$$\phi_- = \frac{g^3\sqrt{T}}{8\pi\tilde{\lambda}}\sqrt{9 - 384\pi^2\frac{\tilde{\lambda}m_3^2}{g^6T^2} + 3\sqrt{9 - 768\pi^2\frac{\tilde{\lambda}m_3^2}{g^6T^2} + 256\pi^2\frac{\tilde{\lambda}^2M_3^2}{g^8T^2}}}. \tag{3.63}$$

For there to be a minimum at positive field values, $\phi_- \in \mathbb{R}$. Hence, both of the radicals must be real. With the help of Eq. (3.59), we find that there is only one condition:

$$m_3^2 < \frac{3g^6T^2}{256\pi^2\tilde{\lambda}} + \frac{\tilde{\lambda}M_3^2}{3g^2} \tag{3.64}$$

As a nice cross-check, the right-hand-side of this inequality reduces to the lower bound from Eq. (3.58) when $\tilde{\lambda}$ is set to be its upper bound from (3.59). Hence, there is no value for m_3^2 which would give a first-order phase transition with this value of $\tilde{\lambda}$.

As already mentioned, $\phi_0 \approx \phi_-$ near the critical temperature. Therefore, we can use Eq. (3.63) to estimate the field value at the centre of the critical bubble. If $\tilde{\lambda}$ is at its maximum value, then m_3^2 must be as well and $\phi_- = 0$. Thus, the approximations we made in the earlier for the size of ϕ_0 fails when $\tilde{\lambda} \approx \tilde{\lambda}_{\max}$.

We define a quantity that measures the relative difference of $\tilde{\lambda}$ from its upper bound:

$$r = 1 - \frac{\tilde{\lambda}}{\tilde{\lambda}_{\max}}. \tag{3.65}$$

The last term in the inner radical simplifies to $9(1-r)^2$. We know that m_3^2 is not parametrically smaller than its upper bound at the critical temperature: With large values of $\tilde{\lambda}$, the mass parameter is forced to be close to the upper bound by its lower bound and at small values of $\tilde{\lambda}$, we know this due to the estimate (3.55). We can now underestimate ϕ_- by setting m_3^2 to be its maximal value which is, at least, the correct order parametrically. The equation (3.63) simplifies to

$$\phi_- > \frac{3g^3\sqrt{T}}{8\pi\tilde{\lambda}}\sqrt{r\left(1 - \frac{r}{2}\right)}. \tag{3.66}$$

We can also overestimate the radical in (3.63) by setting $m_3^2 = 0$ and $\tilde{\lambda}$ to its maximal value (3.59). We now have both upper and lower bounds for ϕ_+:

$$\frac{3g^3\sqrt{T}}{8\pi\tilde{\lambda}}\sqrt{r\left(1 - \frac{r}{2}\right)} < \phi_- < \frac{3g^3\sqrt{T}}{8\pi\tilde{\lambda}}\sqrt{1+\sqrt{2}}. \tag{3.67}$$

The lower limit grows as the square root of r when $\tilde{\lambda}$ is close to its upper bound. Therefore it is valid to use (3.61) even when $\tilde{\lambda} \sim g^3$, if $\tilde{\lambda}$ is not extremely close to its upper bound. Even if $\tilde{\lambda}$ was close to its upper bound, (3.61) would be an overestimate. This would mean that the effective action just has too many terms for the wanted accuracy. From the upper bound of ϕ_-, we can see that (3.61) is never an underestimate. Therefore it is good to be used near the critical temperature.

There is also a possibility of large amounts of supercooling. In a supercooled transition, it is possible that the field value in the centre of a critical bubble is much smaller than the field value in the stable phase, $\phi_0 \ll \phi_-$. Consequently, we would be way overestimating the need for higher order terms with parametric estimates in equations (3.61) and (3.62). Here, we assume that we can expand the cubic term into a quartic polynomial:

$$-\frac{1}{12\pi}\left[\left(M_3^2+\frac{g^2T}{2}\phi^2\right)^{3/2}-M_3^3\right]=-\frac{g^2TM_3}{16\pi}\phi^2-\frac{g^4T^2}{128\pi M_3}\phi^4+\mathcal{O}\left(\frac{g^6T^3}{M_3^3}\phi^6\right). \tag{3.68}$$

This requires that

$$\phi_0^2 \lesssim \frac{2M_3^2}{g^2T} \tag{3.69}$$

as can be seen from Fig. 3.3. The ignored terms are important near the critical temperature, so the expansion should be used only for supercooled transitions. This in turn means that $\tilde{\lambda}$ must not be too close to its upper bound.

We can now simplify the notation by absorbing the expansion of the cubic term to already existing quadratic and quartic terms:

$$U(\phi)=\frac{\hat{m}^2}{2}\phi^2-\frac{\hat{\lambda}T}{4!}\phi^4+\mathcal{O}\left(\frac{g^6T^3}{M_3^3}\phi^6\right). \tag{3.70}$$

The order of $\hat{\lambda}$ is g^3 because the quartic term is dominated by the contribution from (3.68).

The extremality of the critical bubble implies that the terms are of same order in the centre of the bubble:

$$\phi_0^2 \sim \frac{\hat{m}^2}{\hat{\lambda}T}. \tag{3.71}$$

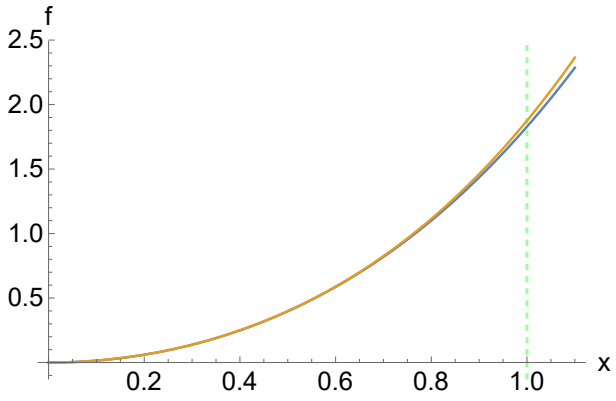

Figure 3.3: The blue plot is $f(x)=(1+x^2)^{3/2}-1$, and it represents the cubic term. The orange plot is the quartic approximation of the blue plot, and it represents the approximation in Eq. (3.68). The dashed line represents the bound from Eq. (3.69).

Comparing this with (3.69) tells the maximal order for the mass parameter to be $\hat{\lambda}T^2$, because $M_3^2 \sim g^2T^2$. A lower bound comes from the field being perturbative around $\phi = 0$. It states $\hat{\lambda}T \gg \hat{m}$. Therefore,

$$\hat{\lambda}^2T^2 \ll \hat{m}^2 \lesssim \hat{\lambda}T^2. \tag{3.72}$$

If the mass is below the range, the transition cannot be studied by perturbative methods and, if the mass is over the range, the expansion of the cubic term in Eq. (3.68) is not valid.

We have now the tools to estimate the volume of the bubble parametrically. The basis of the estimate comes from the leading gradient term containing the information from the radius:

$$R_{\text{B}} \sim \sqrt{\frac{(\boldsymbol{\nabla}\phi)^2}{\phi_0^2}}, \tag{3.73}$$

where $(\boldsymbol{\nabla}\phi)^2$ is understood as a average of the energy density contribution of the term and ϕ_0 is the value of the field in the centre of the bubble.

We can link the gradient term to the potential with the scaling argument presented in Secs. 2.2 and Sec. 4.1. From Eqs. (3.60) and (3.71), we obtain that the mass term contribution to the potential is the same order as the potential itself on the critical bubble. Thus,

$$\bar{m}^2\phi_0^2 \sim (\boldsymbol{\nabla}\phi)^2, \tag{3.74}$$

where the mass parameter $\bar{m}^2$, depending on the situation, is either m_3^2 or $\hat{m}^2$.

The volume can be expressed parametrically with the mass of the nucleating field:

$$V_{\text{B}} \sim \frac{1}{\bar{m}^3}. \tag{3.75}$$

As discussed in Sec. 3.2, there is a natural truncation point for the effective action, which is dropping contributions that are of order unity or smaller. The order of magnitude can be estimated with the form of the Lagrangian term and the volume of the critical bubble. Now, we have also an estimate for the volume in Eq. (3.75). In this thesis, we will reach this precision with transitions where the mass of the nucleating field is $\sim g^3T^2$. From Eqs. (3.61) and (3.71), we can see that $\phi_0^2 \sim T$.

3.3.2 Dimensional Reduction

The first step towards an effective description for the critical bubble is the dimensional reduction which was discussed in Subsec. 3.2.1. Here, we will conduct the procedure for the asymmetric model presented in Sec. 3.3.

The degrees of freedom that are infrared sensitive are the zero Matsubara modes of fields Φ and X. We make the following simple identification between the DoFs of the

EFT and the full theory:

$$\phi = T^{-1/2}\Phi_0, \qquad \chi = T^{-1/2}\mathrm{X}_0, \tag{3.76}$$

where ϕ and χ are three-dimensional fields of the effective field theory and Φ_0 and X_0 are the zero modes of the fields of the full theory (cf. Eq. (3.17)). The conversion factor ensures that the fields of the EFT are canonically normalized.

The effective field theory works at distances that are much longer than the inverse temperature. The identification implies that, at those distances, the correlation functions of the EFT and the FT have certain relations. For example,

$$\langle\Phi_0(\mathbf{x}_1)\Phi_0(\mathbf{x}_2)\rangle_{\mathrm{FT}} = T\langle\phi(\mathbf{x}_1)\phi(\mathbf{x}_2)\rangle_{\mathrm{EFT}}, \tag{3.77}$$

$$\langle\Phi_0(\mathbf{x}_1)\Phi_0(\mathbf{x}_2)\Phi_0(\mathbf{x}_3)\Phi_0(\mathbf{x}_4)\rangle_{\mathrm{FT}} = T^2\langle\phi(\mathbf{x}_1)\phi(\mathbf{x}_2)\phi(\mathbf{x}_3)\phi(\mathbf{x}_4)\rangle_{\mathrm{EFT}}. \tag{3.78}$$

The only internal symmetry in the full theory is the $\mathbb{Z}_2$-symmetries of the scalar fields, $\Phi \to -\Phi$ and $\mathrm{X} \to -\mathrm{X}$. This provides a constraint for the EFT action: It must also contain these symmetries. Otherwise, all terms must be included:

$$S_{\mathrm{DR}} = \int_{\mathbf{x}} \left(\frac{1}{2}(\boldsymbol{\nabla}\phi)^2 + \frac{1}{2}(\boldsymbol{\nabla}\chi)^2 + \frac{m_3^2}{2}\phi^2 + \frac{M_3^2}{2}\chi^2 + \Lambda^{2\epsilon}\frac{\lambda_3}{4!}\phi^4 + \Lambda^{2\epsilon}\frac{g_3^2}{4}\phi^2\chi^2 + \Lambda^{2\epsilon}\frac{f_3}{4!}\chi^4 + \ldots \right) + S_{\mathrm{DR,ct}}. \tag{3.79}$$

The EFT is also regularized with dimensional regularization. Therefore, the cut-off scale of the EFT, Λ, appears in the action to ensure the correct mass dimension for the couplings.

The accuracy goal was laid down at the very end of the previous subsection. To achieve the accuracy, the truncation of the action in Eq. (3.79) just drops terms marked with the ellipsis.

Dimensional regularization provides a handy trick for the matching process, as discussed in Sec. 3.2. We can regulate infrared divergences with dimensional regularization. The infrared physics of the EFT and the full theory are the same and it can be covered under the hood with the incorrect treatment. This vastly simplifies the matching. The incorrect treatment must be the same on both sides and, as a consequence, the renormalization scale of the FT has to be run to the cut-off scale of the EFT, $\mu = \Lambda$, for the matching.

One of the simplifications is that all the loop-integrals on the EFT side vanish. The mass parameters are treated perturbatively because IR-divergences are regulated with dimensional regularization. This leads to another simplification that the resummation, discussed in Subsec. 3.1.3, is done implicitly.

The mass parameter of the effective field theory is found by matching the two-point 1PI-diagrams. On the EFT side, all other contributions vanish except the renormalized mass parameter and the counterterm, $m_3^2 + \delta_{m_3^2}$. On the side of the full theory we include

all the diagrams that are needed for our accuracy goal. For example, the third diagram in Eq. (3.80) contributes to the ϕ-mass at order g^4T^2. Therefore, its ultimate contribution to the exponential suppression comes at order $g^4T^2\,\phi_0^2 \times V$. As discussed in the Sec. 3.2, the natural accuracy goal for the action is everything over the order of unity. Our goal is to achieve this accuracy with transitions that happen at $m_3^2 \lesssim g^3T^2$. This leads to $V \sim g^{-4.5}T^{-3}$ and $\phi_0^2 \sim T$ in the case that needs the most precision. Thus, the diagram is needed. We need no gradient terms which come from the external momentum. Hence, we can compute the diagrams with zero external momentum.

The diagrams needed on the side of the full theory are

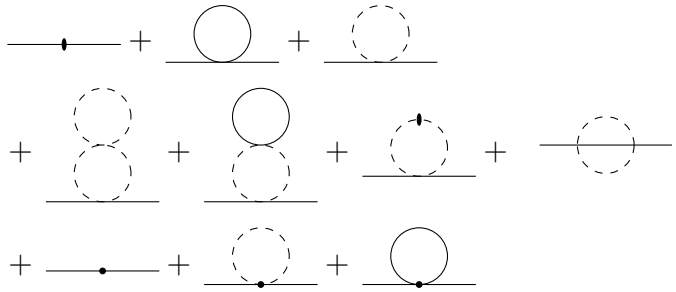

$$
\begin{aligned}
=&m^2 + \frac{g^2T^2}{24} + \frac{\lambda T^2}{24} - \frac{(g^4+fg^2)T^2 + 24g^2M^2}{24(4\pi)^2}\ln\left(\frac{e^\gamma\bar{\Lambda}}{4\pi T}\right) + \frac{g^4T^2}{4(4\pi)^2}\ln\left(\frac{A^{12}\bar{\Lambda}}{4\pi T}\right)\\
&+ \frac{g^4T^2}{8(4\pi)^2}\frac{1}{\epsilon} + \mathcal{O}(\epsilon),
\end{aligned}
\tag{3.80}
$$

where elliptical dots refer to mass insertions and spherical dots refer to counterterm insertions and $A = 1.282...$ is Glaisher's constant. $\bar{\Lambda}$ is defined in accordance with the $\overline{\text{MS}}$-scale:

$$
\bar{\Lambda}^2 = 4\pi e^{-\gamma}\Lambda^2. \tag{3.81}
$$

The diagrams are computed in App. A.1.

Now that we have computed the 1PI two-point functions, we would like to extract the mass parameter of the ϕ-field. There is a factor of temperature from Eq. (3.77). However, it disappears from our identification because we have dropped external legs from the diagrams in Eq. (3.80). This is equivalent to the kinetic term being canonically normalized due to the identification in Eq. (3.76). If the identification was more complicated, it would change the mass identification. We will see below, that there is a factor of temperature in the identification of the couplings.

We can identify in the $\overline{\text{MS}}$-scheme:

$$
\begin{aligned}
m_3^2(\Lambda) =&m^2(\Lambda) + \frac{g^2(\Lambda)T^2}{24} + \frac{\lambda(\Lambda)T^2}{24}\\
&- \frac{(g^4+fg^2)T^2 + 24g^2M^2}{24(4\pi)^2}\ln\left(\frac{e^\gamma\bar{\Lambda}}{4\pi T}\right) + \frac{g^4T^2}{4(4\pi)^2}\ln\left(\frac{A^{12}\bar{\Lambda}}{4\pi T}\right),
\end{aligned}
\tag{3.82}
$$

$$
\delta_{m_3^2} = \frac{g^4T^2}{8(4\pi)^2}\frac{1}{\epsilon}. \tag{3.83}
$$

The parameters of the full theory depend on the renormalization scale which has been run down to the cut-off scale of the effective theory. The dependence which is large enough to matter at our accuracy is shown here. The running of the FT parameters can be read from the App. B.2 and it must be able to cancel the cut-off dependence from physical results. The parameter m_3^2 is dependent on the cut-off scale Λ as can be seen from Eq. (3.89) below. However, the running is cancelled when the χ-field is integrated out in the next subsection.

For the phase transition, the most important contribution from the dimensional reduction is the second term in the three-dimensional mass parameter. It is the one restoring the $\mathbb{Z}_2$-symmetry of the ϕ-field at high temperatures. As this contribution diminishes in comparison to m^2, the symmetry breaks, resulting in a phase transition.

We can do a similar matching for χ-mass. The main difference is that less precision is needed since the χ-mass affects the effective action for the critical bubble only indirectly. The needed diagrams are

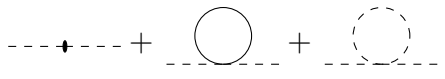

$$= M^2 + \frac{(g^2+f)T^2}{24} + \mathcal{O}(\epsilon), \tag{3.84}$$

Therefore:

$$M_3^2 = M^2 + \frac{(g^2+f)T^2}{24}. \tag{3.85}$$

Lastly, we compute the quartic couplings. The only one needing higher order corrections is the self-coupling of the ϕ-field:

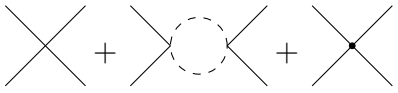

$$= \lambda - \frac{3g^4}{(4\pi)^2}\ln\left(\frac{e^\gamma \bar{\Lambda}}{4\pi T}\right) + \mathcal{O}(\epsilon) \tag{3.86}$$

Here, one cannot just identify λ_3 to be the result from above. We can see this from the dimensions of λ_3 which is one. There is an effect of multiplying the above result by the temperature:

$$\lambda_3 = \lambda(\Lambda)T - \frac{3g^4 T}{(4\pi)^2}\ln\left(\frac{e^\gamma \bar{\Lambda}}{4\pi T}\right). \tag{3.87}$$

A way of seeing this is to look at the tree-level g_3^2:

$$\int_X \frac{g^2}{4}\Phi^2 \mathrm{X}^2 \to \int_{\mathbf{x}} \frac{g^2}{4T}\Phi_0^2 \mathrm{X}_0^2 = \int_{\mathbf{x}} \frac{g^2 T}{4}\phi^2\chi^2, \tag{3.88}$$

where we have first dropped the $n \neq 0$ modes and then used the identification of the fields (3.76). This is actually the full result we need for the coupling between ϕ and χ fields.

The full result from the dimensional reduction:

$$\begin{aligned} m_3^2(\Lambda) =& m^2(\mu) + \frac{g^2(\mu)T^2}{24} + \frac{\lambda(\mu)T^2}{24} \\ & - \frac{(g^4 + fg^2)T^2 + 24g^2M^2}{24(4\pi)^2} \ln\!\left(\frac{e^\gamma \bar{\mu}}{4\pi T}\right) + \frac{g^4T^2}{4(4\pi)^2} \ln\!\left(\frac{A^{12}\bar{\Lambda}^2}{4\pi T\bar{\mu}}\right) \end{aligned} \tag{3.89}$$

$$\delta_{m_3^2} = \frac{g^4T^2}{8(4\pi)^2}\frac{1}{\epsilon}, \tag{3.90}$$

$$M_3^2 = \frac{(g^2 + f)T^2}{24} + M^2, \tag{3.91}$$

$$\lambda_3 = \lambda(\mu)T - \frac{3g^4T}{(4\pi)^2} \ln\!\left(\frac{e^\gamma \bar{\mu}}{4\pi T}\right) \tag{3.92}$$

$$g_3^2 = g^2T \tag{3.93}$$

$$f_3 = fT \tag{3.94}$$

Here, we have used the running of the parameters of the full theory (App. B.2) to replace the cut-off with the renormalization scale. There is still residual dependence on the cut-off in the mass parameter, but it will disappear from the effective action after integrating the χ-field out.

As already mentioned above, the most important effect of the dimensional reduction is the second term in the three-dimensional mass parameter. The effect of it is that the mass parameter m_3^2 can be positive even if the mass parameter of the four-dimensional theory is negative. This gives rise to the phase transition under study at

$$T^2 \approx -\frac{24m^2}{g^2}. \tag{3.95}$$

3.3.3 Integrating out the Inducing Field

In this subsection, we will first identify the hard scale. Then, we will discuss the ways this matching will be different from the matching in the previous subsection, and how we will perform the matching. We will then compute the effective action that describes the critical bubble and gives the exponential suppression of the nucleation rate. At the end, we we will discuss the problems of double counting and complex actions.

In the previous subsection, we integrated out the momentum scale of temperature. However, there can still be fluctuation scales which have much shorter range than the extent of the critical bubble. In the asymmetric model, this scale can be the inverse of χ-mass, $M_3^{-1} \sim g^{-1}T^{-1}$. In situations where the mass of the nucleating ϕ-field has gone down to $m_3^2 \lesssim g^3T^2$, the extent of the critical bubble is larger than the correlation length of χ. Hence, the χ-field is a heavy field to be integrated out. Even if the mass of the ϕ-field had not supercooled much below the mass of χ-field, the latter field can become

heavy through its coupling to the ϕ-field due to the field value of ϕ (cf. Eq. (3.61)). This type of a situation is handled in the next subsection.

This time we will not explicitly construct an effective action and carry out the matching as in the previous section. It would be incredibly messy. Here, the contribution to the χ-mass from coupling to the ϕ-field can be as large as M_3^2. Therefore, adding extra ϕ^2-legs to a diagram does not change the order of the diagram and the series of diagrams must be resummed. Doing the matching in the previous way, would lead to matching n-point functions with n being every even number.

Instead of matching n-point functions, we will be matching the 1PI-actions of ϕ-field. This method allows two nice simplifications: We will see below that the effective action describing the critical bubble is just the 1PI-action of the ϕ-field, in which the IR-physics is regulated with dimensional reduction rather than with the resummed ϕ-mass. The other simplification is an easy way of resumming diagrams for the effective potential part [33].

The resummations can be done by computing a diagram with no external ϕ^2-legs in the χ-propagators. In the result, a replacement $M_3^2 \to M_3^2 + \frac{g^2T}{2}\phi^2$ is done. This resums effectively the ϕ^2-legs in the χ-propagators. The trick basically comes from the fact that the mass of χ-field at $\chi = 0,\ \phi \neq 0$ looks like $\frac{1}{2}\Big(M_3^2 + \frac{g^2T}{2}\phi^2\Big)\chi^2$ in the action in Eq. (3.79). In App. A.3, we will go through the resummation of the one-loop effective potential and show that this procedure works also for the first gradient term on one-loop level.

Another convolution in this matching is the parametric power counting suggests, that there is a need for the first term in the derivative expansion. The two scales, the masses of the ϕ- and the χ-field, are not that widely separated. This means that the diameter of the bubble and the characteristic length scale of χ-fluctuations are close enough that the gradient term caused by the χ-field is needed. However, the numerical results in Subsec. 4.3.2 seem contradict this, as the contribution from the derivative term is rather small in comparison to the whole exponential suppression.

We will once again employ the strict perturbation expansion. This time, it is important to notice that the χ-mass cannot be treated perturbatively, because χ does not appear in the effective theory. Only the IR-physics of ϕ-field are on both sides of the matching. Therefore, only the ϕ-mass can be treated perturbatively. To get to do the strict perturbation theory, the cut-off of the former effective theory must be run down to the scale of the χ-mass so that it becomes the cut-off of the new effective theory $\Lambda \sim M_3$. However, this will not affect how the matching is done.

The 1PI effective action to the wanted accuracy from the full theory side is:

$$S_{\text{1PI}}[\phi] = S_{\text{DR},\phi}[\phi] + \quad + \quad + \quad , \tag{3.96}$$

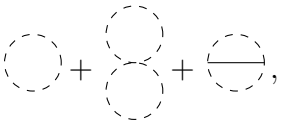

where all the χ-propagators are resummed with external legs of ϕ. The first derivative expansion term from the first diagram is included. In the last diagram, the ϕ-propagator is massless due to the strict pertubation theory.

On the side of the new effective theory, there is only the tree-level action. This comes from the strict perturbation theory in the ϕ-mass: All the loop-integrals on the side of the new EFT are scale free and vanish in dimensional regularization:

$$S_{\text{1PI}}[\phi] = S_{\text{eff}}[\phi]. \tag{3.97}$$

We get the result for the action with which the bubble nucleation is computed:

$$S_{\text{eff}}[\phi] = S_{\text{DR},\phi}[\phi] + \quad + \quad + \quad . \tag{3.98}$$

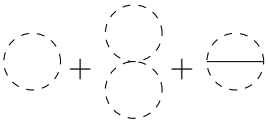

The base cases have been computed in App. A.2. For the potential part we can readily use the substitution trick from above and the resummation of the gradient term has been shown in App. A.3. In the appendix, there is also computation of one-loop resummation. The results for the needed hard diagrams are

$$= \int_{\mathbf{x}} \left[-\frac{1}{3(4\pi)} \left(M_3^2 + \frac{g^2 T \phi^2}{2} \right)^{3/2} + \frac{1}{96(4\pi)} \frac{g^4 T^2 \phi^2}{\left(M_3^2 + \frac{g^2 T \phi^2}{2} \right)^{3/2}} (\boldsymbol{\nabla}\phi)^2 \right], \tag{3.99}$$

$$= \int_{\mathbf{x}} \frac{fT}{8(4\pi)^2} \left(M_3^2 + \frac{g^2 T}{2} \phi^2 \right), \tag{3.100}$$

$$= -\int_{\mathbf{x}} \frac{g^4 T^2}{8(4\pi)^2} \left[\frac{1}{2\epsilon} + \ln \left(\frac{\bar{\Lambda}^2}{4\left(M_3^2 + \frac{g^2 T}{2} \phi^2 \right)} \right) + 1 \right] \phi^2. \tag{3.101}$$

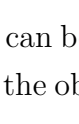

An important point to note is that although the diagrams on the left are non-local, they can be approximated via local gradient expansion on the right. This is due to the fact that the obtained EFT describes physics at longer length scale than the non-locality of the diagrams. The diagrams look local on the longer length scale. The gradient expansion is done for the one-loop diagram in App. A.3. There is already a hint of this when computing the sunset diagram in App. A.2, because the base case of the diagram is already non-local.

The only gradient term, that seems to be needed, is from the one-loop level. We can estimate its size parametrically to be $g^4 T^3$ in the case where $m_3^2 \sim g^3 T^2$. The gradient

part gives $(\boldsymbol{\nabla}\phi)^2 \sim m_3^2\phi^2$ (Eq. (3.74)). Also, $\phi_0^2 \sim T$ and $M_3^2 \sim g^2T^2$ as we saw in Subsec. 3.3.1. Comparing the size of the Lagrangian term to the volume of the critical bubble, $V \sim m_3^{-3}$, we see that the gradient term is, just barely, over the order of unity.

Physically, the most important contribution from the hard scale is the one-loop potential term. It is the one responsible for the first orderedness of the phase transition. When the value of ϕ grows, the term decreases the effective potential. At the critical temperature, this might be enough for the global minimum to jump off from $\phi = 0$, producing a first-order transition.

The sunset diagram provides a nice cross-check for the calculation. The divergences and cut-off dependence related to the χ-field should vanish and they indeed do. The divergence in the sunset diagrams cancels against the mass counterterm and the cut-off in the logarithm cancels the cut-off running of the ϕ-mass parameter. At this order, the effective action describing the critical bubble does not depend on the cut-off and contains no divergences.

The full result for the effective action is

$$S_{\text{eff}} = \int_{\mathbf{x}} \left\{ \frac{Z(\phi)}{2}(\boldsymbol{\nabla}\phi)^2 + \frac{\tilde{m}^2(\phi)}{2}\phi^2 - \frac{1}{3(4\pi)}\left[\left(M_3^2 + \frac{g^2T\phi^2}{2}\right)^{3/2} - M_3^3\right] + \frac{\lambda_3}{4!}\phi^4 \right\}, \tag{3.102}$$

$$Z(\phi) = 1 + \frac{1}{48(4\pi)} \frac{g^4T^2\phi^2}{\left(M_3^2 + \frac{g^2T\phi^2}{2}\right)^{3/2}}, \tag{3.103}$$

$$\begin{aligned}\tilde{m}^2(\phi) =& m^2 + \frac{g^2T^2}{24} + \frac{\lambda T^2}{24} + \frac{fg^2T}{8(4\pi)^2} - \frac{g^4T^2}{4(4\pi)^2} \\ & - \frac{(g^4 + fg^2)T^2 + 24g^2M^2}{24(4\pi)^2} \ln\left(\frac{e^\gamma \bar{\mu}}{4\pi T}\right) + \frac{g^4T^2}{4(4\pi)^2} \ln\left(\frac{A^{12}\left(M_3^2 + \frac{g^2T}{2}\phi^2\right)}{\pi T\bar{\mu}}\right),\end{aligned} \tag{3.104}$$

$$M_3^2 = M^2 + \frac{(g^2 + f)T^2}{24}, \tag{3.105}$$

$$\lambda_3 = \lambda T - \frac{3g^4T}{(4\pi)^2} \ln\left(\frac{e^\gamma \bar{\mu}}{4\pi T}\right). \tag{3.106}$$

This is a kind of culmination point of the thesis: We have finally obtained the effective action which describes the critical bubble to the desired precision! The action has some nice features which will be discussed below. It is real for any configuration of the ϕ-field. Also, it is not divergent and does not depend on the cut-off Λ.

In analytical treatments of bubble nucleation, there has been a problem of double counting, meaning that the effects of some fluctuations have been taken into account twice. By employing the framework of effective field theory, we can eradicate this problem: Some fluctuations belong into the effective action and others into the determinants of the prefactor. In this example, all the χ-fluctuations went into the effective action. So do some

ϕ-fluctuations as well. One might be alerted by the fact that there is the ϕ-propagator appearing in the sunset diagram in Eq. (3.98). However, it is nothing to be worried at all. In the diagram, also the IR of the propagator was regulated with dimensional regularization. Therefore, the diagram contains only momenta above the cut-off scale of the resulting EFT. The sunset diagram, in which the ϕ-propagator has soft momentum can be constructed by contracting two external ϕ-legs from the one-loop diagram of χ in Eq. (3.98). Therefore, the EFT contains the contribution of the sunset with a soft ϕ-momentum. This is true also on higher loop-levels: The effective action will attain only diagrams, where the ϕ-momentum is hard due to mixing with χ-propagators and therefore they, indeed, should be included into the effective action.

Another problem, related to the double counting, has been the problem of complex action. The critical bubble is the saddle-point of the effective action, which comes from it being the easiest way of a metastable state to jump over to the stable state. This loses its meaning if the action has complex values. Also, the nucleation rate cannot be complex. Here, we have demonstrated that there is no imaginary part to the effective action. The imaginary part can only come from the second derivative of the effective potential of the ϕ-field being negative. Only the ϕ-propagators with hard momentum can enter the effective action. Thus, there will be no imaginary part to the action.

The action in Eq. (3.102) contains no counterterms nor any dependence on the cut-off scale of the EFT, even though its precision is enough for the determinant of the pre-factor in Eq. (2.40). This is a consequence of the fact that the one-loop diagram has no logarithmic UV-divergence in three dimensions. Therefore, it is not divergent in dimensional regularization. This is no longer true if the nucleation rate is wanted up to two-loop level in the nucleating field due to the sunset diagram containing a logarithmic divergence. The divergences obviously cancel from the nucleation rate, but there might be a problem coming from the critical bubble depending on the cut-off scale. One might imagine that the cut-off scale dependence goes away when the fluctuations around the critical bubble have been taken into account. However, the problem is minuscule. For it to even matter, one has to first be able to compute the fluctuation determinants and also solve the time-evolution part of the nucleation rate.

3.3.4 Cubic Anisotropy Model

We hop onto studying a different region of the parameter space of the two scalar model, the cubic anisotropy model. Nucleation rate in the model has been studied on the lattice in Ref. [34]. However, the comparison with lattice data remains as future work. The transition was also studied there via integrating out all the fluctuations. To the order that we compute the effective action, the results are the same. This is because the fluctuations

of the nucleating field contribute very little to the free energy. The transition has also been studied via coarse grained potential in Ref. [31], where the method breaks down due to the fluctuation determinants of the inducing field. With our methods, the inducing field is integrated out leaving no fluctuation determinants. However, this poses another problem, because the inducing field is light in the symmetric phase. This is discussed at the end of this subsection. We will first introduce the cubic anisotropy model and the two steps of EFT. Then, we discuss the nature of the symmetry breaking transition with different parameter values (Refs. [35, 36, 37]). We study how the EFT, that we created for the model, breaks down when the transition is no longer strongly first order.

In the cubic anisotropy model, the parameters of the full action in Eq. (3.44) have been set according to

$$M^2 = m^2, \qquad f = \lambda. \tag{3.107}$$

The effect is that the Φ- and the X-field are symmetric. In addition to the $\mathbb{Z}_2$-symmetries of the fields, there is also symmetry of rotating the field basis by $\pi/2$ radians:

$$\begin{pmatrix} \phi \\ \chi \end{pmatrix} \to \begin{pmatrix} -\chi \\ \phi \end{pmatrix} \tag{3.108}$$

One might be worried that since the fields are symmetric, neither one can be integrated out consistently. However, if there is a strong first-order transition, a bubble must break the symmetry during nucleation. One field nucleates and the other becomes heavy on the bubble. We will return to this matter below.

The model has another peculiarity that it maps onto itself with rotations of $\pi/4$ radians in the field space:

$$\begin{pmatrix} \phi \\ \chi \end{pmatrix} \to \frac{1}{\sqrt{2}} \begin{pmatrix} 1 & -1 \\ 1 & 1 \end{pmatrix} \begin{pmatrix} \phi \\ \chi \end{pmatrix} \tag{3.109}$$

The shift in the parameter values that corresponds to the rotation is

$$\lambda \to \frac{1}{2}(\lambda + 3g^2), \qquad g^2 \to \frac{1}{2}(\lambda - g^2). \tag{3.110}$$

This means that there are two sets of parameters for the cubic anisotropy model that describe the same system. There is one exception which is the $O(2)$-symmetric model, $\lambda = 3g^2$, in which the transformation does nothing. There can be a strong first-order transition at $\lambda \ll g^2$ and correspondingly, with $g^2 \approx -3\lambda$. For us, the region $\lambda \ll g^2$ is much more convenient since the transition happens to the direction of a field variable. With $g^2 \approx -3\lambda$, the direction would be rotated by $\pi/4$ and it would be between the field variables.

Let us now move onto summarizing the two steps of integrating out. Both of them are basically done in Subsecs. 3.3.2 and 3.3.3. There is only a little bit of tweaking. We will also discuss one of the fields becoming heavy.

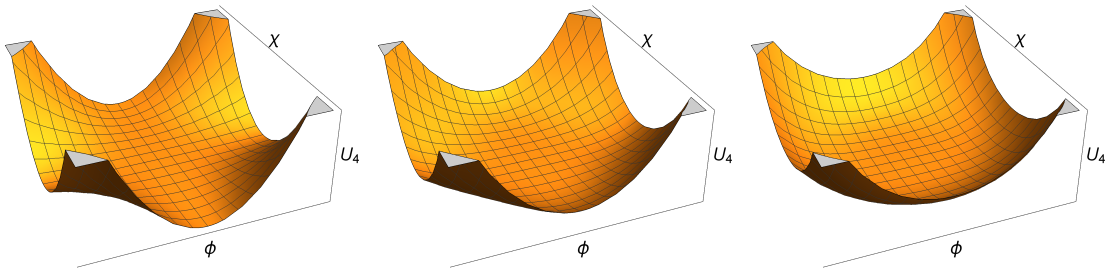

Figure 3.4: The quartic part of the potential plotted. The first figure has a strong cross-coupling, the middle figure has two uncoupled fields (in the diagonal direction) and the last figure has two fields with $O(2)$-symmetry. The figures are in order of increasing λ_3/g_3^2. A strong quartic cross-coupling induces a large contribution to the mass of the field that is not nucleating, as the first figure illustrates.

We can perform the dimensional reduction for the model basically the same way as we did for the asymmetric model in Sec. 3.3.2. Only minor details need to be fixed: $M_3^2(\Lambda) = m_3^2(\Lambda)$, $f_3 = \lambda_3$ and no need for the term with fg^2 for the mass parameter. The first two come from the symmetry between the fields and the last one follows from the fact that f has to be much smaller than the cross-coupling for there to be a first-order transition (cf. (3.46)). The form of the potential in the dimensionally reduced EFT is

$$U_{\text{DR}} = m_3^2(\phi^2 + \chi^2) + \frac{\lambda_3}{4!}(\phi^4 + \chi^4) + \frac{g_3^2}{4}\phi^2\chi^2. \tag{3.111}$$

The second step is to integrate out heavy fields. This is a bit more subtle than in the treatment we did for the asymmetric model. Here, the other field is not heavy in the symmetric phase but becomes one due to coupling to the field nucleating a bubble. This is demonstrated in Fig. 3.4 where the quartic part of the potential in Eq. (3.111) is shown. The leftmost potential corresponds to one with a strong first-order transition. There, we can see that fluctuations orthogonal to the nucleating field gain mass from the quartic coupling. We can always choose to label the nucleating field with ϕ and so the χ-field gains mass from the Lagrangian term $\frac{g_3^2}{4}\phi^2\chi^2$ on the bubble. Because the field integrated out must be heavy, we get that on the bubble $\frac{g_3^2}{2}\phi_0^2 \gg m_3^2$. Otherwise, the χ-field cannot be integrated out.

Assuming that χ can be integrated out, the result for the action which describes the

critical bubble is

$$S_{\text{eff}} = \int_{\mathbf{x}} \left\{ \frac{Z(\phi)}{2} (\boldsymbol{\nabla}\phi)^2 + \frac{\tilde{m}^2(\phi)}{2}\phi^2 - \frac{1}{3(4\pi)} \left[\left(M_3^2 + \frac{g^2 T \phi^2}{2} \right)^{3/2} - M_3^3 \right] + \frac{\lambda_3}{4!}\phi^4 \right\}, \tag{3.112}$$

$$Z(\phi) = 1 + \frac{1}{48(4\pi)} \frac{g^4 T^2 \phi^2}{\left(M_3^2 + \frac{g^2 T \phi^2}{2} \right)^{3/2}}, \tag{3.113}$$

$$\begin{aligned} \tilde{m}^2(\phi) =& m^2 + \frac{g^2 T^2}{24} + \frac{\lambda T^2}{24} - \frac{g^4 T^2}{4(4\pi)^2} \\ & - \frac{g^4 T^2 + 24 g^2 m^2}{24(4\pi)^2} \ln\left(\frac{e^\gamma \bar{\mu}}{4\pi T} \right) + \frac{g^4 T^2}{4(4\pi)^2} \ln\left(\frac{A^{12} \left(M_3^2 + \frac{g^2 T}{2}\phi^2 \right)}{\pi T \bar{\mu}} \right), \end{aligned} \tag{3.114}$$

$$M_3^2 = m^2 + \frac{(g^2 + \lambda) T^2}{24}, \tag{3.115}$$

$$\lambda_3 = \lambda T - \frac{3 g^4 T}{(4\pi)^2} \ln\left(\frac{e^\gamma \bar{\mu}}{4\pi T} \right). \tag{3.116}$$

The action itself looks like the equivalent for the asymmetric model (3.102) but the parameters have slightly different forms. The most important distinction between the two is that here M_3^2 alone does not make the χ-field heavy and can be very small near the transition.

Here, we have truncated the next-to-leading term in M_3^2, as its contribution is below the order of unity. However, it is interesting in few regards. The next order can become somewhat important as the M_3^2 decreases with temperature. Thus, it can be important regarding to the convergence of the derivative series. As discussed in the end of the subsection, the series is an indicator of whether the poor handling of the symmetric phase gives a large error. Another interesting point comes from the next order depending on the cut-off. This can be seen from Eq. (3.89), in which the three-dimensional ϕ-mass in the asymmetric model is shown. The running is resummed in the one-loop χ-diagram into the cubic term. The leading order can be cancelled with the basketball diagram with two χ- and two ϕ-propagators. However, the full running and divergence can be countered only by resumming the one-loop χ-diagrams with insertions of the following sunset:

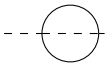 . (3.117)

There is no momentum scale separation between the insertions and the ring and hence, the resummation is very non-trivial. Leaving the resummation undone leaves information of the higher order contributions to the running of M_3^2 with the cut-off scale. If the running is large, the χ-field is non-perturbative, which signals that the perturbative methods do not work, as the nucleating field ϕ is symmetric with the inducing field χ.

Let us now discuss a bit about the nature of the transition, and how it can be seen from the potential of the action. The order of the phase transition has been studied

with the three-dimensional theory in Eq. (3.111) via renormalization group methods in Refs. [35, 36] and via Monte Carlo simulations in Ref. [37]. The results were that there is a second order transition with $0 \leq g_3^2 \leq \lambda_3$ and a first-order transition with $g_3^2 < 0$ or $\lambda_3 < g_3^2$. The borderline cases correspond to two uncoupled scalars. The three situations are illustrated in Fig. 3.4.

The first-order transitions that are near the second order transition cannot be studied via perturbative methods, because the transition is weak, so the expansion around the critical bubble fails due to very differently shaped bubbles contributing to the rate. The question is how can one see this within our method. Let us look at the potential in the action of Eq. (3.112), but stripping a bit of complexity down by $M_3^2 = \tilde{m}^2$ and setting the cross-coupling to be twice the border case, $g_3^2 = 2\lambda_3$:

$$U_{\text{eff}}(\phi) = \frac{\tilde{m}^2}{2}\phi^2 - \frac{1}{3(4\pi)}\left[\left(\tilde{m}^2 + \lambda_3\phi^2\right)^{3/2} - \tilde{m}^3\right] + \frac{\lambda_3}{4!}\phi^4. \tag{3.118}$$

We can scale out the mass parameter by introducing dimensionless parameters $\tilde{x} = \tilde{m}x$, $\tilde{\phi}^2 = \phi/\tilde{m}$, $\alpha = \lambda_3/\tilde{m}$:

$$\tilde{U}_{\text{eff}}(\tilde{\phi}) = \frac{1}{2}\tilde{\phi}^2 - \frac{1}{3(4\pi)}\left[\left(1 + \alpha\tilde{\phi}^2\right)^{3/2} - 1\right] + \frac{\alpha}{4!}\tilde{\phi}^4. \tag{3.119}$$

The critical temperature is at $\lambda_3/m_3 = \alpha \approx 9.66$. This parameter indicates if the self-interaction of the three-dimensional fields is small enough to be treated perturbatively, and it clearly is not small enough. Neither is the cross-coupling perturbatively small: $g_3^2/m_3 \approx 19.3$. This tells us that perturbation theory breaks down due to too large fluctuations, and the nucleation rate cannot be obtained via perturbative methods. If we were to trust the effective potential, the mass of the inducing field would still be rather heavy in the broken phase at the critical temperature, even though the transition is very weak: $1 + \alpha\tilde{\phi}_-^2 \approx 8.23$.

In the cubic anisotropy model, the inducing field is light in the symmetric phase but heavy on a bubble. As discussed in Sec. 3.2, this gives us rights to integrate the field out on top of the bubble but not in the symmetric phase. Therefore, the symmetric phase is not described by the EFT properly. This clearly affects the form of the bubble at its outskirts, but the hope is that the ill-handling the symmetric phase would not affect the bubble as a whole too much. This could be true due to the fact that the tails do not contribute substantially to the exponential suppression from the critical bubble. Also, the outskirts of the critical bubble configuration are overrun by the thermal fluctuations in the symmetric phase and hence, it is not physical in a sense.

We would like to be able to quantify the error. Here, we propose a diagnostic for the tails causing the treatment to fail. The ill-handling of the symmetric phase causes the derivative expansion of the χ-diagrams to diverge in the phase. Therefore, the failure

should be visible from the derivative expansion of the effective action evaluated on the critical bubble. We already have the first order in the derivative expansion of the one-loop diagram in $Z(\phi)$, Eq. (3.113). We can get a hint if the series is broken by computing the second term in it. We will not compute the full second order in the one-loop derivative series, but hints of the derivative series breaking can be obtained already from partial second order:

$$\int_{\mathbf{x}} -\frac{1}{2560(4\pi)} \frac{g^4 T^2}{\left(M_3^2 + \frac{g^2 T}{2}\phi^2\right)^{5/2}} \left(\boldsymbol{\nabla}^2 \phi^2\right)^2. \tag{3.120}$$

The base case in the resummation is calculated in App. A.4, but the resummation is just assumed to work as in the effective potential, i.e. $M_3^2 \to M_3^2 + \frac{g^2 T}{2}\phi^2$ from the base case to the resummed term. The derivative term should at least give a good understanding on the size of the next order in the derivative expansion. If the derivative series works properly, this term should be much smaller on the critical bubble than the derivative contribution in $Z(\phi)$. This comparison is done in Subsec. 4.3.2.

Note, that including more extra derivative terms to the effective action actually changes the shape of the critical bubble. As a consequence, the derivative series does not break, if it is included to the action. The breakdown of the series only happens, if it is evaluated on a critical bubble obtained from an effective action without it. If the description of the critical bubble is good, even though the symmetric phase is ill-handled, the inclusion of the series should not change the centre regions of the critical bubble nor the exponential suppression from it.

In Ref. [31], the nucleation rate was studied via a coarse grained potential. There, it was noted that the fluctuation determinant of the inducing field becomes exponentially large due to being heavy on the bubble, which causes their treatment to fail. With our methods, the χ-field has to be integrated out due to being heavy and therefore, it does not receive a fluctuation determinant of its own. The exponential effects of the fluctuations are already in the effective action. However, the weak point of the treatment moves to the symmetric phase, as discussed above.

3.3.5 Breakdown of the EFT

In cases where there are uncontrollable fluctuations, the EFT breaks down. We will now discuss the breakdown of the EFT in the light of the previous two examples. First, we will focus on problems relating to the fluctuations of the nucleating field and then, to the fluctuations of inducing fields.

The method at hand relies on the importance of the critical bubble. Next-to-leading contributions are obtained via the saddle-point approximation and they end up in fluctuation determinants (cf. Eq. (2.40)). The determinant computed around the critical bubble

contains contributions from configurations that are small deformations of the critical bubble. If the barrier between the stable and metastable phases is lowered, the deformations of the critical bubble are less and less suppressed. Consequently, the determinant becomes more and more important compared to the suppression from the critical bubble. This has been studied in Ref. [38] near spinodal decomposition, where the barrier between the stable and metastable phases vanishes completely. The determinant is just the next-to-leading correction in a series that corresponds to the loop expansion in small coupling around the critical bubble configuration. At some point, this expansion breaks down if the barrier is lowered enough. This corresponds to the transition being driven by regular fluctuations. We can study this breakdown through the coupling expansion and then link it to the properties of the walls of the critical bubble.

In three dimensions, the expansion parameter in the small coupling expansion is not just the quartic coupling because it is dimensionful. The parameter is the coupling divided by the mass. In the previous subsection, where we studied the cubic anisotropy model, we noted that this expansion parameter is very large when the transition is second order. This correspond to the fluctuations of the nucleating field being non-perturbative.

Let us now see how this relates to the critical bubble. In the thin-wall limit, it is possible to have as sturdy a critical bubble as one wants, granted that there is some barrier between the stable and the metastable phases (cf. Eq. (3.42)). Therefore, it is not sufficient to just look at the critical bubble to check the order of the transition. It is rather the relation between the determinant and the bubble. With a thin-wall bubble the determinant contains deformations of the wall of the bubble. A thick-wall bubble is entirely made out of its wall and therefore, we can study the walls via thick-wall bubbles.

The thick-wall case in the asymmetric model was studied in Subsec. 3.3.1. Here, we will study the situation with weak transitions in the asymmetric model, but this applies generally to both models, the asymmetric and the cubic anisotropy. Let us look at the situation in which there is no exponential suppression coming from the critical bubble, i.e. $S \sim 1$. Using the hatted notation that was introduced for the Taylor series coefficients of the effective potential in a weak transition, as in Eq. (3.70), we get that the exponential suppression from the critical bubble is parametrically

$$S \sim \frac{1}{\hat{m}^3} \times \hat{m}^2 \phi_0^2 = \frac{\phi_0^2}{\hat{m}}. \tag{3.121}$$

Next, we can use the parametric order of ϕ_0 from Eq. (3.71):

$$S \sim \frac{\hat{m}}{\hat{\lambda} T}. \tag{3.122}$$

With $S \sim 1$, this gives that the expansion parameter in three dimensions is $\mathcal{O}(1)$ and hence, not small any more.

A thick-wall bubble is a configuration that goes from the previous phase to the future phase. In the thin-wall limit, a thick-wall bubble is a subcritical bubble, but still interpolates between the phases. When a thick wall bubble has no exponential suppression, it means that it is at the order of regular fluctuations. This is an illustration that, when the expansion parameter becomes large in the metastable phase, regular fluctuations can interpolate between the two phases. Therefore, the phase transition is not driven by critical bubbles.

As discussed in Sec. 3.2, the breakdown of the EFT can come from light fluctuations being crucial. This can happen in two ways. The first one is that in the thin-wall limit, the light fluctuations are important within the plateau of the thin-wall bubble, which is discussed more in Subsec. 3.2.3. The other way is that the transition is solely induced by light fluctuations. The cubic anisotropy model might have been an example of this, because the inducing field is light at least in the symmetric phase. It was however found that the perturbative treatment breaks down due to the nucleating field being non-perturbative, before the inducing field becomes light in the broken phase. It might be that the latter happens only in situations, where the perturbative methods would not even be applicable for the reason that the nucleating field is strongly coupled near the transition.

3.3.6 Thin-Wall Limit

In this subsection, we will discuss the thin-wall limit for our examples. The limit was explored more generally in Subsec. 3.2.3. In this limit, the free energy difference of the two phases is very small. The problem of the limit arises, when the light fluctuations, that can relax on the plateau of a thin-wall bubble, become important. An EFT cannot be created, because the light fluctuations cannot be integrated out within the walls. Here, we will identify the dominant light fluctuations and compute the leading contribution to the free energy.

The only light field in the example models is the nucleating field ϕ. Therefore, the leading contribution to the free energy difference between the phases is the one-loop of ϕ, which can be computed very similarly to the one-loop of χ. The result is

$$-\frac{1}{3(4\pi)}\Big(U''_{\text{eff}}(\phi_-)^{3/2} - U''_{\text{eff}}(0)^{3/2}\Big), \tag{3.123}$$

where U_{eff} is the potential of the effective action of the theory under study, i.e. either potential from Eq. (3.102) or (3.112). The difference of terms comes from the fact that this contribution goes into the pressure difference shown in Eq. (3.39).

4. Numerical Methods

We have now developed a formalism for finding the exponential suppression from the Boltzmann factor of the critical bubble. However, the work is still incomplete. There are multiple interesting claims to be checked: the importance of different contributions such as the wave function renormalization in Eqs. (3.103) and (3.113), the convergence of the gradient expansion in the cubic anisotropy model, discussed in Subsecs. 3.3.4 and 3.2.2, and the cross-over from the EFT to the extension in the thin-wall limit discussed in Subsec. 3.2.3. We won't be able to truly study the last one because we are not going to compute the fluctuation determinants. However, it should be observable to some extent from the exponential suppression of the critical bubble.

We need to be able to solve for the critical bubble and its Boltzmann factor to get to examine the points above. This has been done traditionally by solving the equation of motion of the critical bubble in Eq. (2.15) numerically and evaluating the action on top of the solution. For us the equation of motion would be further complicated by wave function renormalization in Eqs. (3.103) and (3.113).

We will solve for the critical bubble numerically using a formalism, created in Ref. [16], which we will call the tunnelling potential method. In the formalism, the quest of finding the saddle-point of an action corresponding to a critical bubble is reshaped into a minimization problem. This is extremely useful since minimization is much easier to perform numerically to arbitrary precision. It has also two other advantages: It can be generalized to multi-field situations [39] and it can probe deep into the thin-wall limit.

However, we shall see that the minimization process is not without any complications, and the chosen numerical implementation is not perfect as discussed at the end of Subsec. 4.2.1. The slight suboptimality leaves tiny defects into the centres of obtained bubble configurations, which can be seen Fig. 4.6. Also, the tails of the bubbles are not described with high precision. With this being said, the results for actions should still be very accurate.

The tunnelling potential method is reviewed and generalized a bit in Sec. 4.1. In Ref. [39], there is a numerical implementation of the tunnelling potential method. We use a slightly improved implementation which is explained in Sec. 4.2. Numerical results, for example, to the points laid down above can be found from Sec. 4.3.

4.1 Tunnelling Potential Method

We will now study a formalism for solving a critical bubble that we call the tunnelling potential method. Its essence is to create a minimization problem that gives the critical bubble configuration and the exponential suppression, instead of solving the critical bubble from its equation of motion. In this section, we will first review the basic method from Ref. [16] and then generalize it to a situation in which multiple real scalars can have kinetic mixing. A generalization to multiple scalars has already been done in Ref. [39]. The review is very brief and contains only the key elements, but the generalization is done in more detail.

The idea of the formalism is to define an auxiliary function U_t (cf. Fig. 4.1), called the tunnelling potential, and a functional $S_\mathrm{t}[U_\mathrm{t}]$, the tunnelling action, so that the minimum of the tunnelling action gives the exponential suppression from the critical bubble. If the Euclidean action describing the critical bubble is

$$S_\mathrm{E}[\phi] = \int \mathrm{d}^d x \left(\frac{1}{2}(\boldsymbol{\nabla}\phi)^2 + U(\phi)\right), \tag{4.1}$$

where ϕ is a real scalar in d dimensions, the corresponding tunnelling action is

$$S_\mathrm{t}[U_\mathrm{t}] = \frac{(2\pi)^{d/2}(d-1)^{d-1}}{\Gamma(d/2+1)} \int_{\phi_+}^{\phi_0} \mathrm{d}\phi \, \frac{\Big(U(\phi) - U_\mathrm{t}(\phi)\Big)^{d/2}}{\Big(-U_\mathrm{t}'(\phi)\Big)^{d-1}}, \tag{4.2}$$

where the integration bounds are from the metastable field value ϕ_+ to the field value at the centre of the bubble ϕ_0 and the dash represents a differentiation with respect to the field value. It is important to note that the tunnelling action is minimized with respect to both U_t and ϕ_0.

The tunnelling potential has to satisfy four things:

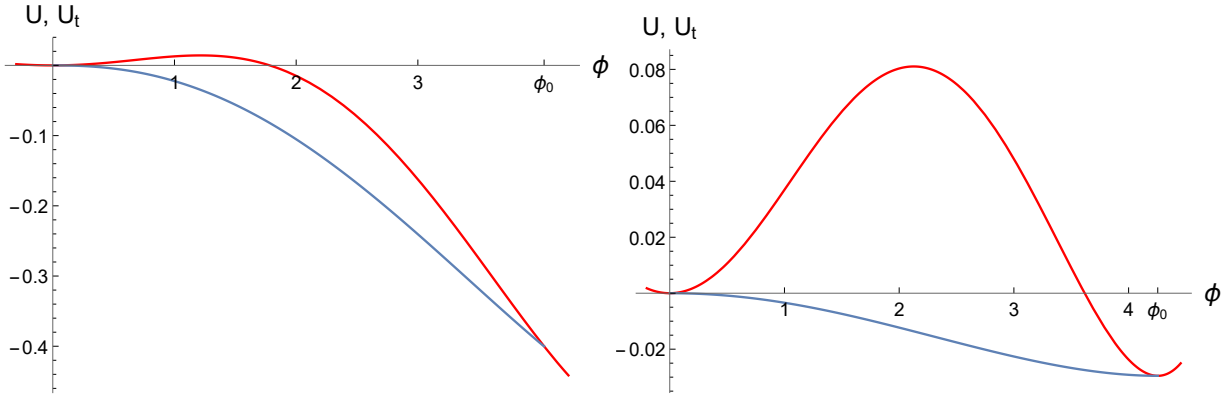

Figure 4.1: Tunnelling potential solutions, shown in blue, for potentials in red. ϕ_0 is the field value at the centre of a bubble. The figure on the left corresponds to a thick-wall bubble and the one on the right corresponds to a thin-wall bubble. The related configurations are shown in Fig. 4.4.

- It is defined on the interval $[\phi_+, \phi_0]$.
- Its boundary conditions are: $U_\mathrm{t}(\phi_+) = U(\phi_+)$ and $U_\mathrm{t}(\phi_0) = U(\phi_0)$.
- $U_\mathrm{t}(\phi) \leq U(\phi)$.
- It is a monotonous function.

Everything else follows from the minimization of the tunnelling action. The last three points will be shown in the generalization.

The information of the critical bubble configuration is contained in the tunnelling potential. It is obtained via solving the radial coordinate corresponding to a field value:

$$r(\phi) = -(d-1)\frac{\sqrt{2\Big(U(\phi) - U_\mathrm{t}(\phi)\Big)}}{U_\mathrm{t}'(\phi)}. \tag{4.3}$$

We will now move onto the generalization of the method to the case where there are multiple real scalars that can mix kinetically. The Euclidean action is

$$S_\mathrm{E}[\phi] = \int \mathrm{d}^d x \left(\frac{1}{2}\boldsymbol{\nabla}\phi_a \, Z_{ab}(\phi)\boldsymbol{\nabla}\phi_b + U(\phi)\right), \tag{4.4}$$

where ϕ is a contains all the fields as its components and indices a and b run over the components. We need the Z-matrix to depend on the field values because we will apply the formalism to the models in the Sec. 3.3. The matrix is required to be positive definite for the stability of the theory and it can be assumed to be symmetric without a loss of generality.

The key points from the base version of the tunnelling potential formalism remain very close to the original ones in the generalization. However, the situation is somewhat more complicated because the field value has now n components, one for each scalar. Therefore, the integration path in the tunnelling action might not be as simple as $[\phi_+, \phi_0]$ in the case of a single real scalar. The path starts from the metastable value ϕ_+ and then, it follows the field values on the critical bubble configuration to the end, which is the field value at the centre of the critical bubble ϕ_0.

As before, the tunnelling potential is defined along the integration path. The other three conditions of the tunnelling potential remain unaltered, which will be shown around Eqs. (4.38), (4.37) and (4.39). The equation for the radius of a certain field value seems exactly the same before in Eq. (4.21), but there is slight modification since the dash is not defined the same way as before.

The tunnelling action could be found from bottom up as is done in Ref. [39], but we will start from the correct action, which is

$$S_\mathrm{t} = \frac{(2\pi)^{d/2}(d-1)^{d-1}}{\Gamma(d/2+1)} \int_{\alpha_+}^{\alpha_0} \mathrm{d}\alpha \left(\frac{\mathrm{d}\phi_a}{\mathrm{d}\alpha} Z_{ab} \frac{\mathrm{d}\phi_b}{\mathrm{d}\alpha}\right)^{d/2} \frac{(U - U_\mathrm{t})^{d/2}}{(-\mathrm{d}U_\mathrm{t}/\mathrm{d}\alpha)^{d-1}}, \tag{4.5}$$

where α is a real number parametrizing the integration path corresponding to the critical bubble.

The action is independent of the parametrization and it will come in handy for the numerical implementation. In this section, there is clearly a natural choice for the parametrization, which we will label with φ:

$$\mathrm{d}\alpha = \mathrm{d}\varphi \equiv \sqrt{\mathrm{d}\phi_a Z_{ab} \mathrm{d}\phi_b}. \tag{4.6}$$

The Z-matrix acts as a metric in the space of field values. With the natural choice, the action looks like

$$S_\mathrm{t} = \frac{(2\pi)^{d/2}(d-1)^{d-1}}{\Gamma(d/2+1)} \int_{\varphi+}^{\varphi_0} \mathrm{d}\varphi \frac{(U-U_\mathrm{t})^{d/2}}{(-U_\mathrm{t}')^{d-1}}, \tag{4.7}$$

where the dash denotes total derivative with respect to the parameter φ.

We will show that this is the correct generalization in two steps. The first step is to show that the two actions agree when the Euclidean action is evaluated on the critical bubble configuration and the tunnelling potential is following:

$$U_\mathrm{t}(\phi) = U(\phi) - \frac{1}{2}\dot{\phi}_a Z_{ab}(\phi)\dot{\phi}_b, \tag{4.8}$$

where dots represent total derivatives with respect to the radial coordinate. Then, we will show that extremizing the action in Eq. (4.7) gives equivalent equations of motion as the extremization of the action in Eq. (4.4). The conversion from the EoM for the bubble to the EoM of the tunnelling potential is done through Eq. (4.8).

We will not actually show that the solution can be found from a minimum but from an extremum. Since the solution is the only minimum in the basic case [16], the extremum is expected to be a minimum.

Before jumping into derivations, I give a list of useful observations:

$$\dot{\phi} = \dot{\varphi}\phi', \tag{4.9}$$

$$\ddot{\phi} = \ddot{\varphi}\phi' + \dot{\varphi}^2\phi'', \tag{4.10}$$

$$\dot{\phi}_a Z^a_{cb} = \dot{\varphi} Z'_{cb}, \tag{4.11}$$

$$\phi'_a Z_{ab} \phi'_b = 1, \tag{4.12}$$

$$\phi'_a Z_{ab} \phi''_b + \frac{1}{2}\phi'_a Z'_{ab}\phi'_b = 0. \tag{4.13}$$

The last equation follows from the second last by differentiating with φ.

There are a few steps to take before it can be shown that the actions give the same value when the field configuration is the critical bubble and the tunnelling potential is given in Eq. (4.8). First, we will invoke the spherical symmetry of the critical bubble configuration [22]. We can see that there is no radial coordinate in the tunnelling action. Thus, we solve for the radial coordinate from the EoM of the critical bubble in terms of the

tunnelling potential. Finally, we will use the scaling arguments from Sec. 2.2 to express the value of the Euclidean action only in terms of the kinetic part. Putting everything together yields the tunnelling action.

The Euclidean action in spherical coordinates with origin at the centre of the critical bubble is

$$S_E[\phi] = \frac{2\pi^{d/2}}{\Gamma(d/2)} \int_0^\infty \mathrm{d}r\, r^{d-1} \Big[\frac{1}{2} \dot{\phi}_a Z_{ab}(\phi) \dot{\phi}_b + U(\phi) \Big]. \tag{4.14}$$

The equation of motion for the critical bubble can be found via the Euler-Lagrange equation:

$$Z_{cb}\ddot{\phi}_b + \frac{d-1}{r} Z_{cb}\dot{\phi}_b + \dot{\phi}_a Z^a_{cb}\dot{\phi}_b - \frac{1}{2}\dot{\phi}_a Z^c_{ab}\dot{\phi}_b = U^c, \tag{4.15}$$

where the upper index is a short hand for differentiation:

$$f^c \equiv \frac{\partial f}{\partial \phi_c}. \tag{4.16}$$

Using the equations (4.9), (4.10) and (4.11) simplifies Eq. (4.15):

$$\Big[\ddot{\varphi} + \frac{d-1}{r}\dot{\varphi} \Big] Z_{cb}\phi'_b + \dot{\varphi}^2 \Big(Z_{cb}\phi''_b + Z_{cb}\phi'_b - \frac{1}{2}\phi'_a Z^c_{ab}\phi'_b \Big) = U^c. \tag{4.17}$$

We can project this equation on ϕ' by contracting it with ϕ'_c. Using equations (4.12) and (4.13), we find that the term in parentheses vanishes and we are left with the term in square brackets on the left-hand side. We can use $\phi'_c U^c = U'$ to obtain

$$\ddot{\varphi} + \frac{d-1}{r}\dot{\varphi} = U'. \tag{4.18}$$

For solving the radius from Eq. (4.18), we need to solve for $\dot{\varphi}$ and $\ddot{\varphi}$ in terms of the tunnelling potential. Using the tunnelling potential in Eq. (4.8) and the definition of $\mathrm{d}\varphi$ (4.6), we get that

$$\dot{\varphi} = -\sqrt{2(U - U_\mathrm{t})}. \tag{4.19}$$

The sign comes from a choice to have φ growing towards the centre of the bubble along the integration path. Differentiating this with respect to r gives:

$$\ddot{\varphi} = U' - U'_\mathrm{t}. \tag{4.20}$$

We can now solve for the radius from Eq. (4.18) by inserting equations (4.19) and (4.20):

$$r = (d-1)\frac{\sqrt{2(U - U_\mathrm{t})}}{-U'_\mathrm{t}}. \tag{4.21}$$

Now that we have solved for the radius, we move onto showing that the Euclidean action on the critical bubble solution can be expressed in terms of the kinetic part on the

critical bubble. The critical bubble, $\phi_{\mathrm{B}}(r)$, is an extremum of the Euclidean action (4.14). Thus, a modification of the critical bubble $\phi_{\mathrm{B}}(\Lambda r)$ is an extremum at $\Lambda = 1$.

$$S_{\mathrm{B}}(\Lambda) = \frac{2\pi^{d/2}}{\Gamma(d/2)} \int_0^\infty \mathrm{d}r r^{d-1} \left[\frac{1}{2} \left(\frac{\mathrm{d}}{\mathrm{d}r} \phi_{\mathrm{B}a}(\Lambda r) \right) Z_{ab}(\phi_{\mathrm{B}}(\Lambda r)) \left(\frac{\mathrm{d}}{\mathrm{d}r} \phi_{\mathrm{B}b}(\Lambda r) \right) + U(\phi_{\mathrm{B}}(\Lambda r)) \right]. \tag{4.22}$$

We denote the kinetic part of the action by K and the potential part by P. By scaling the dummy variable $r \to \Lambda^{-1} r$, we get that

$$S_{\mathrm{B}}(\Lambda) = \Lambda^{2-d} K + \Lambda^{-d} P. \tag{4.23}$$

The extremum is at $\Lambda = 1$:

$$0 = S'_{\mathrm{B}}(1) = (2-d)K - dP. \tag{4.24}$$

Now, we can solve for P. Inserting it to the action gives that

$$S_{\mathrm{B}} = \frac{2}{d} K. \tag{4.25}$$

Finally in Eq. (4.25), the integral measure and derivatives with respect to the radial coordinate can be replaced with the parameter φ via Eq. (4.19) and the radial coordinate can be replace with Eq. (4.6). The result is the tunnelling action in Eq. (4.7). We have now completed the first step of showing the generalization to hold.

The second step is to show that the EoMs from the actions agree. We will translate the EoM from the Euclidean action in Eq. (4.15) to the language of the tunnelling potential method by removing all references to the radial coordinate in favour of the tunnelling potential. There is one step in between, which is that the EoM can be split into two distinct pieces that we will call longitudinal and transversal. Then we can start again from the tunnelling action. Extremizing with respect to the tunnelling potential gives the longitudinal EoM and the same with respect to the path gives the transversal EoM and also, the longitudinal EoM.

The splitting of the EoM in Eq. (4.15) to longitudinal and transversal pieces is almost done in Eq. (4.17). The longitudinal EoM can be found from Eq. (4.18) and inserting this into the square brackets of Eq. (4.15) gives the transversal EoM:

$$\dot{\varphi}^2 \left(Z_{cb} \phi''_b + Z_{cb} \phi'_b - \frac{1}{2} \phi'_a Z^c_{ab} \phi'_b \right) = U^c - U' Z_{cb} \phi'_b. \tag{4.26}$$

The easiest way to translate the the longitudinal EoM is to differentiate Eq. (4.21) with respect to the radial coordinate, then use the chain rule and Eq. (4.19) to eliminate the radial coordinate. The transversal part is easier because one can just use Eq. (4.19).

The EoMs are

$$[(d-1)U' - dU_\mathrm{t}']U_\mathrm{t}' = 2(d-1)(U-U_\mathrm{t})U_\mathrm{t}'', \tag{4.27}$$

$$2(U-U_\mathrm{t})\left(Z_{cb}\phi_b'' + Z_{cb}\phi_b' - \frac{1}{2}\phi_a' Z_{ab}^c \phi_b'\right) = U^c - U' Z_{cb}\phi_b'. \tag{4.28}$$

All we have to do now is to show that extremizing the tunnelling action in Eq. (4.7) gives these EoMs.

In the case of the transversal part, it is clearer to use the general parametrization in the derivation and therefore, we define the action density as

$$\mathcal{S} = \left(\frac{\mathrm{d}\phi_a}{\mathrm{d}\alpha} Z_{ab} \frac{\mathrm{d}\phi_b}{\mathrm{d}\alpha}\right)^{d/2} \frac{(U-U_\mathrm{t})^{d/2}}{(\mathrm{d}U_\mathrm{t}/\mathrm{d}\alpha)^{d-1}}, \tag{4.29}$$

from which we have dropped out a constant factor and an overall sign. In the longitudinal case, it is easiest to use $\alpha = \varphi$, and the density simplifies to

$$\mathcal{S} = \frac{(U-U_\mathrm{t})^{d/2}}{(U_\mathrm{t}')^{d-1}}. \tag{4.30}$$

We can use the Euler-Lagrange equation to extremize the tunnelling action with respect to the tunnelling potential. Here, we use $\alpha = \varphi$:

$$\frac{\partial \mathcal{S}}{\partial U_\mathrm{t}} - \frac{\mathrm{d}}{\mathrm{d}\varphi}\frac{\partial \mathcal{S}}{\partial U_\mathrm{t}'} = -\frac{d}{2}\frac{(U-U_\mathrm{t})^{d/2-1}}{(U_\mathrm{t}')^{d-1}} + (d-1)\frac{\mathrm{d}}{\mathrm{d}\varphi}\left[\frac{(U-U_\mathrm{t})^{d/2}}{(U_\mathrm{t}')^{d}}\right] = 0. \tag{4.31}$$

This gives the longitudinal EoM in Eq. (4.27).

We need to set up a few things before getting to the variation of the action with respect to the path. We will use the general parametrization of the path α, because φ is path dependent. When varying the path, we will shift a point on the path to a different location with $\phi \to \phi + \delta\phi$. On the shifted point, we will keep the same value of the parametrization and the same value of the tunnelling potential. As a consequence, the variation does not alter the values of α, U_t nor $\mathrm{d}U_\mathrm{t}/\mathrm{d}\alpha$ on a point. After the variation is done, we will set $\alpha = \varphi$ to obtain the wanted EoMs.

We cannot vary ϕ_0 like this due to the boundary condition of the tunnelling potential at ϕ_0, $U_\mathrm{t}(\phi_0) = U(\phi_0)$. As the end point is shifted, the value of the tunnelling potential must change on the point. However, this does not actually matter since the action density at the end point is always zero because of the boundary condition. The boundary condition of the critical bubble that $\phi \to \phi_+$, $r \to \infty$ implies that the beginning point of the integration path in the space of field value cannot be varied in the first place.

One last thing, before getting to the actual variation of the action, is that the variation will also reproduce the longitudinal part. If the variation $\delta\varphi$ is along the integration path, the variation of the path can be viewed as a variation of the tunnelling potential

(and a variation of the parametrization which does nothing). Hence, it is expected that the longitudinal EoM comes up again.

We can now employ the Euler-Lagrange equation again, remembering that U_t and $\mathrm{d}U_\mathrm{t}/\mathrm{d}\alpha$ are not varied. We will use $M \equiv \frac{\mathrm{d}\phi_a}{\mathrm{d}\alpha} Z_{ab} \frac{\mathrm{d}\phi_b}{\mathrm{d}\alpha}$ as a shorthand notation.

$$\begin{aligned}
&\frac{\partial \mathcal{S}}{\partial \phi_c} - \frac{\mathrm{d}}{\mathrm{d}\alpha} \frac{\partial \mathcal{S}}{\partial(\mathrm{d}\phi_c/\mathrm{d}\alpha)} \\
=&\frac{d}{2} \frac{\mathrm{d}\phi_a}{\mathrm{d}\alpha} Z^c_{ab} \frac{\mathrm{d}\phi_b}{\mathrm{d}\alpha} M^{d/2-1} \frac{(U-U_\mathrm{t})^{d/2}}{(U_\mathrm{t}')^{d-1}} + \frac{d}{2} M^{d/2} U^c \frac{(U-U_\mathrm{t})^{d/2-1}}{(U_\mathrm{t}')^{d-1}} \\
&- \frac{\mathrm{d}}{\mathrm{d}\alpha} \left[dZ_{cb} \frac{\mathrm{d}\phi_b}{\mathrm{d}\alpha} M^{d/2} \frac{(U-U_\mathrm{t})^{d/2}}{(U_\mathrm{t}')^{d-1}} \right] \\
=&0,
\end{aligned} \tag{4.32}$$

where we have used the symmetricity of the Z-matrix.

Now, we can set the parametrization to the natural choice on the original path, $\alpha = \varphi$. This has an effect that $M = 1$. This yields

$$\frac{\mathrm{d}}{\mathrm{d}\varphi} \left(Z_{ab} \phi_b' \frac{(U-U_\mathrm{t})^{d/2}}{(U_\mathrm{t}')^{d-1}} \right) = \frac{1}{2} \left(U^a + \phi_c' Z^a_{cb} \phi_b' (U - U_\mathrm{t}) \right) \frac{(U-U_\mathrm{t})^{d/2-1}}{(U_\mathrm{t}')^{d-1}} \tag{4.33}$$

For being able to split the EoM into the longitudinal and transversal parts, we use the product rule of the derivative onto the $\frac{\mathrm{d}}{\mathrm{d}\varphi}$-term and move the second term from the right hand side:

$$\frac{\mathrm{d}}{\mathrm{d}\varphi} \left(\frac{(U-U_\mathrm{t})^{d/2}}{(U_\mathrm{t})^{d-1}} \right) Z_{ab} \phi_b' + \frac{(U-U_\mathrm{t})^{d/2}}{(U_\mathrm{t}')^{d-1}} \left[Z'_{ab} \phi_b' + Z_{ab} \phi_b'' - \frac{1}{2} \phi_c' Z^a_{cb} \phi_b' \right] = \frac{1}{2} \frac{(U-U_\mathrm{t})^{d/2-1}}{(U_\mathrm{t}')^{d-1}} U^a \tag{4.34}$$

Now we can project the EoM onto ϕ' by multiplying with ϕ_a'. With Eqs. (4.12) and (4.13), we get:

$$\frac{\mathrm{d}}{\mathrm{d}\varphi} \left(\frac{(U-U_\mathrm{t})^{d/2}}{(U_\mathrm{t}')^{d-1}} \right) = \frac{1}{2} \frac{(U-U_\mathrm{t})^{d/2-1}}{(U_\mathrm{t}')^{d-1}} U' \tag{4.35}$$

This would again give the longitudinal part, which has already been reproduced.

We can insert the solved derivative term in Eq. (4.35) back to our EoM:

$$\frac{(U-U_\mathrm{t})^{d/2}}{(U_\mathrm{t}')^{d-1}} \left[Z'_{ab} \phi_b' + Z_{ab} \phi_b'' - \frac{1}{2} \phi_c' Z^a_{cb} \phi_b' \right] = \frac{1}{2} \frac{(U-U_\mathrm{t})^{d/2-1}}{(U_\mathrm{t}')^{d-1}} (U^a - U' Z_{ab} \phi_b'). \tag{4.36}$$

We have now reproduced also the transversal part in Eq. (4.28).

We have now shown that extremizing the tunnelling action in Eq. (4.5) gives the correct value for the exponential suppression and also the proper EoM for the tunnelling potential. After the extremization, the bubble profile can be retrieved via Eq. (4.21).

As a final touch on the tunnelling potential formalism, we will now show the three conditions for the tunnelling potential: monotonicity, $U_\mathrm{t}(\phi) \leq U(\phi)$ and $U_\mathrm{t}(\phi_+) =$

$U(\phi_+)$, $U_\mathrm{t}(\phi_0) = U(\phi_0)$. The idea is that these hold for the tunnelling potential in Eq. (4.8) that corresponds to the critical bubble. Therefore, we can restrict the general tunnelling potential function to obey them. The restrictions will be very helpful when implementing the minimization numerically.

The second condition follows from the fact that the Z-matrix is positive definite:

$$U_\mathrm{t}(\phi) = U(\phi) - \frac{1}{2}\dot{\phi}_a Z_{ab}(\phi)\dot{\phi}_b \leq U(\phi). \tag{4.37}$$

Also, the third is very straight forward. The boundary conditions of the critical bubble configuration in Eqs. (2.16) and (2.17) imply that $\dot{\phi} = 0$ at $\phi = \phi_+$ and $\phi = \phi_0$. Eq. (4.8) reduces to

$$U_\mathrm{t}(\phi_+) = U(\phi_+), \qquad U_\mathrm{t}(\phi_0) = U(\phi_0). \tag{4.38}$$

Showing the first condition takes slightly longer. We will do it by showing that

$$U_\mathrm{t}' \leq 0. \tag{4.39}$$

One can use the chain rule to have a derivative with respect to the radial coordinate act on the right-hand side of Eq. (4.8):

$$U_\mathrm{t}' = \dot{\varphi}^{-1}\dot{\phi}^a\Big(U^a - Z_{ab}\ddot{\phi}_b - \frac{1}{2}\dot{\phi}_b Z^a_{bc}\dot{\phi}_c\Big), \tag{4.40}$$

where we have used the symmetricity of the Z-matrix. We can simplify the right-hand side with the EoM of the critical bubble in Eq. (4.14) contracted with $\dot{\phi}_c$. The result is

$$U_\mathrm{t}' = \dot{\varphi}^{-1}\frac{d-1}{r}\dot{\phi}^a Z_{ab}\dot{\phi}_b. \tag{4.41}$$

φ decreases monotonously when the radial coordinate is increased and the Z-matrix is positive definite. Thus, we have shown the inequality in Eq. (4.39) to hold.

4.2 Numerical Implementation

A critical bubble can be solved in few special cases analytically within the formalism above. In a general case, a numerical solution is needed. Here, we will go through the numerical implementation used for the results in Sec. 4.3 and the few caveats that it has. The implementation is based on the one in Ref. [39] but it is developed a bit further.

In the previous section, we derived the equations of motion by extremizing the tunnelling action in Eq. (4.5). It was actually enough to vary only the path in the space of field values to obtain all the EoMs. Varying the tunnelling potential just reproduced one of the EoMs. The implementation is based on this observation: We can fix the tunnelling potential on the points of the path and just move the path.

Varying the path gives also the EoM from varying the tunnelling potential because variations of the path along the path alter only the tunnelling potential. This is no longer true in the discretized version of the tunnelling potential method. Variations of the tunnelling potential cannot be reproduced exactly by varying the locations of the discrete points in the space of field values. Leaving some room for the tunnelling potential to change can be beneficial as we will see in Subsec. 4.2.1. One has to be a bit careful though: The particular freedom, that we will give, can give rise to ill-converged bubbles as shown in Fig. 4.8.

We will explain the discretization of the tunnelling action and the implementation of the tunnelling potential in the first subsection. Then, we move onto the minimization process for the tunnelling action. There are things that we would like to evaluate on the critical bubble, such as the next order in a derivative series (Eq. (3.121)). Accuracy wise, it is best to perform this in the language of the tunnelling potential method. The translation is shown in Subsec. 4.2.3. In the last subsection, there are tests conducted on the implementation chosen for the numerical results. In this section, we will not go into the details of solving the bubble configuration numerically, because it can be done straightforwardly using Eq. (4.21).

4.2.1 Tunnelling Action and Potential

In this subsection, we will lay down the form of the discretized tunnelling action which is then minimized to find the approximate exponential suppression from the critical bubble. The most interesting part is the implementation of the tunnelling potential which is discussed after the discretized action is presented.

The integration path in the space of field values is discretized with N consecutive points labelled with index $i \in \{1, ..., N\}$. We use the general form of the tunnelling potential in Eq. (4.5) and choose the parametrization so that, between two consecutive points, $\Delta\alpha = 1$. All the discrete terms in the action are evaluated at mid-points of the field values. The tunnelling action becomes:

$$S_\mathrm{t} = \frac{(2\pi)^{d/2}(d-1)^{d-1}}{\Gamma(d/2+1)} \sum_{i=1}^{N-1} \left(\Delta\phi_a^i Z_{ab}^i \Delta\phi_b^i\right)^{d/2} \frac{(U^i - U_\mathrm{t}^i)^{d/2}}{(-\Delta U_\mathrm{t}^i)^{d-1}}, \tag{4.42}$$

where

$$U_\mathrm{t}^i = (U_\mathrm{t}(\phi^i) + U_\mathrm{t}(\phi^{i+1}))/2, \tag{4.43}$$

$$U^i = (U(\phi^i) + U(\phi^{i+1}))/2, \tag{4.44}$$

$$Z_{ab}^i = Z_{ab}(\tfrac{\phi^i+\phi^{i+1}}{2}), \tag{4.45}$$

$$\Delta\phi_a^i = \phi_a^{i+1} - \phi_a^i, \tag{4.46}$$

$$\Delta U_\mathrm{t}^i = U_\mathrm{t}(\phi^{i+1}) - U_\mathrm{t}(\phi^i). \tag{4.47}$$

We choose that $i = 1$ is at the metastable end and that $i = N$ is at the centre of the bubble, $\phi^1 = \phi_+$ and $\phi^N = \phi_0$.

From the perspective of the minimization, we do not want to give too much freedom for the tunnelling potential. All the terms have ΔU_t to some power in the denominator and, as can be seen from Eq. (4.53) below, the changes are very tiny close to the metastable field value. Restricting the freedom of the tunnelling potential provides stability for the minimization. Also, the fact, that varying only the path gives all the equations of motion, suggests that it is sufficient to fix a value of the tunnelling potential for a given index i and then just move the points in the minimization.

The fixed tunnelling potential must satisfy the conditions shown at the end of Sec. 4.1. In the discrete form, they are

$$U_\mathrm{t}(\phi^1) = U(\phi_+), \tag{4.48}$$
$$U_\mathrm{t}(\phi^N) = U(\phi^N), \tag{4.49}$$
$$U_\mathrm{t}(\phi^i) < U(\phi^i), \quad 1 < i < N, \tag{4.50}$$
$$U_\mathrm{t}(\phi^{i+1}) < U_\mathrm{t}(\phi^i). \tag{4.51}$$

In Ref. [39], the fixing of the tunnelling potential was done with

$$U_\mathrm{t}(\phi^i) = U(\phi_+) + x_i^2(3 - 2x_i)\Big(U(\phi^N) - U(\phi_+)\Big), \quad x_i = \frac{i-1}{N-1}. \tag{4.52}$$

The only condition that does not follow automatically is in Eq. (4.50). An important consequence of this choice is that all the terms is the discrete action (4.42) depend on the last field value ϕ^N.

The choice for the tunnelling potential in Eq. (4.52) works pretty well. However, there is a problem in the convergence to the correct critical bubble, at least in thick-wall cases. Increasing the number of points does not make the radius of the $i = N - 1$ point go towards zero, and its neighbouring points, $i < N - 1$, pack right behind the point. A Taylor series approximation of the critical bubble around $r = 0$ confirmed that the points near the centre of the bubble did not obey the equations of motion. The new implementation for the tunnelling potential, that we present in Eq. (4.55)below, alleviates this problem and the bubble configuration seems to converge properly with increasing N. However, it is still not perfect as can be seen from Fig. 4.6.

Funnily, the problem of the convergence around ϕ_0 lies at the other end of the field values, near ϕ_+. The correct tunnelling potential (Eq. (4.8)) that corresponds to the critical bubble is not analytic at the metastable field value and all of its derivatives are zero:

$$\frac{\mathrm{d}^k U_\mathrm{t}}{\mathrm{d}\varphi^k}(\phi = \phi_+) = 0. \tag{4.53}$$

In the choice of Eq. (4.52), already the second derivative is non-zero. This has two effects: The first one is that the points populate sparsely the values close to the metastable value. This is rather harmless, but the second effect, described below, is the one causing the improper convergence.

The minimization process tries to find the correct tunnelling potential. Besides making the points sparse near ϕ_+, it can also try to push the tunnelling potential values near the metastable end towards $U(\phi_+)$, in accordance with (4.53). The value of the tunnelling potential on every point is dependent on the value of ϕ^N and hence, the values of the tunnelling potential near ϕ_+ can be pushed up by deviating ϕ^N from the value it actually should have. This is the root cause for the too large radial value of the ϕ^{N-1} point. Also, the too small ϕ^N in Fig. 4.6 follows from this.

We have tested two other parametrizations of which the latter is used in the thesis. They are

$$U_\mathrm{t}(\phi^i) = U(\phi_+) + x_i^2(3-\gamma-(2-\gamma)x_i)\Big(U(\phi^N) - U(\phi_+)\Big), \tag{4.54}$$

$$U_\mathrm{t}(\phi^i) = U(\phi_+) + x_i^3(4-\gamma-(3-\gamma)x_i)\Big(U(\phi^N) - U(\phi_+)\Big). \tag{4.55}$$

The parameter γ provides a little freedom within the tunnelling potential. It is constrained by the monotonicity condition (4.51) which gives

$$\frac{-3N+5}{(N-2)^2} < \gamma < \frac{3N-5}{N-2}, \tag{4.56}$$

$$\frac{-6N^2+20N-17}{(N-2)^3} < \gamma < \frac{4N-7}{N-2} \tag{4.57}$$

respectively. There are now two conditions that must be monitored during the minimization process in Eqs. (4.50) and (4.51).

Experimentations with these choices also solidifies the understanding that the region near the metastable field value is problematic. Almost always, the value of γ is at the upper limit which minimizes the change of the tunnelling potential near $i = 1$. The value of γ drops only in the thin-wall limit, presumably to pull the points near ϕ_0, into the upper regions of the wall.

All three choices give similar values for the actions. However, the values from the latter two are extremely close and their bubbles seem to converge correctly near the centre. The choice in Eq. (4.55) is chosen for our numerical results due to being better at describing the tails of bubbles (cf. FIG. 4.2). This stems from the choice for the tunnelling potential being even flatter near $i = 1$. The implementation is tested in Subsec. 4.2.4.

The choice is still not perfect and it has not been proven to converge properly to the critical bubble configuration in the limit of $N \to \infty$. One possibility would be to have a better choice for fixing the tunnelling potential. A way to improve it would be to use a

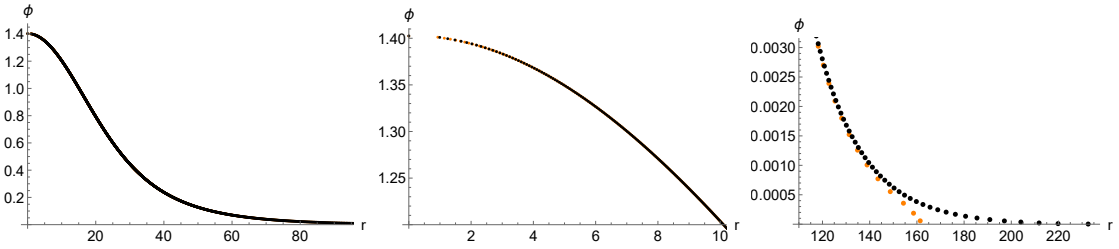

Figure 4.2: Test bubbles using Eqs. (4.55) in black and (4.54) in orange. They give rise to almost identical bubbles. The major difference is the behaviour at extremely large radial values, shown in the last figure, where it can be seen that the choice in (4.55) fares better.

function that already respects the properties of the tunnelling potential at ϕ_+. This would take off the stress related to the interaction between the field point ϕ^N and the tunnelling potential values near ϕ_+. Also, the convergence of the end of the bubble tail would be quicker. Another possibility for improvement is an algorithm that could optimize the choice during the minimization process. However, this already sounds like minimizing also with respect to the tunnelling potential, which would mean approximatively N degrees of freedom more.

4.2.2 Minimization

The tunnelling potential method is used in the thesis because it allows one to find the critical bubble via minimization. Here, we will explain the implementation of the minimization that is used for the results in Sec. 4.3. The minimization process happens in two steps: proper minimization and increasing the number of points, N. After the insertion of new points, the proper minimization is done again. This permits the user to see the convergence in both the value of the action and the shape of the bubble (cf. Figs. 4.3 and 4.4).

Before getting into the actual implementation, it is important to note that there have to be safety measures implemented in the minimization. If the tunnelling potential jumps out of the allowed bounds given in Eqs. (4.48), the minimization can converge to a completely wrong result or, in odd number of dimensions, the tunnelling action can become complex. Each step in the minimization has to be checked to be valid. With different choices in the implementation of the tunnelling potential, one needs to be wary of different conditions. When using the choice in Eq. (4.55), conditions in Eqs. (4.51) and (4.50) need to be checked. The former one simplifies to the condition in Eq. (4.57).

The proper minimization has two options for taking a step towards the minimum: the Newton-Raphson method and the negative eigenvector descent. The latter method might already exist with another name. The minimization with the Newton-Raphson method relies on the Hessian matrix of the action having all positive eigenvalues. If there

exists at least one negative eigenvalue, the Newton-Raphson method does not seek the minimum, so the second minimization option is used until all the eigenvalues are positive.

The Newton-Raphson method, in this case, tries to find a root for the derivative of a function f, i.e. it extremizes the function. The way it works intuitively is to fit a second order polynomial around a starting point $\mathbf{x}_0$:

$$f(\mathbf{x}_0 + \delta\mathbf{x}) \approx f(\mathbf{x}_0) + \frac{\partial f}{\partial \mathbf{x}}(\mathbf{x_0}) \cdot \delta\mathbf{x} + \frac{1}{2}\delta\mathbf{x} \cdot \frac{\partial^2 f}{\partial \mathbf{x}^2}(\mathbf{x_0}) \cdot \delta\mathbf{x}, \tag{4.58}$$

and then it finds $\delta\mathbf{x}$ that extremizes the polynomial. The solution can be found from the following linear equation:

$$\frac{\partial^2 f}{\partial \mathbf{x}^2}(\mathbf{x_0}) \cdot \delta\mathbf{x} = -\frac{\partial f}{\partial \mathbf{x}}(\mathbf{x_0}). \tag{4.59}$$

The negative eigenvector descent works in the case where are some negative eigenvalues. The idea is to take the step to be in the direction of the eigenvector that corresponds to the most negative eigenvalue. One can find the minimum of the discretized tunnelling action in this direction via a derivative assisted binary search and take the step to the minimum.

On the first round before the addition of new points, it is possible that the negative eigenvector descent becomes stuck at a border of allowed values for the tunnelling potential. This can be circumvented with a better choice for initial ϕ^is and γ.

To increase precision, one needs to increase N, the number of field value points. After finishing minimization with N points, it is possible to insert a point between two consecutive points and still be close to the end result of minimization with $2N-1$ points. There are several possible ways of refining this procedure, and we will go through the steps that we have implemented.

The first thing to check in $N \to 2N-1$ transition is that the tunnelling potential is still monotonous. The condition for monotonicity, given in Eq. (4.57), becomes stricter when the number of points is increased, and it can so happen that γ is out of the range after the point insertion. Changing γ alters the whole system, so the best way is not to change purely γ but the points as well. We take the value of the action to tell how much the whole system is disturbed. To change the value of the action as little as possible, we solve the eigenvector corresponding to the lowest eigenvalue of the Hessian matrix. The tunnelling action is a function of ϕ^is and γ. Hence, the eigenvector tells how to change the points as the value of γ is pushed into the new limits.

Values for the new points can be assessed in multiple ways. In our implementation, they were given by

$$\phi^2_{\text{new}} = (3\phi^1 + 6\phi^2 - \phi^3)/8, \tag{4.60}$$

$$\phi^{2i}_{\text{new}} = (9(\phi^i + 6\phi^{i+1}) - (\phi^{i-1} + \phi^{i+1}))/16, \tag{4.61}$$

$$\phi^{2N-2}_{\text{new}} = (3\phi^N + 6\phi^{N-1} - \phi^{N-2})/8, \tag{4.62}$$

where the indices on the right-hand sides correspond to the old indices. Here, we have fitted a parabola through two consecutive old points with $f:\ i \mapsto \phi^i,\ i+1 \mapsto \phi^{i+1}$, so that the second derivative at the mid-point, $f''(i+1/2)$, is the numerical second derivative with respect to the index from the four closest points. The new value for a point comes from $f(i+1/2)$.

After the insertion, there will be frustration related to the γ parameter. To alleviate this, we minimize the tunnelling potential with respect to the parameter before recommencing the proper minimization.

4.2.3 Evaluations on the Critical Bubble

Sometimes, there are contributions, that need to be evaluated on a critical bubble solution, which cannot be included in the tunnelling action. We are interested in two such contributions: one-loop free energy of a nucleating field in Eq. (3.124) and second order in a derivative expansion in Eq. (3.121). The first one should not be included physically since the nucleating field can never be integrated out within the wall of a critical bubble. From the view-point of the minimization, the obstacle for inclusion is an imaginary part in the contribution. The next order in the derivative expansion cannot be included because the tunnelling potential method is not yet capable of dealing with such operators, only possible gradient terms are shown in the action in Eq. (4.4). Sadly, the methods presented here do not work for non-derivative quantities in the thin-wall limit, which would be our interest with the one-loop contribution. This is because the plateau of a thin-wall bubble is not described accurately (cf. Fig. 4.4).

In the current subsection, we will learn how to translate the contributions into the language of the tunnelling potential method. This is beneficial because we do not need to first obtain the critical bubble configuration for the evaluation. This would cause inaccuracies that we bypass. We will first use the spherical symmetry of the critical bubble around its centre and then, use results from Subsec. 4.2.1 to replace all the references to the radial coordinate with the tunnelling potential. The discretization should be the same as in the discretized tunnelling action shown in Eq. (4.42) because a different discretization might have a slight impact on the obtained value.

A contribution can be simplified with the spherical symmetry:

$$\int \mathrm{d}^d x\, f(\phi, (\boldsymbol{\nabla}\phi)^2, \boldsymbol{\nabla}^2\phi) = A_d \int_0^\infty \mathrm{d}r\, r^{d-1}\, f(\phi, \dot{\phi}, \ddot{\phi}, r), \tag{4.63}$$

where A_d is the area of d-dimensional unit sphere. We could have included also higher order gradients but we only need these. We do not need to modify ϕ and we already have r in Eq. (4.21). This leaves us with the measure, $\dot{\phi}$ and $\ddot{\phi}$.

We can use the chain rule for the measure:

$$\mathrm{d}r = \frac{\mathrm{d}r}{\mathrm{d}\varphi}\frac{\mathrm{d}\varphi}{\mathrm{d}\alpha}\mathrm{d}\alpha = \dot{\varphi}^{-1}\frac{\mathrm{d}\varphi}{\mathrm{d}\alpha}\mathrm{d}\alpha, \tag{4.64}$$

and use Eqs. (4.19) and (4.6) for simplification. In the discretized version, we can again use $\Delta\alpha = 1$ between consecutive points. We arrive at

$$\int_0^\infty \mathrm{d}r \to \sum_{n=1}^{\infty} \sqrt{\frac{\Delta\phi_a^i Z_{ab}^i \Delta\phi_b^i}{2(U^i - U_\mathrm{t}^i)}}, \tag{4.65}$$

whose notations are explained below Eq. (4.42).

Once again, we can employ the chain rule:

$$\dot{\phi}_a = \dot{\varphi}\phi_a' = -\sqrt{2(U - U_\mathrm{t})}\phi_a', \tag{4.66}$$

where the second equality follows from Eq. (4.19). In the case of a single field, this can be further simplified with Eq. (4.6). In the discretized form, the one-field situation gives

$$\dot{\phi} \to -\sqrt{\frac{2(U^i - U_\mathrm{t}^i)}{Z^i}}. \tag{4.67}$$

In multi-field cases, the derivative can be approximated with $\phi_a' \to \Delta\phi_a^i / \sqrt{\Delta\phi_b^i Z_{bc}^i \Delta\phi_c^i}$.

For $\ddot{\phi}$, we can use Eqs. (4.10), (4.19) and (4.20):

$$\ddot{\phi}_a = (U' - U_\mathrm{t}')\phi_a' - \sqrt{2(U - U_\mathrm{t})}\phi_a''. \tag{4.68}$$

Again, we provide a simplified form for the single-field case. ϕ' has already been simplified, and ϕ'' does not require any more tools:

$$\phi'' = -\frac{1}{2Z^2}\frac{\mathrm{d}Z}{\mathrm{d}\phi}. \tag{4.69}$$

Now, we can give the discretized version:

$$\ddot{\phi} \to \frac{\Delta U^i - \Delta U_\mathrm{t}^i}{Z^i \Delta\phi^i} + \frac{\sqrt{2(U^i - U_\mathrm{t}^i)}}{2(Z^i)^2}\frac{\Delta Z^i}{\Delta\phi^i}. \tag{4.70}$$

We have now everything needed for the evaluation of the contributions that we want to evaluate on top of a bubble solution.

4.2.4 Tests

Here, we will study the performance of the code with two parameter points from the next section. One of the points corresponds to a thick-wall bubble and the other to a thin-wall bubble, shown in Fig. 4.4. We will first focus on the convergence of the code and then look at how well the equation of motion in Eq. (4.15) is satisfied.

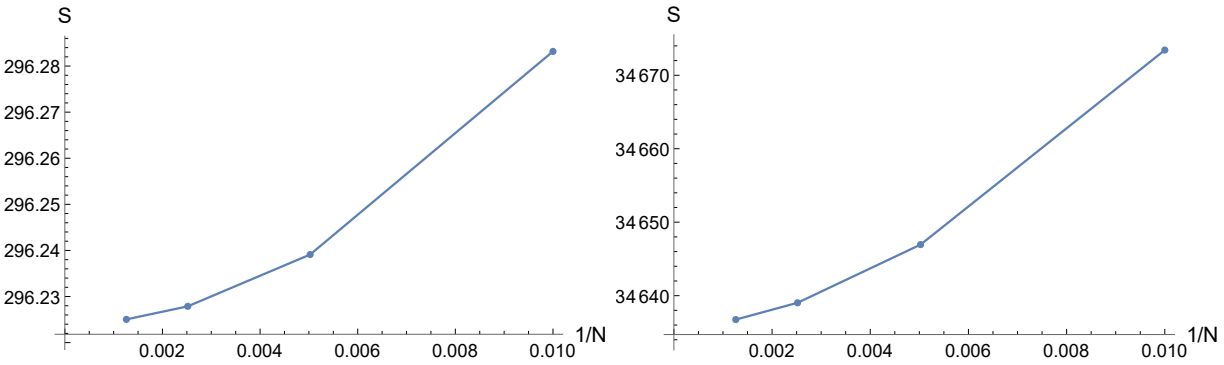

Figure 4.3: The graphs show the convergence of tunnelling action. One on the left corresponds to the thick-wall bubble in Fig. 4.4 and the other to the thin-wall bubble.

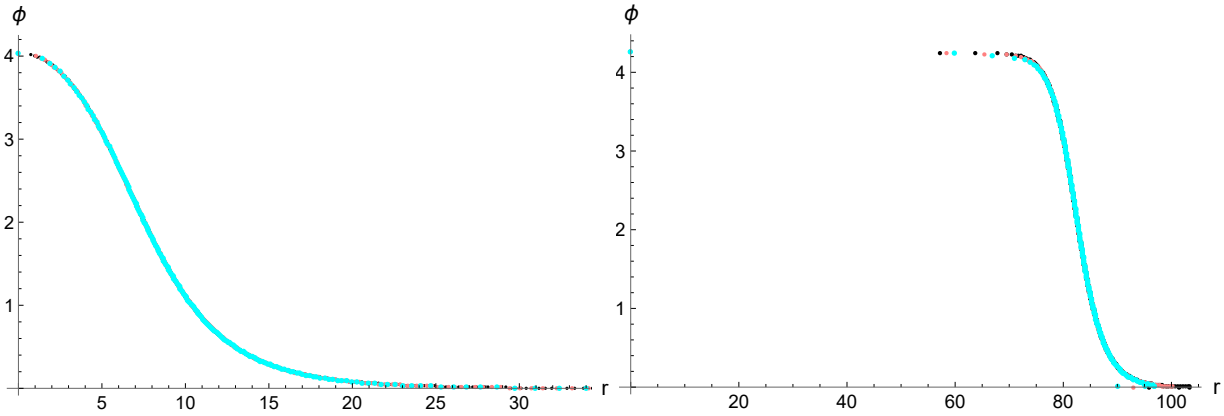

Figure 4.4: The bubble configurations that are extracted from the tunnelling potential solution via Eq. (4.21). Only bubbles with $N = \{199, 397, 793\}$ are shown.

From Fig. 4.3, we can see that the action of a critical bubble converges nicely. The actions with $N = 100$ are proportionally already very close to the results with $N = 800$. Also, the behaviour of the values show that the convergence is very good.

Similarly to the values of the action, the field configurations converge well. This can be seen from Fig. 4.4. The configurations with different numbers of points match on top of each other. This also holds true for $N = 100$ which has been left out for clarity. With the thin-wall bubble, we can also compare the shape of the bubble to the radius obtained for the bubble from the thin-wall approximation from Eq. (3.41). This is done in Fig. 4.7. However, we can see that the thin-wall bubble does not describe the behaviour near the metastable state well, as the radius of the smallest field values decreases.

The fulfilment of the equation of motion in Eq. (4.15) is shown in Fig. 4.5. Red dots are the left-hand side evaluated on each point of the configuration and blue dots are the corresponding right-hand sides. The EoM is well satisfied within the bubble wall. However, both configurations have difficulties near the centre and for the thin-wall bubble at the end of its tail. In Fig. 4.6, the EoM is solved up to quartic order in the radial

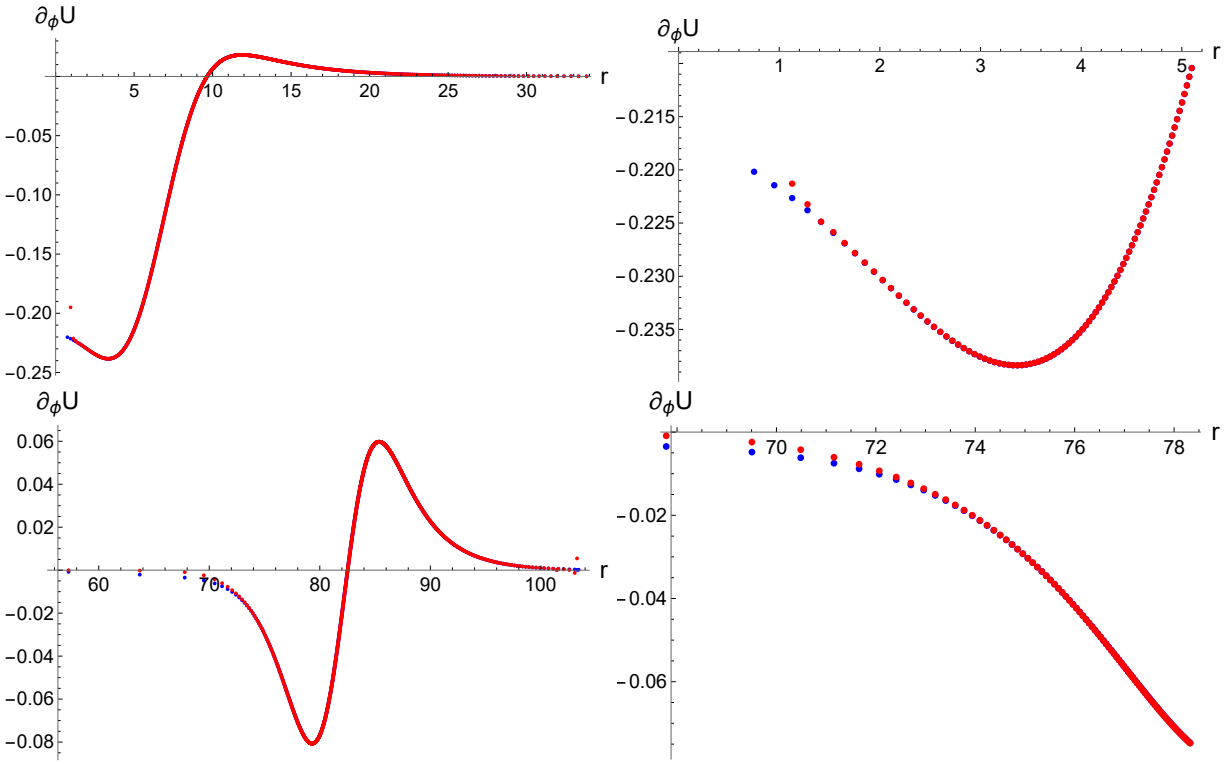

Figure 4.5: The graphs show how well the equation of motion in Eq. (4.15) is satisfied. The red dots are the left-hand sides of the EoM and the blue dots are the right-hand sides. Top graphs correspond to the thick-wall bubble in Fig. 4.4 and the bottom graphs to the thin-wall bubble.

coordinate around $r = 0$. The polynomial solution is adjusted to fit points near $r = 2$. Even though the equation of motion might seem to be violated badly, the consequences for the configuration are rather small. A similar check for the thin-wall bubble is not possible, but we can use the thin-wall approximation of the radius to double check the correctness of the configuration. This is done in Fig. 4.7.

As a last remark, I want to discuss the fact that the critical bubble is truly a secondary quantity from the tunnelling potential method. Most of this subsection is based on studying the critical bubbles from the minimized tunnelling action. However, the method tries to minimize the tunnelling action with respect to the tunnelling potential. Therefore, the action obtained is always much more precise than the configuration. As an example, there is clearly an ill-converged bubble in Fig. 4.8. During minimization, the γ-parameter was pushed extremely close to its lower limit. As a consequence, the point next to ϕ_0 is pushed to $r \approx 350$. Also, the rest of the points at the top do not behave properly. The value of the tunnelling action of the bubble is still very close to the correct value being only under one percent off. The point is that, the bubbles that behave nicely correspond to action values that are very precise and hence trustworthy.

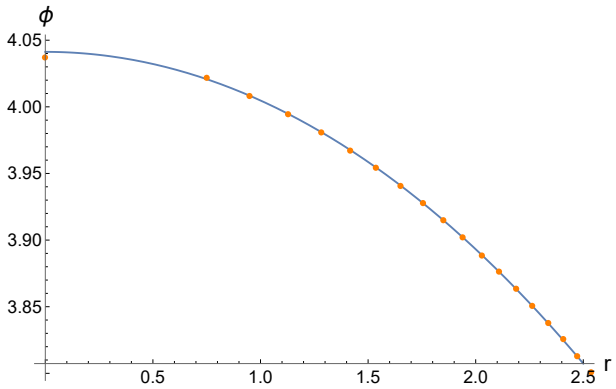

Figure 4.6: A quartic polynomial solution to the equation of motion in Eq. (4.15) around $r = 0$ is adjusted to points near $r = 2$. The bubble is rather near its correct shape even though the EoM is not satisfied around the centre (cf Fig. 4.5).

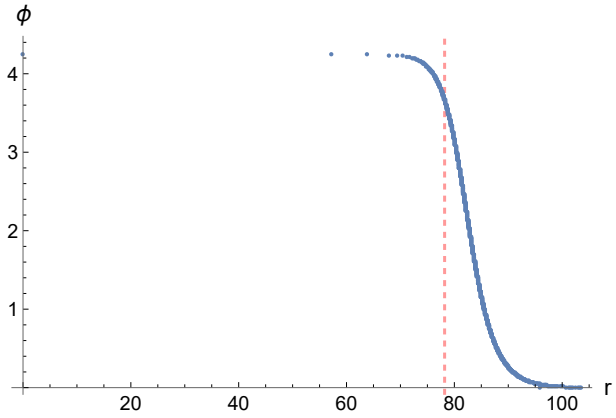

Figure 4.7: The thin-wall bubble is compared to the radius obtained from thin-wall approximation in Eq. (3.41).

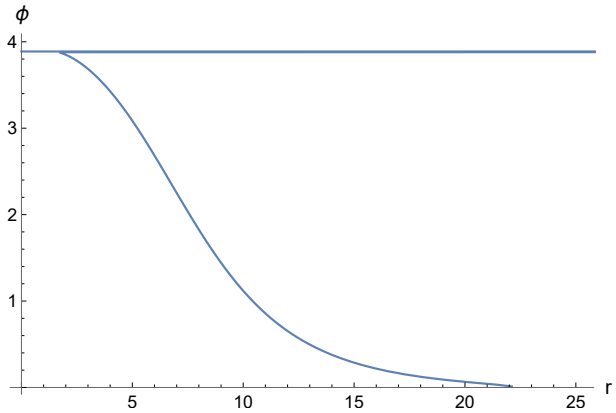

Figure 4.8: An ill-converged bubble that corresponds to the thick-wall bubble in Fig. 4.4.

4.3 Numerical Results

Here, we will cover the main points of the thesis with only one benchmark point for the asymmetric model and the cubic anisotropy model. Hence, this section is not a compre-

hensive study of the parameter space of the two scalar model presented in Sec. 3.3. In Subsec. 4.3.1, we study the temperature dependence of the exponential suppression from the critical bubble with renormalization scale dependence. We will also compute, in a particular transition, quantities that are relevant for the gravitational background spectrum and check their uncertainty via varying the renormalization scale. In Subsec. 4.3.2, we examine the importance of the wave function renormalization and the convergence of the derivative series. Lastly, we look into the thin-wall limit and the cross-over from the EFT method to its extension presented in Subsec. 3.2.3.

The benchmark point for the asymmetric model is chosen as follows:

$$g_0^2 = 0.4, \tag{4.71}$$

$$f_0 = 0.4, \tag{4.72}$$

$$\lambda_0 = 0.0199, \tag{4.73}$$

$$m_0^2 = -1, \tag{4.74}$$

$$M_0^2 = -1, \tag{4.75}$$

$$\mu_0 = 2\pi\sqrt{-\frac{24m_0^2}{g_0^2}}. \tag{4.76}$$

The cross-coupling and the self-coupling of the χ-field are fixed to roughly match the weak coupling. As discussed in Subsec. 3.3.1, there is a maximum value for the self-coupling of the ϕ-field with which there can be a symmetric and a broken minimum at the same temperature. The self-coupling is chosen to be half of the maximum value. The values are set at a scale that approximately matches $2\pi T_{\text{SD}}$, where T_{SD} is the temperature at the spinodal decomposition. The running of the constants is done with results in App. B.2.

With the cubic anisotropy model, we use

$$g_0^2 = 0.4, \tag{4.77}$$

$$\lambda_0 = 0.006, \tag{4.78}$$

$$m_0^2 = -1, \tag{4.79}$$

$$\mu_0 = 2\pi\sqrt{-\frac{24m_0^2}{g_0^2}}. \tag{4.80}$$

The self-coupling is much smaller than the upper limit for first-order transition, which is approximately g_0^2. The transition has to be very strong so that the mass of the χ-field is much larger than its uncertainty which is order $g^4 \ln g$. This prevents us from studying comprehensively the possibility of the derivative series breaking down. Hence, only one temperature point is tested in Subsec. 4.3.2.

4.3.1 Asymmetric Model

In this section, we will study the asymmetric model with the benchmark point from above. First, we will examine the temperature dependence of the exponential suppression and its dependence on the renormalization scale. Then, we study quantities that are relevant for the gravitational wave background from a particular transition.

Near a transition temperature, there happens an extraordinary cancellation between the terms in the effective potential. These cancellations do not happen to the running of the constants. Therefore, the renormalization scale dependence of the effective potential is huge compared to the potential itself, even though the running of each term in the potential is minuscule in comparison to the individual terms. This is shown in Fig. 4.9. It is clear that the description of the system at a particular temperature near its phase transition is far from accurate. However, we are interested in the transition as the system cools down and not in its state at a specific temperature.

Before assessing the true uncertainties in the quantities related to a transition, we will argue that the transition happens with almost identical exponential suppression as the renormalization scale is varied: The temperature at which a fraction of e^{-1} is still in the symmetric phase is presented in Ref. [7], and it can be solved from the following equation:

$$8\pi v_{\text{wall}}^3 A = \left(\frac{\mathrm{d}}{\mathrm{d}t} S\right)^4 e^S, \tag{4.81}$$

where v_{wall} is the speed of the bubble walls as the bubbles expand, A is the prefactor in

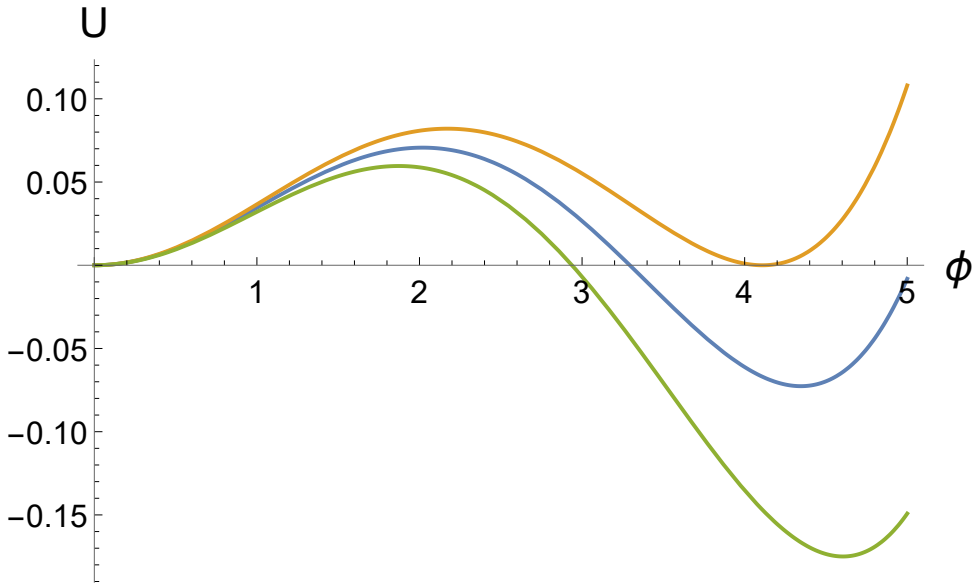

Figure 4.9: The effective potential is very dependent on the renormalization scale near the phase transition compared to its size size. The renormalization scales are $\mu = \{\pi T, 2\pi T, 4\pi T\}$, beginning from the top.

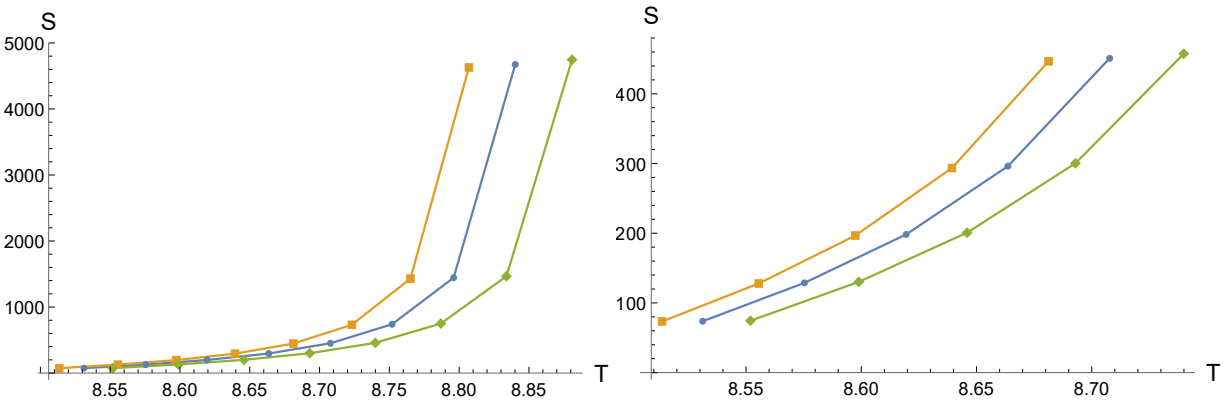

Figure 4.10: The temperature dependence of the exponential suppression from the critical bubble. The renormalization scales are $\mu = \{\pi T, 2\pi T, 4\pi T\}$, beginning from the left.

the nucleation rate, $\Gamma = Ae^{-S}$, and t refers to time. All of the quantities are dependent on temperature, but the equation as a whole is dominated by the exponential dependence on the action. Even a rather slight change in the action changes the right-hand side drastically, e.g. $\Delta S = 7$ leads to multiplication of the RHS approximately by 1100. Hence, the exponential suppression is, to a good approximation, the same as the renormalization scale is varied.

In Fig. 4.10, the exponential suppression from the critical bubble is plotted as a function of temperature. The curves are almost identical but shifted slightly in the temperature. From the figure, we can see that the renormalization scale dependence becomes uncertainty in the transition temperature from the perspective of the transition.

For the gravitational wave spectrum produced by a first-order transition, there are only a few important quantities [8]: the temperature of bubble wall collisions, the transition strength, α, the inverse duration of the transition, β, the Hubble rate at the transition H_*, the bubble wall speed and the speed of sound.

The transition strength is defined via the released trace anomaly $\theta = \frac{1}{4}(e - 3p)$ and the enthalpy density w:

$$\alpha = \frac{4\Delta\theta}{3w}, \tag{4.82}$$

$$\Delta\theta = \frac{1}{4}T^2\frac{\mathrm{d}}{\mathrm{d}T}U_{\text{eff}}(\phi_-) - \frac{3}{4}TU_{\text{eff}}(\phi_-), \tag{4.83}$$

$$w = \frac{4\pi^2}{45}T^4. \tag{4.84}$$

If the broken minimum is described by the potential U_{eff} in Eq. (3.102), the released trace anomaly can be expressed with it. This is done in the second equation, where ϕ_- refers to the broken phase. The enthalpy density is approximated with the enthalpy of two massless non-interacting scalars (cf. e.g. Ref. [26]). The transition strength and released trace anomaly are shown in Fig. 4.11.

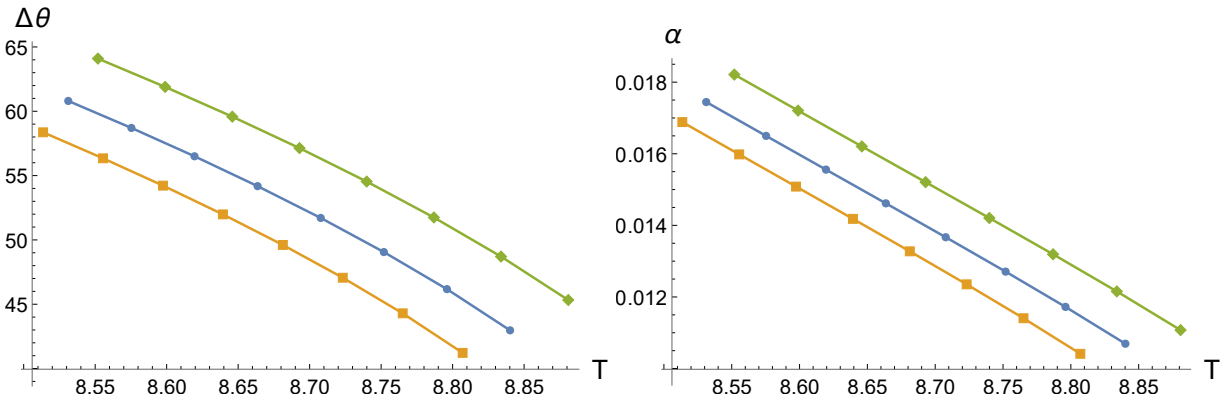

Figure 4.11: Released trace anomaly and the transition strength. Corresponding points along each graph roughly correspond to the same transition. This follows from each point having the almost the same exponential suppression (cf. Fig. 4.10). The renormalization scales are $\mu = \{\pi T, 2\pi T, 4\pi T\}$, beginning from the left.

The inverse duration of the transition is

$$\beta = \frac{\mathrm{d}}{\mathrm{d}t}\ln(\Gamma) \approx -\frac{\mathrm{d}}{\mathrm{d}t}S = H_* T \frac{\mathrm{d}}{\mathrm{d}T}S. \tag{4.85}$$

We first approximated that the derivative of the logarithm of the nucleation rate is dominated by the exponential suppression from the critical bubble and then assumed that the transition happens in a radiation dominated universe.

As discussed above, a transition happens with approximately the same exponential suppression from the critical bubble when the renormalization scale is varied. In Tab. 4.1, we show the quantities that can be obtained directly from the nucleation rate calculation. The transition is characterized by an exponential suppression of $S = 130$. The value is somewhat motivated by the electro-weak phase transition [8]. The running of these quantities describing the GW spectrum is rather small. However, we did not test how large the uncertainties in the spectrum itself are.

μ	πT	$2\pi T$	$4\pi T$
T_*	8.57	8.58	8.60
$T\frac{\mathrm{d}}{\mathrm{d}T}S$	12300	11900	11300
$\Delta\theta$	55.7	58.3	61.9
α	0.0157	0.0163	0.0172

Table 4.1: The table contains quantities that are important for the gravitational wave background from a transition. The values are for a transition characterized by $S = 130$. The quantity from the second row relates to the inverse duration of the transition β in Eq. (4.85). $\Delta\theta$ is the released trace anomaly and α is the transition strength from Eqs. (4.83) and (4.82).

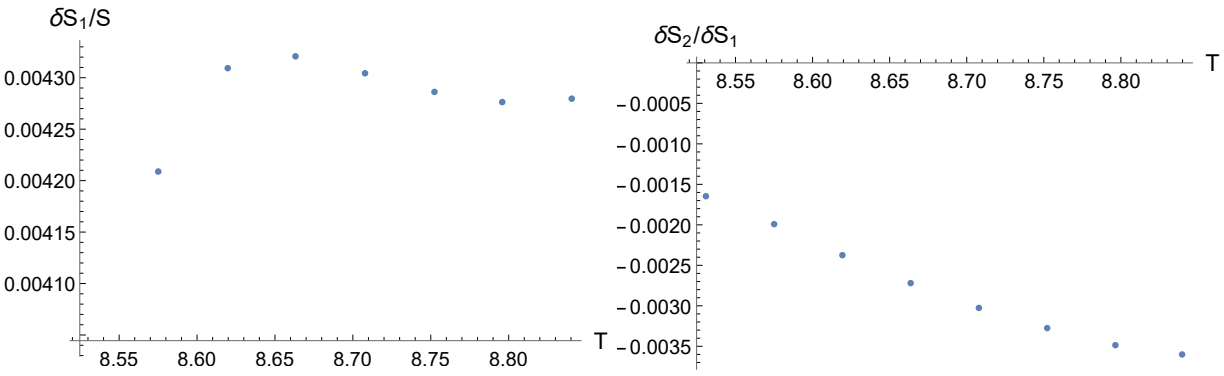

Figure 4.12: Figures show that the derivative series from one-loop diagram converges well in the benchmark point of the asymmetric model. δS_1 is the contribution from the first term in the one-loop derivative expansion, contained in Z in Eq. (3.103), and δS_2 is a part of the second term shown in Eq. (3.121). The renormalization scale is set as $\mu = 2\pi T$.

4.3.2 Derivative Series

In this subsection, we will look into the contributions of extra derivative terms. The leading such contribution is the first order derivative term from one-loop of χ, which is included into the wave function renormalizations in Eqs. (3.103) and (3.113). Another contribution we will examine is a part of the second order derivative term from one-loop, shown in Eq. (3.121). This contribution comes from the same diagram as the wave function renormalization but it is next order in derivatives. The contributions are evaluated with methods from Subsec. 4.2.3.

There are two objectives in this subsection. One is to see whether the extra contribution to the wave function renormalization is important as suggested by Subsec. 3.3.1. The other is to study the convergence of the effective action. The latter point is more prominent in the cubic anisotropy model, introduced in Sec. 3.3.4, because the inducing field is light in the symmetric phase. Due to reasons explained in the beginning of the section, we can only study a rather strong transition. It can very well be that it is not representative.

The claim, that the wave function renormalization factors in Eqs. (3.103) and (3.113) are important contributions to the exponential suppression, is not supported by the numerical results. At least in comparison with the full exponential suppression, the contribution is very small. This is illustrated in Fig. 4.12 on the left and in Tab. 4.2, where the contribution is denoted with δS_1. It might be that the contribution becomes important with different parameter values, but it is rather insignificant with the chosen benchmark values.

Next, we would like to examine the convergence of the derivative expansion. Obviously, a part of the next order does not tell the full story, and neither would the full next

Model	CAM	AM
S	3960	3740
δS_1	9.58	8.03
δS_2	-0.256	-0.103

Table 4.2: The table shows the convergence of the one-loop derivative series. CAM refers to the benchmark point of the cubic anisotropy model and AM to the asymmetric model with $\lambda_0 = 0.006$. δS_1 is the contribution from one-loop modification of the wave function renormalization and δS_2 is the partial second order in the one-loop derivative series, shown in Eq. (3.121). The temperature and renormalization scale are set as $T = 13$ and $\mu = 2\pi T$.

order, but it can tell something.

In Fig. 4.12 on the right, the partial second order in the one-loop derivative expansion δS_2 is compared to the first order. This is done with the benchmark point of the asymmetric model. It shows excellent convergence: The partial second order is minuscule compared to the first order, which, in turn, is minuscule compared to the full action.

In Tab. 4.2, we compare similar transitions from the cubic anisotropy model and the asymmetric model. The comparison is for checking whether the small χ-mass in the symmetric phase causes the derivative expansion to converge slower, or even break the convergence. Indeed, it seems that the convergence is slower but the difference is not drastic.

4.3.3 Thin-Wall Limit

In Secs. 3.2.3 and 3.3.6, it was discussed that, ultimately, the EFT created in Sec. 3.2 does not describe the critical bubble. This happens because the light degrees of freedom can relax within the plateau of the critical bubble and change the exponential suppression drastically. Very near the critical temperature, the relaxation of light degrees of freedom in the new phase can be responsible for the stability of the new phase. In these extreme cases, the EFT does not even contain a critical bubble at its tree-level.

In this section, we examine the cross-over in which the contribution from the plateau can be either incorporated into the fluctuation determinant or into the exponential suppression. In the former way, the critical bubble is solved from the EFT and, in the latter, the fluctuations have already been integrated out.

We have not presented a consistent effective theory approach for integrating out light degrees of freedom and, therefore, we resort to the thin-wall approximation presented in Subsec. 3.2.3. Also, the methods presented in Subsec. 4.2.3 do not work for evaluations of non-derivative quantities. For the estimation of the one-loop contribution from the ϕ-field, we use the radius obtained from Eq. (3.41) where the pressure is evaluated without

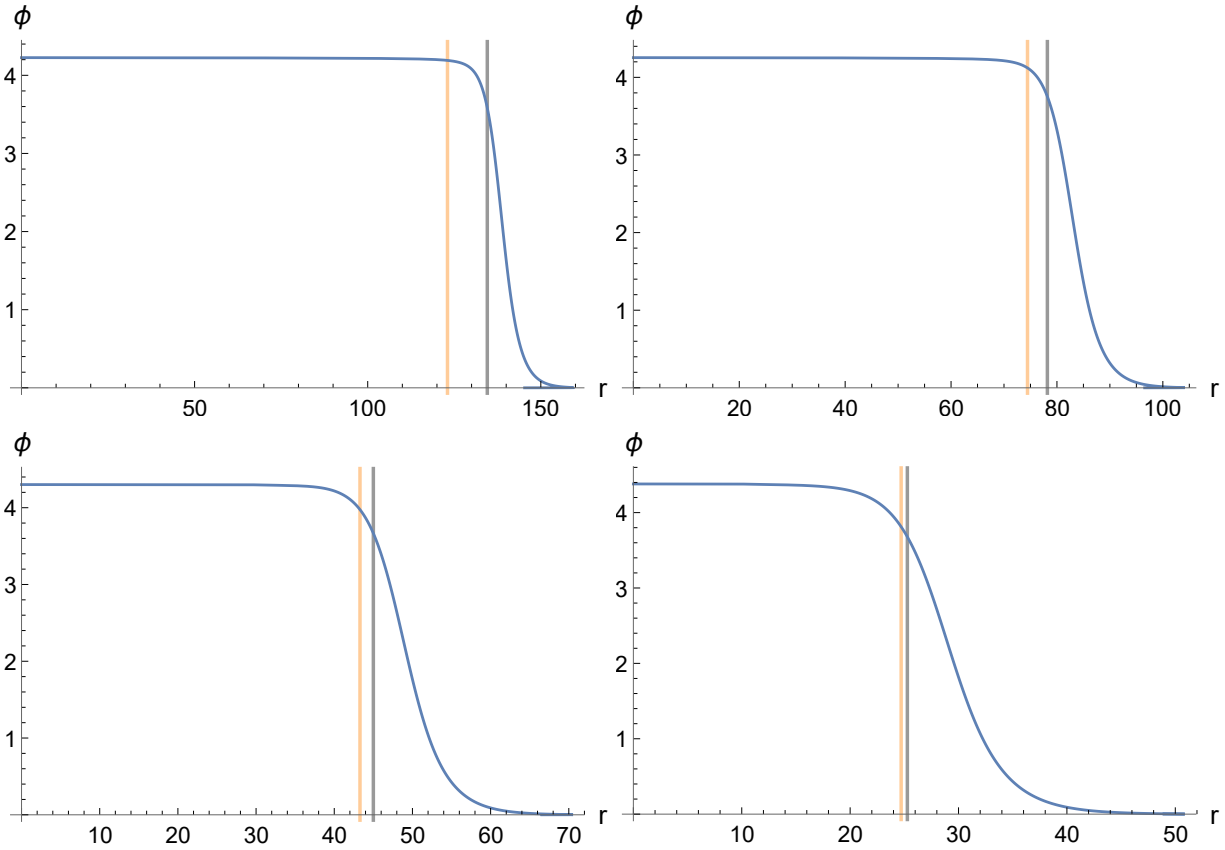

Figure 4.13: Four critical bubbles that have plateaux which is much larger than the correlation length of the ϕ-field. The two vertical lines correspond to the thin-wall approximations for the radius. The contribution of the ϕ-fluctuations to the pressure is not taken into account in the outer radii. The renormalization scale is set as $\mu = 2\pi T$ and the temperatures are $T = \{8.875, 8.870, 8.859, 8.840\}$.

the contribution from the ϕ-field. These radius estimates are shown in Fig. 4.13 as the outer vertical lines. They are all slight over-estimations of the size of the plateaux and, hence, give over-estimations for the ϕ-contributions.

The mass of the ϕ-field in the broken phase is $m_{\mathrm{Br}} > 0.431$ which means that the correlation length of the field, m_{Br}^{-1}, is much smaller than the radii of the plateaux presented in Fig. 4.13. Hence, the field can relax on the plateaux and, consequently, it can be integrated out into the action of the critical bubble.

As long as the ϕ-fluctuations on the plateau do not change the shape of the critical bubble too much, their contribution can be found from the fluctuation determinants of the ϕ-field. However, extremely near the critical temperature, the size of the critical bubble can be very dependent on the inclusion of the ϕ-fluctuations into the pressure of the broken phase. Then, the determinant, evaluated on the critical bubble configuration, does not give the correct value for the contribution from the fluctuations. In Fig. 4.13, this is illustrated with two vertical lines: the outer line corresponds to the radius from the thin-wall approximation without the ϕ-fluctuations in the pressure, and the inner line is

the thin-wall radius with the fluctuations included to the pressure. If the lines are close to each other, the ϕ-fluctuations do not change the bubble shape much.

The values from actions corresponding to the critical bubbles in Fig. 4.13 are listed in Tab. 4.3. Also, the estimations of ϕ-fluctuations are listed. The estimations are obtained via

$$\delta S_{1\mathrm{L}\phi} = \frac{4}{3}\pi R_1^3 \delta p_{1\mathrm{L}\phi}, \tag{4.86}$$

where the subscript of R_1 refers to the thin-wall approximation without including the ϕ-fluctuations into the pressure and the other subscript refers to the one-loop contribution from the ϕ-fluctuations.

The ϕ-fluctuations are very important in the exponential suppression in the least supercooled transition shown in Tab. 4.3. Sadly, we can see that the thin-wall approximation is not good yet: The thin-wall approximation without the ϕ-fluctuations should match the value from the action from the tunnelling potential method, but there is a clear discrepancy between the values. This is an indication of the fact that the thin-wall approximation including the fluctuations does not yet give an accurate value for the exponential suppression from the critical bubble.

Temperature	8.875	8.870	8.859	8.840
Tunnelling potential method	93900	34600	12700	4670
Thin-wall approximation 1	87700	29600	9790	3090
Thin-wall approximation 2	73300	26800	9060	2960
One-loop of ϕ	-16300	-3480	-759	-165

Table 4.3: The second row contains actions obtained via the tunnelling potential formalism. Thin-wall approximation 1 refers to the thin-wall approximation that omits the ϕ one-loop contribution to the pressure. Last row has the estimated contributions from the ϕ-fluctuations on the plateau of a thin-wall bubble. The estimation is done via the thin-wall radius that omits the ϕ-fluctuations.

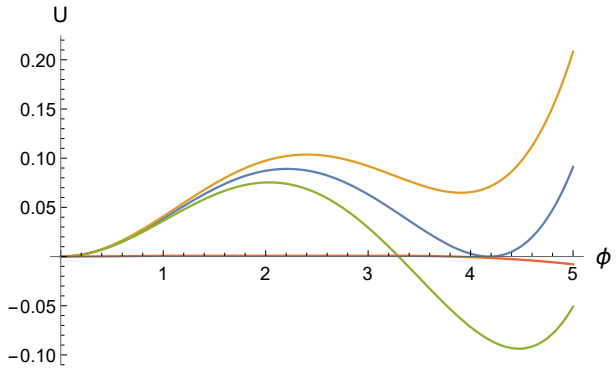

Figure 4.14: The renormalization scale dependence of the potential is much larger than the real part of the ϕ one-loop shown in red.

Lastly, I want to note that the ϕ-fluctuations are not the next in line as an improvement to the accuracy of the actions in Eqs. (3.102) and (3.112). The running of the potential is larger than the contribution of the fluctuations in the broken phase, shown in Fig. 4.14. The accuracy of the potential is not enough to describe the state of the system near the phase transition. However, it is not expected that an increase in precision would not alter the surface tension of the bubble wall nor the contribution from the one-loop level of the ϕ-field much. The precision changes mostly the accuracy of the critical temperature and, hence, the temperature of the thin-wall limit.

5. Conclusions and Outlook

We have applied the modern EFT framework to obtain an effective description for the critical bubble configuration of a high temperature phase transition. The effective description can then be used to yield the statistical part of the nucleation rate, i.e. the Boltzmann weighted hypersurface area in the field configuration space, through which the nucleation can happen, which contains the exponentially large contributions to the rate. With the framework, more precise predictions can be made for the nucleation rate of a cosmological phase transition from the corresponding particle physics model. These, in turn, can be used to make more precise predictions for observable consequences from the transition, such as the gravitational wave spectrum.

The phase transitions, that may have taken place in the early universe, are described via thermal field theory. For the statistical part, it is enough to use the imaginary time formulation of TFT, that captures the physics of thermal equilibrium. The critical bubble corresponding to the transition is never visible from the tree-level of the Euclidean action describing the TFT, because the phase transition is induced by thermal fluctuations. Therefore, we need to construct an effective description via integrating out fluctuations from the scales that are much shorter than the spatial variations in the critical bubble. The EFT framework is particularly suitable when there is a separation of scales. Usually, in thermal transitions, there is at least one high momentum scale, which is the scale of the temperature. This scale can be dealt with by using dimensional reduction [11, 12]. In symmetry breaking transitions, there can naturally also be a heavy scale, which is much lighter than the scale of the temperature. This scale can still drastically change the nature of the transition. Sometimes, the scales are not as straightforward. It is possible that a light field becomes heavy on the bubble configuration. It is currently unknown, how large an error comes from the incorrect treatment of the old phase.

The resulting effective field theory is able to describe the critical bubble and the fluctuations around it. By employing the EFT framework, there is no double counting of fluctuations. The fluctuations, that have been integrated out, create a background on which the critical bubble exists, and the remaining fluctuations, which are described by the EFT, are the ones comprising the bubble and its fluctuations. Another problem following from the double counting, which is an imaginary part to the effective action,

does not occur. It comes from integrating out the fluctuations of the nucleating field. In a thick-wall bubble, it is unphysical to integrate them out into the background, as they make up the critical bubble. In the thin-wall limit, however, these fluctuations can be integrated out within the plateau of the critical bubble, because there is room for them to relax and affect the pressure within the bubble.

In addition to dodging the double counting problem, the EFT framework has other benefits. It is possible to use the power counting to see what contributions are important and necessary to take into account. It is also much easier to compute the wanted contributions within the EFT framework than by doing the needed resummations explicitly or by coarse graining the potential. This is because a single momentum scale can be dealt with at a time, and its intricacies can be taken care of without other scales causing havoc. By using the power counting of the EFT, it is also possible to make the running of the action with the renormalization scale tiny, which corresponds to the results being precise.

Applying the EFT framework to gauge fields was not part of the thesis, and it is left for future work. The hope is that with the framework, a gauge independent result for the nucleation rate could be formulated, as has been done for the vacuum decay rate calculation [15]. A possible obstruction to this goal in symmetry breaking transitions is that the gauge fields are non-perturbative in the symmetric phase due to the Linde problem [13].

Another still open question is the ill-handling of the symmetric phase in the cubic anisotropy model. The fields are symmetric in the symmetric phase and this symmetry breaks only as a bubble nucleates. The non-nucleating field becomes heavy and can be integrated out on the bubble, which is actually crucial, because the first-order transition is induced by the field that becomes heavy. The method at hand does not discriminate between the bubble and the symmetric phase, so the inducing field is also integrated out in the symmetric phase, even though there is no hierarchy allowing this. Therefore, the symmetric phase is not described correctly in the final EFT. The resulting error should be quantified to see whether the methods can be trusted. The same problem, from a different perspective, can be seen in Ref. [31], where the effective description for the critical bubble was tackled with a coarse grained potential. There, the problem was that the fluctuation determinants of the inducing field gave a contribution too large, due to the strong coupling to the nucleating field. Our problem is different because we are integrating out too much, in a sense. This problem also relates to the transitions induced by gauge fields since the magnetic components are very light in the symmetric phase.

There is also future work related to the example models of Sec. 3.3. We did not compute the fluctuation determinants, which play in a key role in showing the validity of the nucleation rate calculation [38]. The calculation relies on the critical bubble and a saddle-point approximation around it, which takes into account nucleating bubbles

that are not exactly the critical bubble. In transitions that are weakly first order, the bubbles that nucleate can be quite different from the critical bubble, and the saddle-point approximation fails. The determinants are next-to-leading order in the saddle-point approximation, and therefore signal if the approximation breaks down.

Another point is that the effective action should be calculated even more precisely. Even though the next order does not contribute exponentially, it is still important for reducing the uncertainty in the transition temperature. Near the phase transition, there is a huge cancellation between the different terms of the effective potential, but the renormalization scale running does not cancel. Thus, there is a large running in comparison to the potential, as can be seen from Fig. 4.9. This running translates into uncertainty in the transition temperature of a phase transition.

Lastly, the results for exponential contributions to the nucleation rate in the example models should be double checked against different methods. The rate can be computed with lattice simulations [34], and the comparison with lattice data is left as future work.

There are other minor results in the thesis. One is the naive thermal nucleation rate of a classical field, whose result is in Eq. (2.40). As there is already a more comprehensive work on the rate including non-trivial time-evolution [21], the role of the simpler calculation is merely to help create intuition on the rate calculation. Another result is the generalization of the tunnelling potential formalism to apply to kinetically mixed scalar fields, where the mixing can depend on the field value. The tunnelling action is shown in Eq. (4.5). The last minor result is the improvement in the numerical implementation of the tunnelling potential action in Sec. 4.2, which aides the result to converge better near the stable and the metastable phases.

There is future work relating to all three points above. The classical nucleation rate was for a fixed background potential. An interesting and quite possibly extremely challenging task would be to calculate the real time nucleation rate in a situation, where the transition was induced by another field. Here, the relaxation time of the inducing field would affect the rate, and not only the relaxation of the nucleating field. As the accuracy requirements for the effective action might grow in the future, the tunnelling potential method would need to be generalized to handle higher order derivative terms. Currently, the possible derivative terms are limited to the form of $\boldsymbol{\nabla}\phi_a\, Z_{ab}(\phi)\boldsymbol{\nabla}\phi_b$ in Eq. (4.4). The numerical implementation of the tunnelling potential is not perfect, and it has not even been shown to actually converge to the correct solution as the discretization is made finer. One possible improvement would be to use a more refined choice for the implementation of the tunnelling potential, that would better conform to the features of the tunnelling potential result (cf. Eq. (4.55)). This could improve the critical bubble configuration obtained from the method, and the convergence of the action, although it is already pretty good as shown in Fig. 4.3.

A. Integrals for matching

In this appendix, we compute the relevant integrals for the matching procedures in Subsecs. 3.3.2 and 3.3.3. In the first section, we focus on the sum-integrals needed for the dimensional reduction. In the second, we compute the base cases for the diagrams of the heavy scale, which are then resummed via arguments in Ref. [33]. The resummation of the one-loop potential is done explicitly in the third section alongside the resummation of the first one-loop derivative term. Finally, a partial second order of the one-loop derivative expansion is calculated without resummation.

A.1 Sum-integrals

We will first show the results for the calculations, and then proceed to show them via Eqs. (3.23) and (3.24). Only the last diagram does not fall directly out of these and it can be take from e.g. Ref. [12].

$$= \mu^{2\epsilon} \oint_P \frac{1}{P^2} = \frac{T^2}{12} + \mathcal{O}(\epsilon). \tag{A.1}$$

$$= \mu^{2\epsilon} \oint_P \frac{1}{(P^2)^2} = \frac{1}{(4\pi)^2}\frac{1}{\epsilon} + \frac{2}{(4\pi)^2}\ln\left(\frac{e^\gamma \bar{\mu}}{4\pi T}\right) + \mathcal{O}(\epsilon). \tag{A.2}$$

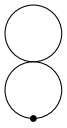

$$= \mu^{4\epsilon} \oint_P \frac{1}{(P^2)^2} \oint_Q \frac{1}{Q^2} = \frac{T^2}{12(4\pi)^2}\frac{1}{\epsilon} + \frac{T^2}{6(4\pi)^2}\ln\left(\frac{A^{12} e^\gamma \bar{\mu}^2}{(4\pi)^2 T^2}\right) + \mathcal{O}(\epsilon). \tag{A.3}$$

$$= \mu^{4\epsilon} \oint_{PQ} \frac{1}{P^2 Q^2 (P+Q)^2} = 0. \tag{A.4}$$

We will do a bit more general integral first, because all the three results come from

it nicely:

$$\begin{aligned}\oint\!\!\!\!\!\!\sum_P \frac{1}{(P^2)^l} &= 2T\sum_{n=1}^{\infty}\int_{\mathbf{p}}\frac{1}{(\mathbf{p}^2+(2\pi nT)^2)^l}\\ &= \frac{2T\,\Gamma(l-d/2)}{(4\pi)^{d/2}\,(2\pi T)^{2l-d}\,\Gamma(l)}\sum_{n=1}^{\infty}\frac{1}{n^{2l-d}}\\ &= \frac{2T\,\Gamma(l-d/2)\,\zeta(2l-d)}{(4\pi)^{d/2}\,(2\pi T)^{2l-d}\,\Gamma(l)}.\end{aligned} \tag{A.5}$$

On the first line, we noted that the $n=0$ integral vanishes as a scale-free integral. Then, we used Eq. (3.23) for the integrals and Eq. (3.24) for the sum.

We can now just expand the result in powers of ϵ with $d=3-2\epsilon$. The two first diagrams come from $l=1$ and $l=2$. To get the third diagram, it is useful to have the first diagram including $\mathcal{O}(\epsilon)$:


$$= \mu^{2\epsilon}\oint\!\!\!\!\!\!\sum_P \frac{1}{P^2} = \frac{T^2}{12}+\frac{T^2}{6}\ln\!\left(\frac{A^{12}\bar{\mu}}{4\pi T}\right)\epsilon+\mathcal{O}\big(\epsilon^2\big). \tag{A.6}$$

This is due to the ϵ^{-1} term in the second diagram, which causes an ϵ term to contribute at $\mathcal{O}(1)$ to the third diagram.

A.2 Three-dimensional Integrals

We will first compute all the base cases of the diagrams needed for results in Eqs. (3.99), (3.100) and (3.101). The results still need to be resummed via Ref. [33] explained in Subsec. 3.3.3. Here, we will also include the symmetry factors and powers of coupling constants into the results, but we are not going to carry explicitly the cut-off scale cluttering the calculations. It is needed only for the result of the sunset diagram, and it is added back in Eq. (A.23).

The results of the section are


$$= \int_{\mathbf{x}} -\frac{1}{3(4\pi)}(M_3^2)^{3/2}, \tag{A.7}$$


$$= \int_{\mathbf{x}} \frac{f_3}{8(4\pi)^2}M_3^2, \tag{A.8}$$


$$= -\int_{\mathbf{x}} \frac{g^4T^2}{8(4\pi)^2}\left[\frac{1}{2\epsilon}+\ln\!\left(\frac{\bar{\Lambda}^2}{4M_3^2}\right)+1\right]\phi^2, \tag{A.9}$$

where we have defined $\bar{\Lambda}$ in accordance with the $\overline{\text{MS}}$-scale (Eq. (3.81)).

The first diagram is:

$$\begin{aligned} \bigcirc &= -\ln \int \mathcal{D}\chi \exp(-S_{\chi 0}) \\ &= -\ln \left(\det \left(\frac{\delta(\mathbf{x}-\mathbf{y})(-\nabla_{\mathbf{x}}^2 + M_3^2)}{\pi} \right)^{-1/2} \right), \end{aligned} \tag{A.10}$$

where

$$S_{\chi 0} = \int_{\mathbf{x}} \left[\chi(\mathbf{y}) \delta(\mathbf{x}-\mathbf{y}) \left(-\nabla_{\mathbf{x}}^2 + M_3^2 \right) \chi(\mathbf{x}) \right] \tag{A.11}$$

is the free action of the χ-field.

A determinant is the product of the eigenvalues, which can be found with the eigenfunctions of the operator that are plane waves:

$$\int_{\mathbf{x}} \delta(\mathbf{x}-\mathbf{y}) \left(-\nabla_{\mathbf{x}}^2 + M_3^2 \right) e^{i\mathbf{k}\cdot\mathbf{x}} = \left(\mathbf{k}^2 + M_3^2 \right) e^{i\mathbf{k}\cdot\mathbf{y}}. \tag{A.12}$$

The eigenvalues are $\mathbf{k}^2 + M_3^2$.

Using the box regulator:

$$\begin{aligned} \bigcirc &= -\ln \left(\left(\prod_{\mathbf{k}} \frac{\mathbf{k}^2 + M_3^2}{\pi} \right)^{-1/2} \right) \\ &= \frac{1}{2} \sum_{\mathbf{k}} \left(\ln \left(1 + \frac{M_3^2}{\mathbf{k}^2} \right) + \ln \left(\frac{\mathbf{k}^2}{\pi} \right) \right) \\ &= \frac{V}{2} \int_{\mathbf{k}} \left(\ln \left(1 + \frac{M_3^2}{\mathbf{k}^2} \right) + \ln \left(\frac{\mathbf{k}^2}{\pi} \right) \right), \end{aligned} \tag{A.13}$$

where we have taken the continuum limit in the last equality.

The second integral vanishes as it is a scale free integral and the first integral can be solved the following way:

$$\begin{aligned} \int_{\mathbf{k}} \ln \left(1 + \frac{M_3^2}{\mathbf{k}^2} \right) &= \int \mathrm{d}\left(M_3^2 \right) \frac{\partial}{\partial (M_3^2)} \int_{\mathbf{k}} \ln \left(1 + \frac{M_3^2}{\mathbf{k}^2} \right) \\ &= \int \mathrm{d}\left(M_3^2 \right) \int_{\mathbf{k}} \frac{1}{\mathbf{k}^2 + M_3^2} \\ &= \int \mathrm{d}\left(M_3^2 \right) \frac{1}{(4\pi)^{d/2}} \Gamma(1-d/2) (M_3^2)^{d/2-1} \\ &= \frac{1}{(4\pi)^{d/2}} \Gamma(1-d/2) \frac{2}{d} (M_3^2)^{d/2} + C, \end{aligned} \tag{A.14}$$

where we have used Eq. (3.23) in the third equality. The constant can be set to zero because it is independent of M_3^2. Therefore, the result is

$$\bigcirc = \int_{\mathbf{x}} \frac{\Gamma(1-d/2)}{(4\pi)^{d/2} d} (M_3^2)^{d/2}, \tag{A.15}$$

where we have replaced the volume with an integral over the volume. We can now take $d \to 3$ to find the result in Eq. (A.7).

The next diagram is directly solvable through Eq. (3.23) and the three dimensional free Euclidean propagator:

$$= \int_{\mathbf{x}} \frac{f_3}{8} \langle \chi(\mathbf{x})\chi(\mathbf{x})\rangle_0^2$$

$$= \int_{\mathbf{x}} \frac{f_3}{8} \left(\int_{\mathbf{k}} \frac{1}{\mathbf{k}^2 + M_3^2} \right)^2$$

$$= \int_{\mathbf{x}} \frac{f_3}{8} \left(\frac{1}{(4\pi)^{d/2}} \Gamma(1-d/2) \left(M_3^2\right)^{1/2} \right)^2 . \tag{A.16}$$

Again, the limit $d \to 3$ gives the result in Eq. (A.8).

The last diagram of the effective potential is the two-loop sunset diagram:

$$= -\int_{\mathbf{x}} \int_{\mathbf{y}} \frac{g_3^4}{4} \phi(\mathbf{x})\phi(\mathbf{y}) \langle \phi(\mathbf{x})\phi(\mathbf{y})\rangle_0 \langle \chi(\mathbf{x})\chi(\mathbf{y})\rangle_0^2 . \tag{A.17}$$

It differs from the first two diagrams in that it already has external ϕ-legs and the propagators are between two distinct spatial locations. We will now get some foretaste on how the diagrams are expanded into a derivative expansion in App. A.3. However, we only need the first term so the expansion is cut short before the actual derivative terms.

We are doing strict perturbation theory in the ϕ-mass and therefore, its propagator is massless.

$$= -\int_{\mathbf{x}} \int_{\mathbf{y}} \frac{g_3^4}{4} \phi(\mathbf{x})\phi(\mathbf{y}) \int_{\mathbf{q}} \frac{e^{i\mathbf{q}\cdot(\mathbf{x}-\mathbf{y})}}{\mathbf{q}^2} \int_{\mathbf{k}} \frac{e^{i\mathbf{k}\cdot(\mathbf{x}-\mathbf{y})}}{\mathbf{k}^2 + M_3^2} \int_{\mathbf{p}} \frac{e^{i\mathbf{p}\cdot(\mathbf{x}-\mathbf{y})}}{\mathbf{p}^2 + M_3^2} . \tag{A.18}$$

To be able to get the potential term, we would like to identify the external momentum in which the diagram can be expanded. With a shift in the integration variables, $\mathbf{k} \to \mathbf{k} - \mathbf{q} - \mathbf{p}$, the only momentum in the exponent is $\mathbf{k}$:

$$= -\int_{\mathbf{x}} \int_{\mathbf{y}} \frac{g_3^4}{4} \phi(\mathbf{x})\phi(\mathbf{y}) \int_{\mathbf{k}} \int_{\mathbf{q}} \int_{\mathbf{p}} \frac{e^{i\mathbf{k}\cdot(\mathbf{x}-\mathbf{y})}}{\mathbf{q}^2(\mathbf{p}^2 + M_3^2)((\mathbf{k}-\mathbf{p}-\mathbf{q})^2 + M_3^2)} . \tag{A.19}$$

Using the Fourier transform of the ϕ-field, we obtain:

$$= -\frac{g_3^4}{4} \int_{\mathbf{k}} \phi(\mathbf{k})\phi(-\mathbf{k}) \int_{\mathbf{q}} \int_{\mathbf{p}} \frac{1}{\mathbf{q}^2(\mathbf{p}^2 + M_3^2)((\mathbf{k}-\mathbf{p}-\mathbf{q})^2 + M_3^2)} , \tag{A.20}$$

and now we can identify $\mathbf{k}$ as the external momentum.

The external momentum is of order $\mathbf{k}^2 \sim \bar{m}^2$ on the bubble solution due to the size of the critical bubble. The mass of the χ-field is $M_3^2 \sim g^2T^2$. Therefore, we can expand the integrand in the powers of $\mathbf{k}^2$, if $\bar{m}^2 \ll g^2T^2$.

In the transition near the critical temperature and the mass being of order $\tilde{m}^2 \sim g^3T^2$, we only need the zeroth order term because the next term would already be too small:

$$g^4T^2 \frac{\mathbf{k}^2}{M_3^2} \phi^2 \sim g^5T^3 , \tag{A.21}$$

where the temperature appears from the three-dimensional couplings and the mass of the χ-field comes from being the only dimensionful parameter in the integrals over $\mathbf{p}$ and $\mathbf{q}$.

Now we can continue from the equation (A.19) with setting $\mathbf{k} = 0$ in the denominator and perform the integrals over $\mathbf{k}$ and $\mathbf{y}$:

$$\text{  } = -\int_{\mathbf{x}} \frac{g_3^4}{4}\phi(\mathbf{x})^2 \int_{\mathbf{q}}\int_{\mathbf{p}} \frac{1}{\mathbf{q}^2(\mathbf{p}^2+M_3^2)((\mathbf{p}+\mathbf{q})^2+M_3^2)} \tag{A.22}$$

The term is now manifestly local.

The integrals over $\mathbf{p}$ and $\mathbf{q}$ are computed with the help from Ref. [11]:

$$\Lambda^{4\epsilon}\int_{\mathbf{p}}\int_{\mathbf{q}} \frac{1}{(\mathbf{p}^2+m_1^2)(\mathbf{q}^2+m_2^2)((\mathbf{p}+\mathbf{q})^2+m_3^2)} = \frac{1}{(4\pi)^2}\left[\frac{1}{4\epsilon}+\ln\left(\frac{\bar{\Lambda}}{m_1+m_2+m_3}\right)+\frac{1}{2}\right] \tag{A.23}$$

Here, we have not been so careful with the appearance of the cut-off scale because the integrals above have not produced logarithmic divergences that would show in dimensional regularization. The sunset diagram is logarithmically divergent in three dimensions. Hence, the cut-off scale is added back in. We obtain the result in Eq. (A.9) by combining Eqs. (A.22) and (A.23).

A.3 Resummations on One-Loop Level

We will now reproduce the full one-loop result in Eq. (3.99), including the first derivative term. We will start by looking at a single term in the one-loop series with n external ϕ^2-legs. From the term, we will identify the part that corresponds to the integral over the loop momentum in Eq. (A.30). Expanding the part in external momenta gives the derivative series. The expansion can then be used to calculate the first two terms in the derivative series. The one-loop effective potential is reproduced in App. A.3.1 and the first derivative term is calculated in App. A.3.2. Methods from this section are used to calculated a part of the second derivative term from one-loop in App. A.4.

The one-loop contribution to the effective action with n external ϕ^2-legs is

$$S_{n,\text{one-loop}} = \frac{(-1)^{n+1}}{n!}\left(\frac{g^2T}{4}\right)^n \int_{\mathbf{x}_1}\cdots\int_{\mathbf{x}_n} \phi^2_{\mathbf{x}_1}\cdots\phi^2_{\mathbf{x}_n}\left\langle\chi^2_{\mathbf{x}_1}\cdots\chi^2_{\mathbf{x}_n}\right\rangle_{0,\text{c}}. \tag{A.24}$$

There are $2^{n-1}(n-1)!$ ways of Wick contracting the loop from the χ-correlator:

$$S_{n,\text{one-loop}} = \frac{(-1)^{n+1}}{2n}\left(\frac{g^2T}{2}\right)^n \int_{\mathbf{x}_1}\cdots\int_{\mathbf{x}_n} \phi^2_{\mathbf{x}_1}\cdots\phi^2_{\mathbf{x}_n}\left\langle\chi_{\mathbf{x}_1}\chi_{\mathbf{x}_2}\right\rangle_0\cdots\left\langle\chi_{\mathbf{x}_n}\chi_{\mathbf{x}_1}\right\rangle_0. \tag{A.25}$$

Using the form of the three-dimensional Euclidean propagator:

$$S_{n,\text{one-loop}} = \frac{(-1)^{n+1}}{2n}\left(\frac{g^2T}{2}\right)^n \int_{\mathbf{x}_1}\cdots\int_{\mathbf{x}_n}\int_{\mathbf{k}_1}\cdots\int_{\mathbf{k}_n} \phi^2_{\mathbf{x}_1}\cdots\phi^2_{\mathbf{x}_n} e^{i\sum_{j=1}^n \mathbf{k}_j\cdot(\mathbf{x}_j-\mathbf{x}_{j+1})}\prod_{j=1}^n\left(\mathbf{k}_j^2+M_3^2\right)^{-1}, \tag{A.26}$$

where $\mathbf{x}_{n+1}$ is the same as $\mathbf{x}_1$.

Now we will do a shift of the integration variables:

$$\mathbf{k}_j \to \mathbf{q} + \mathbf{k}_j,\ j < n \tag{A.27}$$

$$\mathbf{k}_n \to \mathbf{q} \tag{A.28}$$

The advantage is that $\mathbf{q}$ does not appear in the exponential, which means that $\mathbf{q}$ is the loop momentum and $\mathbf{k}$'s are associated with external momenta:

$$S_{n,\text{one-loop}} = \frac{(-1)^{n+1}}{2n}\left(\frac{g^2T}{2}\right)^n \int_{\mathbf{x}_1}\dots\int_{\mathbf{x}_n}\int_{\mathbf{k}_1}\dots\int_{\mathbf{k}_{n-1}} \phi^2_{\mathbf{x}_1}\dots\phi^2_{\mathbf{x}_n} e^{i\sum_{j=1}^{n-1}\mathbf{k}_j\cdot(\mathbf{x}_j-\mathbf{x}_{j+1})} \times \underbrace{\int_{\mathbf{q}}\left(\mathbf{q}^2+M_3^2\right)^{-1}\prod_{j=1}^{n-1}\left((\mathbf{q}+\mathbf{k}_j)^2+M_3^2\right)^{-1}}_{\equiv I_{\mathbf{q}}(\{\mathbf{k}\},M_3,n)}. \tag{A.29}$$

In the expression above, the integral over $\mathbf{q}$ is the loop integral. It can be expanded in the external momenta as was done with the sunset diagram in App. A.2. In App. A.3.2, we will see how the external momenta are transformed into gradients in the terms of an effective action.

What we want to do next is to shape the integral over $\mathbf{q}$ into such a form that the expansion in $\mathbf{k}$'s is nice:

$$I_{\mathbf{q}}(\{\mathbf{k}\},M_3,n) = \int_{\mathbf{q}} \frac{1}{((\mathbf{q}+\mathbf{k}_1)^2+M_3^2)\dots((\mathbf{q}+\mathbf{k}_{n-1})^2+M_3^2)(\mathbf{q}^2+M_3^2)}. \tag{A.30}$$

Using Feynman parameters

$$\frac{1}{a_1\dots a_n} = \int_0^1 \mathrm{d}t_1\dots\mathrm{d}t_n \frac{\delta\Big(1-\sum_j t_j\Big)(n-1)!}{(t_1a_1+\dots+t_na_n)^n} \tag{A.31}$$

the $\mathbf{q}$ integral eventually becomes

$$I_{\mathbf{q}}(\{\mathbf{k}\},M_3,n) = \int_{\mathbf{q}}\int_0^1 \mathrm{d}t_1\dots\mathrm{d}t_n \frac{\delta\Big(1-\sum_j t_j\Big)(n-1)!}{\left(\mathbf{q}^2+M_3^2+K^2\right)^n}, \tag{A.32}$$

where we have defined $K^2 \equiv \sum_{j=1}^{n-1} t_j\mathbf{k}_j^2 - \left(\sum_{j=1}^{n-1} t_j\mathbf{k}_j\right)^2$.

The derivative expansion is obtained by expanding the integrand into series in K^2:

$$I_{\mathbf{q}}(\{\mathbf{k}\},M_3,n) = \int_{\mathbf{q}}\int_0^1 \mathrm{d}t_1\dots\mathrm{d}t_n\delta\Big(1-\sum_j t_j\Big)\sum_{l=0}^{\infty}(-1)^l\frac{(n-1+l)!}{l!}\frac{(K^2)^l}{\left(\mathbf{q}^2+M_3^2\right)^{n+l}}. \tag{A.33}$$

We can perform the integral over $\mathbf{q}$ by using Eq. (3.23):

$$I_{\mathbf{q}}(\{\mathbf{k}\},M_3,n) = \frac{1}{(4\pi)^{d/2}}\int_0^1 \mathrm{d}t_1\dots\mathrm{d}t_n\delta\Big(1-\sum_j t_j\Big)\sum_{l=0}^{\infty}(-1)^l\frac{\Gamma(n+l-d/2)}{l!}\frac{(K^2)^l}{(M_3^2)^{n+l-d/2}}. \tag{A.34}$$

The gradient expansion comes from different values of l. For $l = 0$, there are no external momenta and, after summing over n, this reproduces the one-loop effective potential. $l = 1$ gives the first derivative term. These are computed in the next two subsections.

A.3.1 Reproducing the One-Loop Effective Potential

Here, we will reproduce the one-loop contribution to the effective potential in Eq. (3.102). We need the $l = 0$ term from (A.34) for a term in the one-loop series in Eq. (A.29). The whole one-loop contribution comes from resumming all the terms. We will do this the other way round by starting from the correct one-loop result and seeing that it matches with the terms that we have obtained from Eq. (A.29).

After the t_1 integral, the term $l = 0$ of the expansion of $I_{\mathbf{q}}(\{\mathbf{k}\}, M_3, n)$ is

$$I_{\mathbf{q},l=0}(\{\mathbf{k}\}, M_3, n) = \frac{1}{(4\pi)^{d/2}} \frac{1}{(n-1)!} \Gamma(n - d/2)(M_3^2)^{d/2-n}. \tag{A.35}$$

Inserting this back to the equation (A.29) and integrating over $\mathbf{k}$'s and $\mathbf{x}$'s gives:

$$S_{n,11,0} = \int_{\mathbf{x}} \frac{(-1)^{n+1}}{(4\pi)^{d/2}} \frac{1}{2n!} \Gamma(n - d/2)(M_3^2)^{d/2-n} (\frac{g^2 T}{2} \phi^2)^n \tag{A.36}$$

One of the $\mathbf{x}$ integrals was left over and it was relabelled with $\mathbf{x}$.

We already have a result for the one-loop effective potential that can be obtained via the resummation method of Ref. [33] with the result of Eq. (A.15). We can now double-check the resummation by comparing its expansion with the terms that we have in Eq. (A.36):

$$\begin{aligned}
&\int_{\mathbf{x}} \frac{1}{(4\pi)^{d/2}} \frac{\Gamma(1 - d/2)}{d} (M_3^2 + \frac{g^2 T}{2} \phi^2)^{d/2} \\
&= \int_{\mathbf{x}} \frac{1}{(4\pi)^{d/2}} \frac{\Gamma(1 - d/2)}{d} \left((M_3^2)^{d/2} + \sum_{n=1}^{\infty} \frac{1}{n!} (M_3^2)^{d/2-n} (\frac{g^2 T}{2} \phi^2)^n \prod_{i=0}^{n-1} (d/2 - i) \right) \\
&= \sum_{n=0}^{\infty} \int_{\mathbf{x}} \frac{1}{(4\pi)^{d/2}} \frac{(-1)^{n+1}}{2n!} \Gamma(n - d/2)(M_3^2)^{d/2-n} (\frac{g^2 T}{2} \phi^2)^n.
\end{aligned} \tag{A.37}$$

As we can see, resumming over the external legs of ϕ^2, i.e. summing over n, gives us the result that we already anticipated.

A.3.2 First Gradient Term

The first term in the derivative series is obtained from the $l = 1$ term of the $I_{\mathbf{q}}(\{\mathbf{k}\}, M_3, n)$ expansion (A.34).

Due to the form of $K^2 = \sum_{j=1}^{n-1} t_j \mathbf{k}_j^2 - \left(\sum_{j=1}^{n-1} t_j \mathbf{k}_j\right)^2$,the t-integrals are more complicated. We need to use:

$$\int_0^1 \mathrm{d}t_1 ... \mathrm{d}t_n \delta\Big(1 - \sum_j t_j\Big) t_1 = \frac{1}{n!} \tag{A.38}$$

$$\int_0^1 \mathrm{d}t_1 ... \mathrm{d}t_n \delta\Big(1 - \sum_j t_j\Big) t_1^2 = \frac{2}{(n+1)!} \tag{A.39}$$

$$\int_0^1 \mathrm{d}t_1 ... \mathrm{d}t_n \delta\Big(1 - \sum_j t_j\Big) t_1 t_2 = \frac{1}{(n+1)!}. \tag{A.40}$$

After integrating over t's, we have:

$$I_{\mathbf{q},l=1}(\{\mathbf{k}\}, M_3, n) = -\frac{1}{(4\pi)^{d/2}} \frac{\Gamma(n+1-d/2)}{n!} \left(\sum_{j=1}^{n-1} \mathbf{k}_j^2 - \frac{2}{n+1} \sum_{j=1}^{n-1} \sum_{i=1}^{j} \mathbf{k}_j \cdot \mathbf{k}_i \right) (M_3^2)^{d/2-n-1}. \tag{A.41}$$

From Eq. (A.29), we see that we need to compute the following type of integral:

$$I_{\mathbf{k}} = \int_{\mathbf{x}_1} ... \int_{\mathbf{x}_n} \int_{\mathbf{k}_1} ... \int_{\mathbf{k}_{n-1}} \phi_{\mathbf{x}_1}^2 ... \phi_{\mathbf{x}_n}^2 e^{i \sum_{h=1}^{n-1} \mathbf{k}_h \cdot (\mathbf{x}_h - x_{h+1})} \mathbf{k}_i \cdot \mathbf{k}_j, \quad i \leq j. \tag{A.42}$$

We can perform all $\mathbf{k}$ integrals except $\mathbf{k}_i$ and $\mathbf{k}_j$ giving us delta functions of coordinates. With the help of the delta functions, we then perform the $\mathbf{x}$ integrals except $\mathbf{x}_i$, $\mathbf{x}_j$ and $\mathbf{x}_{j+1}$. For clarity, we replace $\mathbf{x}_i$ with $\mathbf{z}$, $\mathbf{x}_j$ with $\mathbf{x}$ and $\mathbf{x}_{j+1}$ with $\mathbf{y}$:

$$I_{\mathbf{k}} = \int_{\mathbf{z}} \int_{\mathbf{x}} \int_{\mathbf{y}} \int_{\mathbf{k}_i} \int_{\mathbf{k}_j} \phi_{\mathbf{z}}^{2i} \phi_{\mathbf{x}}^{2(j-i)} \phi_{\mathbf{y}}^{2(n-j)} e^{i(\mathbf{k}_i \cdot (\mathbf{z}-\mathbf{x}) + \mathbf{k}_j \cdot (\mathbf{x}-\mathbf{y}))} \mathbf{k}_i \cdot \mathbf{k}_j, \quad i \leq j. \tag{A.43}$$

We can represent $\mathbf{k}$'s as derivatives acting on the exponential function:

$$I_{\mathbf{k}} = \int_{\mathbf{z}} \int_{\mathbf{x}} \int_{\mathbf{y}} \int_{\mathbf{k}_i} \int_{\mathbf{k}_j} \phi_{\mathbf{z}}^{2i} \phi_{\mathbf{x}}^{2(j-i)} \phi_{\mathbf{y}}^{2(n-j)} (\boldsymbol{\nabla}_{\mathbf{z}} \cdot \boldsymbol{\nabla}_{\mathbf{y}}) e^{i(\mathbf{k}_i \cdot (\mathbf{z}-\mathbf{x}) + \mathbf{k}_j \cdot (\mathbf{x}-\mathbf{y}))}, \quad i \leq j. \tag{A.44}$$

The gradients operate on the fields after integrating by parts:

$$I_{\mathbf{k}} = 4i(n-j) \int_{\mathbf{z}} \int_{\mathbf{x}} \int_{\mathbf{y}} \int_{\mathbf{k}_i} \int_{\mathbf{k}_j} \phi_{\mathbf{z}}^{2i-1} \phi_{\mathbf{x}}^{2(j-i)} \phi_{\mathbf{y}}^{2(n-j)-1} e^{i(\mathbf{k}_i \cdot (\mathbf{z}-\mathbf{x}) + \mathbf{k}_j \cdot (\mathbf{x}-\mathbf{y}))} \boldsymbol{\nabla}_{\mathbf{z}} \phi_{\mathbf{z}} \cdot \boldsymbol{\nabla}_{\mathbf{y}} \phi_{\mathbf{y}}, \quad i \leq j \tag{A.45}$$

Now we can finally perform the remaining integrals apart from the $\mathbf{x}$ integral:

$$I_{\mathbf{k}} = 4i(n-j) \int_{\mathbf{x}} \phi^{2n-2} (\boldsymbol{\nabla} \phi)^2, \quad i \leq j \tag{A.46}$$

Before assembling our term, we will tidy up the nasty looking sums in (A.41). We can factor out everything else from these sums apart from the coefficient of (A.46):

$$\sum_{j=1}^{n-1} 4j(n-j) - \frac{2}{n+1} \sum_{j=1}^{n-1} \sum_{i=1}^{j} 4i(n-j) = \frac{n^2(n-1)}{3} \tag{A.47}$$

We can now assemble the term with $2n$ external ϕ-legs:

$$S_{n,1\mathrm{l},l=1} = \int_{\mathbf{x}} \frac{(-1)^n}{(4\pi)^{d/2}} \frac{1}{6} \frac{\Gamma(n+1-d/2)}{(n-2)!} (M_3^2)^{d/2-n-1} \left(\frac{g^2T}{2}\right)^n \phi^{2n-2} (\boldsymbol{\nabla}\phi)^2. \tag{A.48}$$

We will again start from the resummed term and expand it to show its correctness:

$$\begin{aligned}
S_{1\mathrm{l},l=1} &= \int_{\mathbf{x}} \frac{g^4T^2}{24} \frac{1}{(4\pi)^{d/2}} \Gamma(3-d/2) \frac{1}{(M_3^2 + \frac{g^2T}{2}\phi^2)^{3-d/2}} \phi^2 (\boldsymbol{\nabla}\phi)^2 \\
&= \int_{\mathbf{x}} \frac{g^4T^2}{24} \frac{1}{(4\pi)^{d/2}} \Gamma(3-d/2) \phi^2 (\boldsymbol{\nabla}\phi)^2 \sum_{n=0}^{\infty} \frac{1}{n!} \Big(M_3^2\Big)^{d/2-3-n} \left(\frac{g^2T}{2}\phi^2\right)^n \prod_{i=0}^{n-1} (d/2-3-i) \\
&= \sum_{n=0}^{\infty} \int_{\mathbf{x}} (-1)^n \frac{1}{6} \frac{1}{(4\pi)^{d/2}} \frac{\Gamma(n+3-d/2)}{n!} \left(\frac{g^2T}{2}\right)^{n+2} \phi^{2n+2} (\boldsymbol{\nabla}\phi)^2 \Big(M_3^2\Big)^{d/2-3-n} \\
&= \sum_{n=2}^{\infty} \int_{\mathbf{x}} \frac{1}{6} \frac{(-1)^n}{(4\pi)^{d/2}} \frac{\Gamma(n+1-d/2)}{(n-2)!} \left(\frac{g^2T}{2}\right)^n \phi^{2n-2} (\boldsymbol{\nabla}\phi)^2 \Big(M_3^2\Big)^{d/2-1-n} \\
&= \sum_{n=2}^{\infty} S_{n,1\mathrm{l},l=1}.
\end{aligned} \tag{A.49}$$

As there are no $l = 1$ terms with $n < 2$, the term on the first line is the correct resummed first derivative term from the one-loop diagram.

A.4 Partial Second Order in the One-Loop Derivative Expansion

We will compute the result that is shown in Eq. (3.121) and is used to examine the convergence of the derivative series in Subsec. 4.3.2. We are not actually going to conduct the whole resummation but just calculate the base case and just assume the resummation. This result is just meant to be suggestive about the convergence of the derivative series.

The term that we wish to calculate from Eq. (A.34) is $n = 2$, $l = 2$:

$$I_{\mathbf{q},l=2}(\{\mathbf{k}\}, M_3, 2) = \frac{1}{(4\pi)^{d/2}} \frac{\Gamma(4-d/2)}{60} \frac{(\mathbf{k}_1^2)^2}{(M_3^2)^{4-d/2}}. \tag{A.50}$$

Thus, the whole term from Eq. (A.29) becomes

$$S_{2,1\mathrm{l},l=2} = -\frac{g^4T^2}{16} \int_{\mathbf{x}_1} \int_{\mathbf{x}_2} \int_{\mathbf{k}_1} \phi_{\mathbf{x}_1}^2 \phi_{\mathbf{x}_2}^2 e^{i\mathbf{k}_1\cdot(\mathbf{x}_1-\mathbf{x}_2)} \frac{1}{(4\pi)^{d/2}} \frac{\Gamma(4-d/2)}{60} \frac{(\mathbf{k}_1^2)^2}{(M_3^2)^{4-d/2}} \tag{A.51}$$

$$= -g^4T^2 \frac{\Gamma(4-d/2)}{960} \frac{(M_3^2)^{d/2-4}}{(4\pi)^{d/2}} \int_{\mathbf{x}_1} \int_{\mathbf{x}_2} \int_{\mathbf{k}_1} \phi_{\mathbf{x}_1}^2 \phi_{\mathbf{x}_2}^2 e^{i\mathbf{k}_1\cdot(\mathbf{x}_1-\mathbf{x}_2)} (\mathbf{k}_1^2)^2 \tag{A.52}$$

$$= -g^4T^2 \frac{\Gamma(4-d/2)}{960} \frac{(M_3^2)^{d/2-4}}{(4\pi)^{d/2}} \int_{\mathbf{x}_1} \int_{\mathbf{x}_2} \int_{\mathbf{k}_1} \phi_{\mathbf{x}_1}^2 \phi_{\mathbf{x}_2}^2 \boldsymbol{\nabla}_{\mathbf{x}_1}^2 \boldsymbol{\nabla}_{\mathbf{x}_2}^2 e^{i\mathbf{k}_1\cdot(\mathbf{x}_1-\mathbf{x}_2)} \tag{A.53}$$

$$= -g^4T^2 \frac{\Gamma(4-d/2)}{960} \frac{(M_3^2)^{d/2-4}}{(4\pi)^{d/2}} \int_{\mathbf{x}_1} \int_{\mathbf{x}_2} \int_{\mathbf{k}_1} \boldsymbol{\nabla}_{\mathbf{x}_1}^2 \phi_{\mathbf{x}_1}^2 \boldsymbol{\nabla}_{\mathbf{x}_2}^2 \phi_{\mathbf{x}_2}^2 e^{i\mathbf{k}_1\cdot(\mathbf{x}_1-\mathbf{x}_2)} \tag{A.54}$$

$$= -g^4T^2 \frac{\Gamma(4-d/2)}{960} \frac{(M_3^2)^{d/2-4}}{(4\pi)^{d/2}} \int_{\mathbf{x}} (\boldsymbol{\nabla}^2\phi^2)^2, \tag{A.55}$$

which gives the result for Eq. (3.121) when $d \to 3$ and after replacing M_3^2 with the assumed resummed version $M_3^2 + \frac{g^2 T}{2}\phi^2$.

B. Renormalization and Running of the Couplings

In this appendix, we renormalize the example model of two real scalars to the order needed in Sec. 3.3. The renormalization procedure follows the one presented in Subsec. 3.1.2. We also compute the running of couplings in the renormalization scale. This is needed to cancel the dependence of the effective action on the cut-off scale.

B.1 Renormalization

We give first the list of the results of this subsection, which contains all the counterterms up to the wanted order for the example calculation in Sec. 3.3, and then proceed with the calculations.

$$\delta_{m^2} = \frac{g^2 M^2}{2(4\pi)^2}\frac{1}{\epsilon}. \tag{B.1}$$

$$\delta_{\lambda} = \frac{3g^4}{2(4\pi)^2}\frac{1}{\epsilon}. \tag{B.2}$$

$$\delta_{g^2} = \frac{1}{(4\pi)^2}\left(\frac{fg^2}{2} + 2g^4\right)\frac{1}{\epsilon}. \tag{B.3}$$

The results are obtained by requiring that the results in Eqs. (B.4) (B.5) and (B.6) are finite in the limit of $\epsilon \to 0$. We use the $\overline{\text{MS}}$-scheme, so only the divergent part is included to the counterterm.

As stated in Subsec. 3.1.2, the renormalization of a thermal field theory is done at zero temperature. This means that the sum-integrals are reduced to four-dimensional Euclidean integrals. Simple use of Eq. (3.23) is enough for solving all of the needed integrals.

The one-loop two-point diagram is not dependent on the external momentum and therefore does not give rise to a wave function renormalization counterterm. The only

divergence is associated with the mass counterterm:

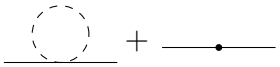

$$= -\frac{\mu^{2\epsilon} g^2}{2} \int_Q \frac{1}{Q^2 + M^2} - \delta_{m^2}$$
$$= \frac{g^2 M^2}{2(4\pi)^2} \frac{1}{\epsilon} - \delta_{m^2} + \mathcal{O}\Big(g^2 M^2\Big) \tag{B.4}$$

Let us now renormalize the four-point function of ϕ. The four-point function does depend on the external momentum. However, we know that there are no divergences related to the external momentum due to the renormalizable nature of our model. If there was such a divergence, there would be an extra term in the Lagrangian, whose form would be $\phi^2(\boldsymbol{\nabla}\phi)^2$. The theory would not be renormalizable if it included this term. Therefore, the diagram can be evaluated with zero external momentum:

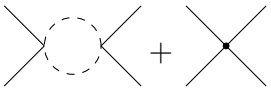

$$= \frac{3\mu^{4\epsilon} g^4}{2} \int_Q \frac{1}{(Q^2 + M^2)^2} - \mu^{2\epsilon} \delta_\lambda$$
$$= \mu^{2\epsilon} \left[\frac{3g^4}{2(4\pi)^2} \frac{1}{\epsilon} - \delta_\lambda + \mathcal{O}\Big(g^4\Big) \right]. \tag{B.5}$$

Finally, onto δ_{g^2}:

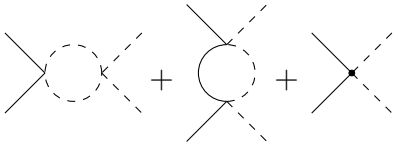

$$= \mu^{2\epsilon} \left[\frac{1}{(4\pi)^2} \Big(\frac{1}{2} f g^2 + 2g^4 \Big) \frac{1}{\epsilon} - \delta_{g^2} + \mathcal{O}\Big(g^4,\, f g^2\Big) \right]. \tag{B.6}$$

B.2 Running of the Couplings

To the order that we do the matchings in Sec. 3.3, there is already dependence on the cut-offs. In the current section, we calculate the running of the couplings to replace the cut-off dependence with the renormalization scale dependence. We show the results here before calculating them:

$$\lambda(\mu') = \lambda(\mu) - \frac{3g^4}{(4\pi)^2} \ln\left(\frac{\mu}{\mu'}\right), \tag{B.7}$$

$$g^2(\mu') = g^2(\mu) - \frac{4g^4 + f g^2}{(4\pi)^2} \ln\left(\frac{\mu}{\mu'}\right), \tag{B.8}$$

$$m^2(\mu') = m^2(\mu) - \frac{g^2 M^2}{(4\pi)^2} \ln\left(\frac{\mu}{\mu'}\right). \tag{B.9}$$

There is a neat way to calculate the running of the couplings [40]: The bare couplings

(cf. (3.30) and (3.31)) do not depend on the scale and therefore:

$$\mu\frac{\mathrm{d}\lambda_0}{\mathrm{d}\mu} = 0 \qquad \Rightarrow \qquad \mu\frac{\mathrm{d}\lambda}{\mathrm{d}\mu} = -2\epsilon\lambda - 2\epsilon\delta_\lambda - \mu\frac{\mathrm{d}\delta_\lambda}{\mathrm{d}\mu} \tag{B.10}$$

$$\mu\frac{\mathrm{d}g_0^2}{\mathrm{d}\mu} = 0 \qquad \Rightarrow \qquad \mu\frac{\mathrm{d}g^2}{\mathrm{d}\mu} = -2\epsilon g^2 - 2\epsilon\delta_{g^2} - \mu\frac{\mathrm{d}\delta_{g^2}}{\mathrm{d}\mu} \tag{B.11}$$

$$\mu\frac{\mathrm{d}f_0}{\mathrm{d}\mu} = 0 \qquad \Rightarrow \qquad \mu\frac{\mathrm{d}f}{\mathrm{d}\mu} = -2\epsilon f \tag{B.12}$$

$$\mu\frac{\mathrm{d}m_0^2}{\mathrm{d}\mu} = 0 \qquad \Rightarrow \qquad \mu\frac{\mathrm{d}m^2}{\mathrm{d}\mu} = -\mu\frac{\mathrm{d}\delta_{m^2}}{\mathrm{d}\mu} \tag{B.13}$$

On this level, the running of M^2 and ϕ^2 are too small to be needed and they are not shown. The counterterm for f is zero on this level as well.

Let us first tackle the running of λ. To compute the derivative of δ_λ up to the wanted order, we need the first order of the running of g^2:

$$\mu\frac{\mathrm{d}\delta_\lambda}{\mathrm{d}\mu} = \frac{3g^2}{(4\pi)^2}\frac{1}{\epsilon}\mu\frac{\mathrm{d}g^2}{\mathrm{d}\mu} = -\frac{6g^4}{(4\pi)^2} \tag{B.14}$$

Substituting this result back gives:

$$\mu\frac{\mathrm{d}\lambda}{\mathrm{d}\mu} = \frac{3g^4}{(4\pi)^2} \tag{B.15}$$

The running of g^4 is of higher order when solving this differential equation and can be ignored. Therefore we can easily integrate the equation above to obtain Eq. (B.7).

Similarly, we can construct differential equations that describe the running of g^2 and m^2. The running of f in Eq. (B.12) is needed for the differential equation for g^2, which is then needed for the equation of m^2. The differential equations are

$$\mu\frac{\mathrm{d}g^2}{\mathrm{d}\mu} = \frac{4g^4 + fg^2}{(4\pi)^2}, \tag{B.16}$$

$$\mu\frac{\mathrm{d}m^2}{\mathrm{d}\mu} = \frac{g^2M^2}{(4\pi)^2}. \tag{B.17}$$

Once again, the runnings on the right-hand side are higher order and thus, can be ignored. A straightforward integration gives the results in Eqs. (B.8) and (B.9).

Bibliography

[1] B. P. et al. Abbott. Observation of gravitational waves from a binary black hole merger. *Phys. Rev. Lett.*, 116:061102, Feb 2016.

[2] Chiara Caprini and Daniel G Figueroa. Cosmological backgrounds of gravitational waves. *Classical and Quantum Gravity*, 35(16):163001, jul 2018.

[3] K. Kajantie, M. Laine, K. Rummukainen, and M. Shaposhnikov. Is there a hot electroweak phase transition at $m_H \gtrsim m_W$? *Phys. Rev. Lett.*, 77:2887–2890, Sep 1996.

[4] K. Kajantie, M. Laine, K. Rummukainen, and M. Shaposhnikov. The electroweak phase transition: a non-perturbative analysis. *Nuclear Physics B*, 466(1):189 – 258, 1996.

[5] Jose R. Espinosa, Thomas Konstandin, and Francesco Riva. Strong Electroweak Phase Transitions in the Standard Model with a Singlet. *Nucl. Phys. B*, 854:592–630, 2012.

[6] M. E. Shaposhnikov. Electroweak baryogenesis. *Contemporary Physics*, 39(3):177–194, 1998.

[7] K. Enqvist, J. Ignatius, K. Kajantie, and K. Rummukainen. Nucleation and bubble growth in a first-order cosmological electroweak phase transition. *Phys. Rev. D*, 45:3415–3428, May 1992.

[8] Chiara Caprini et al. Detecting gravitational waves from cosmological phase transitions with LISA: an update. *JCAP*, 03:024, 2020.

[9] Peter Brockway Arnold and Olivier Espinosa. The Effective potential and first order phase transitions: Beyond leading-order. *Phys. Rev. D*, 47:3546, 1993. [Erratum: Phys.Rev.D 50, 6662 (1994)].

[10] Alessandro Strumia and Nikolaos Tetradis. A consistent calculation of bubble-nucleation rates. *Nuclear Physics B*, 542(3):719 – 741, 1999.

[11] K. Kajantie, M. Laine, K. Rummukainen, and M. Shaposhnikov. Generic rules for high temperature dimensional reduction and their application to the standard model. *Nuclear Physics B*, 458(1):90 – 136, 1996.

[12] Eric Braaten and Agustin Nieto. Effective field theory approach to high-temperature thermodynamics. *Phys. Rev. D*, 51:6990–7006, Jun 1995.

[13] A.D. Linde. Infrared problem in the thermodynamics of the yang-mills gas. *Physics Letters B*, 96(3):289 – 292, 1980.

[14] Mathias Garny and Thomas Konstandin. On the gauge dependence of vacuum transitions at finite temperature. *JHEP*, 07:189, 2012.

[15] Dimitrios Metaxas and Erick J. Weinberg. Gauge independence of the bubble nucleation rate in theories with radiative symmetry breaking. *Phys. Rev. D*, 53:836–843, Jan 1996.

[16] J.R. Espinosa. A fresh look at the calculation of tunneling actions. *Journal of Cosmology and Astroparticle Physics*, 2018(07):036–036, jul 2018.

[17] Curtis G. Callan and Sidney Coleman. Fate of the false vacuum. ii. first quantum corrections. *Phys. Rev. D*, 16:1762–1768, Sep 1977.

[18] Sidney Coleman. Fate of the false vacuum: Semiclassical theory. *Phys. Rev. D*, 15:2929–2936, May 1977.

[19] A.D. Linde. Decay of the false vacuum at finite temperature. *Nuclear Physics B*, 216(2):421 – 445, 1983.

[20] Ian Affleck. Quantum-statistical metastability. *Phys. Rev. Lett.*, 46:388–391, Feb 1981.

[21] Arjun Berera, Joël Mabillard, Bruno W. Mintz, and Rudnei O. Ramos. Formulating the kramers problem in field theory. *Phys. Rev. D*, 100:076005, Oct 2019.

[22] Honda M. Sato R. et al. Blum, K. O(n) invariance of the multi-field bounce. *J. High Energ. Phys*, 2017:1–11, May 2017.

[23] Sidney Coleman. Quantum tunneling and negative eigenvalues. *Nuclear Physics B*, 298(1):178 – 186, 1988.

[24] Carsten Greiner and Berndt Müller. Classical fields near thermal equilibrium. *Phys. Rev. D*, 55:1026–1046, Jan 1997.

[25] Erick J. Weinberg. Vacuum decay in theories with symmetry breaking by radiative corrections. *Phys. Rev. D*, 47:4614–4627, May 1993.

[26] M. Laine and A. Vuorinen. *Basics of Thermal Field Theory: A Tutorial on Perturbative Computations*. Springer International Publishing, 2016.

[27] Aneesh V. Manohar. Introduction to Effective Field Theories. In *Les Houches summer school: EFT in Particle Physics and Cosmology*, 4 2018.

[28] Sidney Coleman and Erick Weinberg. Radiative corrections as the origin of spontaneous symmetry breaking. *Phys. Rev. D*, 7:1888–1910, Mar 1973.

[29] Jaume Garriga. Instantons for vacuum decay at finite temperature in the thin wall limit. *Phys. Rev. D*, 49:5497–5506, 1994.

[30] Marcelo Gleiser, Gil C. Marques, and Rudnei O. Ramos. Evaluation of thermal corrections to false vacuum decay rates. *Phys. Rev. D*, 48:1571–1584, Aug 1993.

[31] Alessandro Strumia and Nikolaos Tetradis. Bubble-nucleation rates for radiatively induced first-order phase transitions. *Nuclear Physics B*, 554(3):697 – 718, 1999.

[32] Jaume Garriga. Nucleation rates in flat and curved space. *Phys. Rev. D*, 49:6327–6342, 1994.

[33] R. Jackiw. Functional evaluation of the effective potential. *Phys. Rev. D*, 9:1686, 1974.

[34] Guy D. Moore, Kari Rummukainen, and Anders Tranberg. Nonperturbative computation of the bubble nucleation rate in the cubic anisotropy model. *JHEP*, 04:017, 2001.

[35] Peter Brockway Arnold, Stephen R. Sharpe, Laurence G. Yaffe, and Yan Zhang. Weakly first order phase transitions: The Epsilon expansion versus numerical simulations in the cubic anisotropy model. *Phys. Rev. Lett.*, 78:2062–2065, 1997.

[36] Peter Brockway Arnold and Laurence G. Yaffe. Epsilon expansion analysis of very weak first order transitions in the cubic anisotropy model: Part 1. *Phys. Rev. D*, 55:7760–7775, 1997.

[37] Peter Brockway Arnold, Stephen R. Sharpe, Laurence G. Yaffe, and Yan Zhang. Weakly first order phase transitions: The Epsilon expansion versus numerical simulations in the cubic anisotropy model. *Phys. Rev. Lett.*, 78:2062–2065, 1997.

[38] A. Strumia, N. Tetradis, and C. Wetterich. The Region of validity of homogeneous nucleation theory. *Phys. Lett. B*, 467:279–288, 1999.

[39] J.R. Espinosa and T. Konstandin. A fresh look at the calculation of tunneling actions in multi-field potentials. *Journal of Cosmology and Astroparticle Physics*, 2019(01):051–051, jan 2019.

[40] Matthew D. Schwartz. *Quantum Field Theory and the Standard Model*. Cambridge University Press, 3 2014.